

Electronic Thesis and Dissertation Repository

8-16-2012 12:00 AM

Thermal and Electrical Behaviors of Selected Geomaterials

Joon Kyu Lee, *The University of Western Ontario*

Supervisor: Professor Julie Q. Shang, *The University of Western Ontario*

A thesis submitted in partial fulfillment of the requirements for the Doctor of Philosophy degree
in Civil and Environmental Engineering

© Joon Kyu Lee 2012

Follow this and additional works at: <https://ir.lib.uwo.ca/etd>



Part of the [Geotechnical Engineering Commons](#)

Recommended Citation

Lee, Joon Kyu, "Thermal and Electrical Behaviors of Selected Geomaterials" (2012). *Electronic Thesis and Dissertation Repository*. 824.

<https://ir.lib.uwo.ca/etd/824>

This Dissertation/Thesis is brought to you for free and open access by Scholarship@Western. It has been accepted for inclusion in Electronic Thesis and Dissertation Repository by an authorized administrator of Scholarship@Western. For more information, please contact wlsadmin@uwo.ca.

THERMAL AND ELECTRICAL BEHAVIORS OF
SELECTED GEOMATERIALS

(Spine title: Thermal and Electrical Behaviors of Selected Geomaterials)

(Thesis format: Integrated-Article)

by

Joon Kyu Lee

Graduate Program in Civil and Environmental Engineering

A thesis submitted in partial fulfillment
of the requirements for the degree of
Doctor of Philosophy

The School of Graduate and Postdoctoral Studies
The University of Western Ontario
London, Ontario, Canada

© Joon Kyu Lee 2012

THE UNIVERSITY OF WESTERN ONTARIO
SCHOOL OF GRADUATE AND POSTDOCTORAL STUDIES

CERTIFICATE OF EXAMINATION

Supervisor

Dr. Julie Q. Shang

Supervisory Committee

Examiners

Dr. Silvana Micic

Dr. Abouzar Sadrekarimi

Dr. Liying Jiang

Dr. Kai Sing Ho

The thesis by

Joon Kyu Lee

entitled:

Thermal and Electrical Behaviors of Selected Geomaterials

is accepted in partial fulfillment of the

requirements for the degree of

Doctor of Philosophy

Date _____

Chair of the Thesis Examining Board

ABSTRACT

Geomaterials can be often classified into two groups: virgin geomaterials such as soil and rock, and by-product materials such as mine tailings, coal fly/bottom ash, foundry sand, kiln dust, blast furnace/steel slag, reclaimed concrete and asphalt. Studies on these materials and their mixtures have been carried out extensively for geoengineering applications, including the characterization of mechanical properties such as the strength, compressibility, compactivity and permeability, as well as mineralogical and geochemical properties. The goal of this study is to investigate the thermal and electrical properties of selected geomaterials and their mixtures for enhancement of knowledge and engineering applications. The thesis consists of three parts as follows:

The first part presents the electrical conductivity measured on compacted kaolin clay using a circular two-electrode cell in conjunction with a specially designed compaction apparatus, which has the advantage of reducing errors owing to sample handling. The experimental results are analyzed to observe the influencing factors on the soil electrical conductivity. The performance of existing analytical models for predicting the soil electrical conductivity is evaluated by calculating empirical constants in these models.

The second part investigates the thermal and packing behaviors of mine tailings and tire crumbs mixtures in dry and wet states, which are important in engineering applications for utilizing recycled tire particles as lightweight fill materials with improved thermal insulation. The thermal and packing properties measurements of the mine tailings and tire crumbs mixtures with different mixing ratios are presented, which are then analyzed to establish the thermal properties relationships with respect to the mixing ratio of tire crumbs, porosity, bulk density,

water content, compactive effort and tire crumbs size. The multiple linear regression analysis shows that the thermal conductivity of the dry and wet mixtures can be estimated using a general model consisting of the factors affecting the thermal conductivity.

The third part evaluates the thermal conductivity, compressive strength, elastic modulus and temperature changes of compacted mine tailings and fly ash mixtures during the curing period as functions of the fly ash ratio, molding water content and compaction energy. The microporosity structure of the fly ash treated mine tailings is also examined.

Keywords: Thermal conductivity, electrical conductivity, mine tailings, tire crumbs, coal fly ash, compaction, packing, fabric, statistics, regression model, recycling.

CO-AUTHORSHIP

This thesis is prepared in accordance with the regulations for Integrated-Article (Formerly Manuscript) format thesis stipulated by the School of Graduate and Postdoctoral Studies at The University of Western Ontario. All the experimental works were carried out at The University of Western Ontario by the author under the supervision of Professor Julie Shang. The co-authorship of Chapters 2 to 5 is as follows:

Chapter 2: Influencing factors on electrical conductivity of compacted kaolin clay

J.K. Lee and J.Q. Shang

Published in *Geomechanics and Engineering, An International Journal*, Techno Press, 2011, Vol. 3, No. 2, 131-151.

Contributions:

J.K. Lee designed experimental program, conducted experiments, interpreted test results, and wrote the draft of the paper.

J.Q. Shang initiated the study and assisted the interpretation of the test results and the writing of the paper.

Chapter 3: Thermal properties of dry mixtures of mine tailings and tire crumbs

J.K. Lee and J.Q. Shang

Submitted for publication in *Journal of Environmental Engineering, ASCE*.

Contributions:

J.K. Lee designed experimental program, conducted experiments, interpreted test results, and wrote the draft of the paper.

J.Q. Shang assisted the interpretation of the test results and the writing of the paper.

Chapter 4: Thermal conductivity of compacted mixtures of mine tailings and tire crumbs

J.K. Lee and J.Q. Shang

Submitted for publication in *Geotechnical Testing Journal*, ASTM.

Contributions:

J.K. Lee designed experimental program, conducted experiments, interpreted test results, and wrote the draft of the paper.

J.Q. Shang assisted the interpretation of the test results and the writing of the paper.

Chapter 5: Evolution of thermal and mechanical properties of mine tailings and fly ash mixtures during curing period

J.K. Lee and J.Q. Shang

Submitted for publication in *Canadian Geotechnical Journal*, NRC Research Press.

Contributions:

J.K. Lee designed experimental program, conducted experiments, interpreted test results, and wrote the draft of the paper.

J.Q. Shang assisted the interpretation of the test results and the writing of the paper.

To my parents

ACKNOWLEDGMENTS

Having studied at Western has been a great experience, both professionally and personally, which will never be forgotten in my life.

I would like to express my deepest gratitude and appreciation to my supervisor Professor Julie Shang whose invaluable encouragement and insightful suggestions guided me throughout this research. It is my pleasure and privilege to work with her during my PhD program.

Sincere appreciation is expressed to the faculties, staffs and fellow students in the Department of Civil and Environmental Engineering at the University of Western Ontario for their support, motivation and friendship. In particular, I am grateful to Ms. M. Richards, Mr. T. Stephens and Mr. W. Logan for their assistance during this research.

Special thanks are also extended to Professors Sangseom Jeong, Junhwan Lee and Sooil Kim of Yonsei University. They all have given me continuous interest and encouragement during my graduate studies as well as instructed me in building a good knowledge of geotechnical engineering.

My family is always supportive for my education and always provides me unconditional and endless love.

TABLE OF CONTENTS

	page
CERTIFICATE OF EXAMINATION	ii
ABSTRACT.....	iii
CO-AUTHORSHIP	v
DEDICATION.....	vii
ACKNOWLEDGMENTS	viii
TABLE OF CONTENTS.....	ix
LIST OF TABLES.....	xiv
LIST OF FIGURES	xv
NOMENCLATURE	xx
CHAPTER 1 INTRODUCTION	1
1.1 Background.....	1
1.2 Research Objectives.....	3
1.3 Thesis Outline	3
1.4 Original Contribution.....	5
References.....	6
CHAPTER 2 INFLUENCING FACTORS ON ELECTRICAL CONDUCTIVITY OF COMPACTED KAOLIN CLAY.....	8
2.1 Introduction.....	8

2.2 Background	10
2.2.1 Influencing Factors on Soil Electrical Conductivity.....	10
2.2.2 Electrical Conductivity Models for Soil	12
2.3 Experimental Investigation	14
2.3.1 Materials and Equipments.....	14
2.3.2 Experimental Method.....	16
2.4 Results and Discussion	17
2.4.1 Effect of Soil Porosity: Saturated Samples.....	17
2.4.2 Effect of Gravimetric Water Content.....	19
2.4.3 Effect of Degree of Saturation	20
2.4.4 Effect of Volumetric Water Content.....	21
2.5 Conclusions.....	23
References.....	24

CHAPTER 3 THERMAL PROPERTIES OF DRY MIXTURES OF

MINE TAILINGS AND TIRE CRUMBS.....	41
3.1 Introduction.....	41
3.2 Objective and Scope	43
3.3 Heat Transfer in Geomaterials	44
3.4 Particle Packing Characteristics.....	46
3.5 Experimental Study.....	51

3.5.1 Materials	51
3.5.2 Apparatus	53
3.5.3 Sample Preparation	54
3.5.4 Methodology	54
3.6 Results and Discussion	56
3.6.1 Packing Behaviors of Mixtures.....	56
3.6.2 Thermal Behaviors of Mixtures	59
3.7 Statistical Analysis.....	62
3.7.1 Regression Model for Thermal Conductivity	63
3.7.2 Analysis Chart for Volumetric Heat Capacity	65
3.8 Summary and Conclusions	66
References.....	68

CHAPTER 4 THERMAL CONDUCTIVITY OF COMPACTED MIXTURES OF

MINE TAILINGS AND TIRE CRUMBS.....	86
4.1 Introduction.....	86
4.2 Experimental Design.....	88
4.2.1 Materials	88
4.2.2 Specimen Preparation	89
4.2.3 Devices and Methodology	91
4.3 Methods of Data Analysis.....	92

4.4 Results and Discussion	93
4.4.1 Compaction Characteristics	93
4.4.2 Thermal Conductivity Characteristics	93
4.4.3 Anisotropy of Thermal Conductivity.....	97
4.5 Statistical Analyses	98
4.6 Conclusions.....	101
References.....	103

CHAPTER 5 EVOLUTION OF THERMAL AND MECHANICAL PROPERTIES OF

MINE TAILINGS AND FLY ASH MIXTURES DURING CURING PERIOD 118

5.1 Introduction.....	118
5.2 Materials	120
5.2.1 Mine Tailings	121
5.2.2 Fly Ash.....	121
5.2.3 Water.....	122
5.3 Specimen Preparation and Testing Conditions	122
5.4 Experiments	124
5.4.1 Thermal Properties Analyzer	124
5.4.2 Unconfined Compression Test.....	125
5.4.3 Mercury Intrusion Porosimetry.....	126
5.4.4 Scanning Electron Microscopy.....	128

5.5 Results and Discussion	128
5.5.1 Compaction Characteristics	128
5.5.2 Thermal Conductivity	129
5.5.3 Temperature	131
5.5.4 Unconfined Compressive Strength	132
5.5.5 Elastic Modulus	133
5.5.6 Pore Size Distribution	134
5.5.7 SEM Image	136
5.5.8 Thermal Conductivity as Related to Packing and Mechanical Properties	137
5.6 Summary and Conclusions	138
References.....	140
CHAPTER 6 CONCLUSIONS	160
6.1 Summary and Conclusions	160
6.2 Suggestions for Future Research	162
APPENDIX A: Definition and Meaning of Statistical Measures	163
APPENDIX B: Photographs of Materials and Experiments.....	164
CURRICULUM VITAE.....	170

LIST OF TABLES

	page
Table 2.1 Index properties of kaolin clay tested	29
Table 2.2 Summary of soil sample properties	30
Table 2.3 Cementation exponent (m) and tortuosity factor (c) for various soils.....	31
Table 2.4 Calculated values of the empirical constants using Eq. (2.6).....	32
Table 3.1 Densities and thermal properties of basic geomaterial constituents	75
Table 3.2 Index properties of mine tailings and tire crumbs	75
Table 3.3 Particle size statistics of mine tailings and tire crumbs	75
Table 3.4 Summary of packings and thermal properties of the mixtures tested.....	76
Table 3.5 Summary of multiple linear regression analysis result.....	77
Table 4.1 Physical properties of mine tailings and tire crumbs	106
Table 4.2 Summary of horizontal, vertical and overall thermal conductivities of compacted mixtures tested.....	107
Table 4.3 Results of ANOVA for response variable	109
Table 4.4 Results of stepwise multiple linear regression analysis.....	109
Table 5.1 Physical properties of test materials	146
Table 5.2 Oxide composition of test materials (adapted from Wang et al. 2006).....	146
Table 5.3 Summary of specimens tested.....	147

LIST OF FIGURES

	page
Figure 2.1 Circular two-electrode cell and compaction apparatus	33
Figure 2.2 Schematic of the electrical conductivity measurement system	34
Figure 2.3 Compacted annular soil samples in the cell	34
Figure 2.4 Variation of electrical conductivity against clay-to-solution ratio for decanted solutions	35
Figure 2.5 Formation factor of saturated samples with different salinities against soil porosity .	35
Figure 2.6 General relationships between formation factor and soil porosity for measured and reported data	36
Figure 2.7 Tortuosity of saturated samples with different salinities against soil porosity	36
Figure 2.8 Influence of gravimetric water content and dry unit weight on bulk soil electrical conductivity	37
Figure 2.9 Influence of degree of saturation and salinity on bulk soil electrical conductivity	38
Figure 2.10 Relationship between κ_b / κ_w and degree of saturation	38
Figure 2.11 Influence of volumetric water content and salinity on bulk soil electrical conductivity	39
Figure 2.12 Variation of bulk soil electrical conductivity against salinity for different volumetric water contents	39
Figure 2.13 Relationship between $(\kappa_b - \kappa_s) / \kappa_w$ and volumetric water content	40
Figure 2.14 Relationship between κ_b / κ_w and volumetric water content	40
Figure 3.1 Porosity in binary packing against volumetric mixing ratio of coarse particles in mixtures (modified from Lade et al. (1998))	78

Figure 3.2 SEM images: (a) mine tailings; (b) tire crumbs	78
Figure 3.3 Particle size distribution curves: (a) mine tailings; (b) tire crumbs.....	79
Figure 3.4 Variations of minimum and maximum bulk unit weights for mixtures of mine tailings and tire crumbs.....	80
Figure 3.5 Variations of minimum and maximum porosities for mixtures of mine tailings and tire crumbs.....	80
Figure 3.6 Correlation between minimum and maximum porosities	81
Figure 3.7 Change in porosity ranges for mixtures of mine tailings and tire crumbs.....	81
Figure 3.8 Relationships between thermal conductivity and volumetric mixing ratio of tire crumbs for loosest and densest packings for mine tailings and tire crumbs mixtures .	82
Figure 3.9 Relationships between volumetric heat capacity and volumetric mixing ratio of tire crumbs for loosest and densest packings for mine tailings and tire crumbs mixtures .	82
Figure 3.10 Effect of weight mixing ratio of mine tailings and tire crumbs mixtures on thermal conductivity	83
Figure 3.11 Thermal conductivity of various dry geomaterials.....	83
Figure 3.12 Effect of weight mixing ratio of mine tailings and tire crumbs mixtures on volumetric heat capacity	84
Figure 3.13 Standard residuals of a regression model with two variables.....	84
Figure 3.14 Change of volumetric heat capacity at different volumetric mixing ratios of tire crumbs and porosities	85
Figure 4.1 Particle size distributions of test materials	110
Figure 4.2 A compacted specimen of mine tailings and small tire crumbs mixtures with	

the mixing ratio of tire crumbs of 0.2 and the water content of 15% (i.e., TC0.2-SP-S-W15)	110
Figure 4.3 Variations of maximum dry density and optimum water content with mixing ratio of tire crumbs	111
Figure 4.4 Variations of bulk density and thermal conductivity with water content for compacted mine tailings and small tire crumbs mixtures with different mixing ratios of tire crumbs	112
Figure 4.5 Variations of bulk density and thermal conductivity with water content for compacted mine tailings and small tire crumbs mixtures with different compactive efforts	113
Figure 4.6 Variations of (a) bulk density, (b) thermal conductivity, and (c) volumetric air content with water content for compacted mixtures with different tire crumbs sizes	114
Figure 4.7 Relationship between thermal conductivity and bulk density for all compacted mixtures	115
Figure 4.8 Anisotropy of thermal conductivity for compacted mine tailings and tire crumbs mixtures: (a) horizontal versus vertical thermal conductivity; (b) effects of water content and mixing ratio of tire crumbs on anisotropy ratio; (c) effects of water content, compactive effort and tire crumbs size on anisotropy ratio	116
Figure 4.9 Predicted thermal conductivity of compacted mine tailings and tire crumbs mixtures using the statistical model versus actual data	117
Figure 5.1 Particle size distributions of (a) Musselwhite mine tailings and	

(b) Atikokan fly ash	148
Figure 5.2 pH variation of mine tailings and fly ash slurries.....	149
Figure 5.3 Compaction curves and conditions studied	149
Figure 5.4 Typical stress and strain curve of compacted mine tailings and fly ash mixtures	150
Figure 5.5 Variations of thermal conductivity with curing time: effects of	
(a) fly ash ratio, (b) molding water content, and (c) compaction energy.....	150
Figure 5.6 Variations of temperature with curing time: effects of	
(a) fly ash ratio and (b) molding water content and compaction energy	152
Figure 5.7 Variations of unconfined compressive strength with curing time: effects of	
(a) fly ash ratio and (b) molding water content and compaction energy	153
Figure 5.8 Variations of elastic modulus with curing time: effects of	
(a) fly ash ratio and (b) molding water content and compaction energy	154
Figure 5.9 Mercury intrusion porosimetry results of the 120 hours-cured specimens with	
different fly ash ratios (20, 40 and 60%): (a) cumulative pore volume;	
(b) differential pore volume	155
Figure 5.10 Mercury intrusion porosimetry results of the 120 hours-cured specimens compacted	
at different compaction conditions: (a) cumulative pore volume;	
(b) differential pore volume	156
Figure 5.11 SEM images of the 120 hours-cured samples with different fly ash ratios:	
(a) FA = 20%; (b) FA = 40%; (c) FA = 60%	157
Figure 5.12 Relationship between initial thermal conductivity and bulk unit weight	158
Figure 5.13 Relationship between final thermal conductivity and cumulative pore volume	159
Figure 5.14 Relationship between unconfined compressive strength and thermal conductivity	159

Figure B.1 By-product materials: (a) Musselwhite gold mine tailings and (b) scrap tire particles.....	165
Figure B.2 SEM images of Atikokan coal fly ash: at (a) 300 times magnification and (b) 1,000 time magnification.....	166
Figure B.3 Thermal conductivity monitoring and curing of specimens of coal fly ash treated mine tailings in an environmental chamber.....	167
Figure B.4 Unconfined compression test - failure shapes of coal fly ash treated mine tailings (FA20-SP-OWC, immediately after compaction)	168
Figure B.5 Unconfined compression test - failure shapes of coal fly ash treated mine tailings (FA20-SP-OWC, 120 hours after compaction)	169

NOMENCLATURE

a, b	empirical constants
C_a	volumetric heat capacity of air ($\text{J}/\text{m}^3\text{K}$)
C_c	coefficient of curvature
C_i	volumetric heat capacity of a constituent ($\text{J}/\text{m}^3\text{K}$)
C_m	volumetric heat capacity of mine tailings ($\text{J}/\text{m}^3\text{K}$)
C_s	volumetric heat capacity of soil solid ($\text{J}/\text{m}^3\text{K}$)
C_t	volumetric heat capacity of tire crumbs ($\text{J}/\text{m}^3\text{K}$)
C_u	coefficient of uniformity
C_v	volumetric heat capacity ($\text{J}/\text{m}^3\text{K}$)
C_w	volumetric heat capacity of water ($\text{J}/\text{m}^3\text{K}$)
CE	compactive effort index
c	tortuosity factor
D	average particle size between two sieve sizes (μm)
D_{10}	effective size of particles (μm)
D_{50}	median particle diameter (μm)
D_{50m}	median diameter of mine tailings (μm)
D_{50t}	median diameter of tire crumbs (μm)
D_m	mode particle diameter (μm)
D_{mm}	mode diameter of mine tailings (μm)
D_{mt}	mode diameter of tire crumbs (μm)
\bar{D}	mean particle diameter (μm)
\bar{D}_m	mean diameter of mine tailings (μm)

\bar{D}_t	mean diameter of tire crumbs (μm)
d	specimen diameter (m)
d_p	pore diameter (m)
E	elastic modulus (MPa)
e	void ratio
e_c	void ratio of coarse particles
e_f	void ratio of fine particles
e_{\max}	maximum void ratio
e_{\min}	minimum void ratio
F	formation factor
f	fraction of particles between two sieve sizes
G_s	specific gravity
G_{sm}	specific gravity of mine tailings
G_{st}	specific gravity of tire crumbs
h	specimen height (m)
I	electric current (A)
K	kurtosis
m	cementation exponent
m_{MT}	mass of mine tailings (g)
m_{TC}	mass of tire crumbs (g)
N	coordination number
n	porosity
n_c	porosity of coarse particles
n_f	porosity of fine particles
n_{\max}	maximum porosity

n_{\min}	minimum porosity
n_{mix}	porosity of a binary mixture
n_{opt}	porosity at the optimal packing
P	mercury intrusion pressure (MPa)
P_{FA}	percentage of fly ash weight in total mixture weight (%)
p	saturation exponent
Q	thermal energy per a unit volume (J/m^3)
q	heat flux (W/m^2)
q_u	unconfined compressive strength (MPa)
R_{FA}	fly ash ratio (%)
R_m	mixing ratio of tire crumbs in a mixture
R_{mV}	volumetric mixing ratio of tire crumbs
$R_{mV-\text{opt}}$	volumetric mixing ratio of tire crumbs at the optimal packing
R_{mW}	weight mixing ratio of tire crumbs
r	residual
r_i	radius of inner electrode (m)
r_o	radius of outer electrode (m)
r_s	standard residual
S	degree of saturation (%)
SE	standard error
Sk	skewness
T	temperature (K or $^{\circ}\text{C}$)
T_s	surface tension (N/m)
t	curing time (hours)
t_s	soil sample thickness (m)

V	imposed AC voltage (V)
V_a	volumetric fraction of air
V_c	cumulative pore volume per unit weight (mL/g)
V_d	derivative of the cumulative pore volume with respect to pore size (mL/g/ m)
V_i	volumetric fraction of a constituent
V_m	volumetric fraction of mine tailings
V_s	volumetric fraction of soil solid
V_t	volumetric fraction of tire crumbs
V_w	volumetric fraction of water
W_{FA}	weight of fly ash (g)
W_{MT}	weight of mine tailings (g)
w	gravimetric water content (%)
w_{opt}	optimum water content (%)
X_i	independent variable
x	distance in the direction of the heat flow (m)
Y	dependent variable
α, β	empirical constants
β_i	regression coefficient
γ_b	bulk unit weight (kN/m ³)
γ_d	dry unit weight (kN/m ³)
$\gamma_{d \max}$	maximum dry unit weight (kN/m ³)
γ_{\max}	maximum bulk unit weight (kN/m ³)
γ_{\min}	minimum bulk unit weight (kN/m ³)
γ_w	unit weight of water (kN/m ³)
ε	random error

η	anisotropy ratio of thermal conductivity
θ	volumetric water content or contact angle (degrees)
θ_a	volumetric air content (m^3/m^3)
κ_0	bulk soil electrical conductivity of a fully saturated soil (S/m)
κ_b	bulk soil electrical conductivity of a unsaturated soil (S/m)
κ_s	surface electrical conductivity (S/m)
κ_w	pore water electrical conductivity (S/m)
λ	thermal conductivity (W/mK)
λ_f	final thermal conductivity (W/mK)
λ_h	horizontal thermal conductivity (W/mK)
λ_i	initial thermal conductivity (W/mK)
λ_m	measured thermal conductivity (W/mK)
λ_p	predicted thermal conductivity (W/mK)
λ_v	vertical thermal conductivity (W/mK)
ρ	particle density (g/cm^3)
ρ_b	bulk density (g/cm^3)
ρ_d	dry density (g/cm^3)
σ	standard deviation
σ_m	standard deviation of mine tailings (μm)
σ_t	standard deviation of tire crumbs (μm)
τ	tortuosity

CHAPTER 1

INTRODUCTION

1.1 Background

Natural soil, crushed rock and cement concrete have been traditionally used as fills of earthworks. Heat and electrical conduction through the geomaterials may have significant impact in geotechnical engineering design and construction (Mitchell and Soga 2005). The heat flow is of importance to frost action, ground stabilization by freezing and heating, construction in permafrost regions, geothermal energy exploitation, underground storage (Farouki 1985; Andersland and Ladanyi 2004). The electrical current flow in geomaterials is essential in ground improvement by electrokinetics, detection of ground contamination, corrosion protection of underground structures, subsurface characterization, oil and hydrocarbon recovery (McCarter and Desmazes 1997; Rowe et al. 2001; Wheatcroft 2002; Rittirong et al. 2008; Rousseau et al. 2009).

Due to rapid industrialization and urbanization, a variety of by-products have been generated worldwide, causing environmental concerns. As an alternative for their disposal, the reuse of some by-products in civil engineering applications has been practiced. The promising materials that can be recycled for use as fill materials, such as granular/stabilized base and backfill of embankments, include mine tailings, scrap tires, and coal fly ash (FHWA 2000). Mine tailings can be often used for road construction, hydraulic barrier and backfilling of underground voids instead of natural soils (Sivakugan et al. 2006; Fall et al. 2009). Typically, there are two distinct strategies for reusing mine tailings: uncemented tailings and cemented tailings. In the former case, the mine tailings are compacted or placed in the form of slurry for backfilling

without any binding agents, provided that they are non-reactive (Shelley and Daniel 1993; Sivakugan et al. 2006). In the latter case, the mine tailings are mixed with binders such as Portland cement, lime and fly ash (Misra et al. 1996; Yellishetty et al. 2008). In particular, the cemented tailings technique is beneficial for mitigating acid mine drainage caused by reactive tailings, resulting from agglomeration process that immobilizes the reactive components of the mine tailings (Amaratunga 1995). Scrap tires in lieu of natural geomaterials are either shredded or grinded to various sizes for practical purposes. The processed scrap tires have low density, high durability, good thermal insulation, and high energy absorption. Owing to these advantages, they can be applied either alone or mixed with other geomaterials as backfills of embankments, retaining walls and bridge abutments, leachate drainage layers in landfill, subgrade thermal insulators, and vibration damping media for railways (ASTM 2008). Coal fly ash from coal-burning facilities is commonly used alone or as an admixture in construction due to its pozzolanic and cementitious properties. The addition of fly ash and/or cement to problematic soils that include dredged soils, expansive soils and organic soils results in improving their engineering properties such as strength and stiffness (Phani Kumar and Sharma 2004; Kim et al. 2010; Tastan et al. 2011). Fly ash is also used to control mine tailings oxidation due to its alkaline nature as well as to improve the quality of the leachates through contaminant soils owing to formation of toxic elements precipitates (Yeheyis et al. 2009). Thus, a number of researchers have studied engineering characteristics of various by-products and their mixtures. However, the majority of research is focused on characterizing the deformation, volume change and stability behaviors as well as on assessing the environmental impact. The studies on thermal and electrical characteristics of the by-products and their mixtures have not been reported extensively in the open literature.

1.2 Research Objectives

The goal of this study is to measure and analyze the thermal and electrical properties of selected geomaterials and their mixtures, including kaolin clay, rubberized tailings and coal fly ash treated tailings, in order to enhance the scientific understanding and to facilitate engineering applications. To achieve this goal, the following specific objectives are devised:

1. To investigate the factors influencing the electrical behavior of the kaolin clay as well as the factors affecting the thermal behaviors of the rubberized tailings and coal fly ash treated tailings;
2. To explore the effect of fabric on the thermal behaviors of the rubberized tailings and coal fly ash treated tailings;
3. To establish the empirical models for predicting thermal properties of the rubberized tailings as related to their compositions and physical states; and
4. To examine the development of thermal and mechanical properties of coal fly ash treated tailings during the curing period.

1.3 Thesis Outline

The thesis is prepared in a manuscript format stipulated by the Faculty of Graduate Studies at The University of Western Ontario. Chapters 2 to 5 are written as independent articles. The research objectives are stated separately in each chapter.

Chapter 2 presents the results of the electrical conductivity measurement on compacted kaolin clay. The influences of packing properties (porosity and dry unit weight), amount of water in a soil (gravimetric water content, degree of saturation and volumetric water content), and pore water salinities on the electrical conductivity of the kaolin clay are investigated. The

experimental data are analyzed to compare the existing prediction models of soil electrical conductivity, along with determining the empirical constants in these models.

Chapter 3 presents the thermal and packings properties of dry mixtures of mine tailings and tire crumbs with different mixing ratios, which are then interpreted to explore the roles of tire particles inclusion in modifying the thermal and packing behaviors of mineral aggregates as well as to examine their correlations with regard to the porosity of the mixtures. A statistical study using multiple linear regression analysis is carried out to develop a prediction model for the thermal conductivity. An analysis chart for estimating the volumetric heat capacity is proposed to relate the volumetric mixing ratio of tire crumbs and porosity of the mixtures.

Chapter 4 studies the thermal conductivity of compacted mine tailings and tire crumbs mixtures as affected by the molding water content, mixing ratio, compactive effort and tire crumbs size. The thermal conductivity anisotropy of the compacted mixtures is also observed. Statistical data analysis is conducted to identify the significance of these influencing factors. A stepwise multiple linear regression analysis is performed to establish an empirical model for predicting the thermal conductivity of the compacted mixtures of mine tailings and tire crumbs.

Chapter 5 evaluates the thermal and mechanical properties of compacted mixtures of mine tailings and fly ash over the curing period of 120 hours through the measurement of thermal conductivity, temperature, unconfined compressive strength and elastic modulus of the mixtures. The effects of the amount of fly ash added to mine tailings, molding water content and compaction energy on these properties are examined. The pore size distribution and surface texture are analyzed to characterize the microfabrics of fly ash treated mine tailings.

Relationships between the thermal conductivity and properties that capture packing and mechanical characteristics of mine tailings and fly ash mixtures are demonstrated.

Chapter 6 presents conclusions of this study and recommendations for further research.

1.4 Original Contribution

The original contributions of this thesis are:

1. This thesis addresses the thermal and electrical behaviors of selected geomaterials (i.e., kaolin clay, rubberized tailings, and coal fly ash treated mine tailings) as influenced by their compositions and physical states (Chapters 2 to 5). It identifies critical factors that govern the thermal and electrical properties of the geomaterials. In the case of rubberized tailings, empirical models for predicting their thermal conductivity are developed as a function of the significant influencing factors (Chapters 3 and 4).
2. The thesis confirms the effect of the fabric change induced by different mixing ratios and natures of host materials, water contents and packing states on the thermal characteristics of geomaterials (Chapters 3 to 5). The change of these factors leads to the difference in the thermal properties that reflects the matrix transition, micropore structure change and fabric anisotropy.
3. The thesis investigates the short-term evolution of thermal and mechanical properties of coal fly ash treated mine tailings (Chapter 5). The relations of the thermal conductivity and the strength gain in the chemically treated tailings are established.

References

- Amaratunga, L.M. (1995). "Cold-bond agglomeration of reactive pyrrhotite tailings for backfill using low cost binders: gypsum -hemihydrate and cement." *Minerals Engineering*, 8(12), 1455-1465.
- Andersland, O.B., and Ladanyi, B. (2004). *Frozen ground engineering*, 2nd ed., American Society of Civil Engineers and John Wiley & Sons, New Jersey.
- ASTM. (2008). "Standard practice for use of scrap tires in civil engineering applications." *D6270-08*, West Conshohocken, Pa.
- Fall, M., Celestin, J.C., Ham, F.S. (2009). "Suitability of bentonite-paste tailings mixtures as engineering barrier material for mine waste containment facilities." *Minerals Engineering*, 22(9-10), 840-848.
- Farouki, O.T. (1986). *Thermal properties of soils*, Series on Rock and Soil Mechanics Vol. 11, Trans Tech Publications, Clausthal-Zellerfeld.
- Federal Highway Administration (FHWA) (2000). "Recycled materials in European Highway Environmental: Uses, Technologies, and Policies." *FHWA-PL-00-025*, International Technology Exchange Program, U.S. Department of Transportation, Alexandria.
- Kim, Y.T., Ahn, J., Han, W.J., and Gabr, M.A. (2010). "Experimental evaluation of strength characteristics of stabilized dredged soil." *Journal of Materials in Civil Engineering*, 22(5), 539-544.
- McCarter, W.J., and Desmazes, P. (1997). "Soil characterization using electrical measurements." *Geotechnique*, 47(1), 179-183.
- Misra, M., Yang, K., and Mehta, R.K. (1996). "Application of fly ash in the agglomeration of reactive mine tailings." *Journal of Hazardous Materials*, 51(1-3), 181-192.
- Mitchell, J.K., and Soga, K. (2005). *Fundamentals of soil behavior*, 3rd ed., John Wiley & Sons, New Jersey.

- Phani Kumar, B.R., and Sharma, R. (2004). "Effect of fly ash on engineering properties of expansive soils." *Journal of Geotechnical and Geoenvironmental Engineering*, 130(7), 764-767.
- Rittirong, A., Douglas, R.S., Shang, J.Q., and Lee, E.C. (2008). "Electrokinetic improvement of soft clay using electrical vertical drains." *Geosynthetics International*, 15(5), 369-381.
- Rousseau, C., Baraud, F., Leleyter, L., and Gil, O. (2009). "Cathodic protection by zinc sacrificial anodes: impact on marine sediment metallic contamination." *Journal of Hazardous Materials*, 167(1-3), 953-958.
- Rowe, R.K., Shang, J.Q., and Xie, Y. (2001). "Complex permittivity measurement system for detecting soil contamination." *Canadian Geotechnical Journal*, 38(3), 498-506.
- Shelley, T., and Daniel, D.E. (1993). "Effect of gravel on hydraulic conductivity of compacted soil liners." *Journal of Geotechnical Engineering*, 119(1), 54-68.
- Sivakugan, N., Rankine, R.M., Rankine, K.J., and Rankine, K.S. (2006). "Geotechnical considerations in mine backfilling in Australia." *Journal of Cleaner Production*, 14(12-13), 1168-1175.
- Tastan, E.O., Edil, T.B., Benson, C.H., and Aydilek, A.H. (2011). "Stabilization of organic soils with fly ash." *Journal of Geotechnical and Geoenvironmental Engineering*, 137(9), 819-833.
- Wheatcroft, R.A. (2002). "In situ measurements of near-surface porosity in shallow-water marine sands." *IEEE Journal of Oceanic Engineering*, 27(3), 561-570.
- Yeheyis, M.B., Shang, J.Q., and Yanful, E.K. (2009). "Long-term evaluation of coal fly ash and mine tailings co-placement: A site-specific study." *Journal of Environmental Management*, 91(1), 237-244.
- Yellishetty, M., Karpe, V., Reddy, E.H., and Subhash, K.N. (2008). "Reuse of iron ore mineral wastes in civil engineering constructions: a case study." *Resources, Conservation and Recycling*, 52(11), 1283-1289.

CHAPTER 2

INFLUENCING FACTORS ON ELECTRICAL CONDUCTIVITY OF COMPACTED KAOLIN CLAY

2.1 Introduction

The interaction between an external electric field and a soil-water system can be characterized in terms of the electrical conductivity, which represents the mobility of electrical charges through soil mass. The electrical conductivity of any earth material reflects its physical, chemical and geological properties. It is noteworthy that the electrical resistivity is also used in engineering practice, which is the reciprocal of the electrical conductivity.

The study on electrical response of soil-water systems is an emerging field with applications in areas including agriculture, soil science, geotechnical and environmental engineering. Reliable measurement of soil electrical conductivity is essential for broad engineering applications, such as the assessment of soil salinity and water content (Kalinski and Kelly 1993; Hamed et al. 2003), monitoring solute transport through soils (Kachanoski et al. 1992; Vanclouster et al. 1995), exploration of oil and hydrocarbon in brine-bearing reservoirs (Kim and Manghnani 1992; Wheatcroft 2002), estimation of hydraulic properties of soils (Lovell 1985; Gorman and Kelly 1990), performance evaluation of compacted-soil liners (Kalinski and Kelly 1994; Abu-Hassanein et al. 1996), characterization of liquefaction potential of soils (Erchul and Gluarte 1982; Arulanandan and Muraleetharan 1988), and engineering applications of electrokinetics (Mohamedelhassan and Shang 2003; Rittirong et al. 2008; Shang et al. 2009).

Electrical conductivity of soils can be measured in the laboratory, generally by using either time domain reflectometry (TDR) or soil resistivity boxes. However, TDR technique is expensive, and overestimates the electrical conductivity of highly saline soils (e.g., higher than 0.05 S/m, Nichol et al. 2002) that leads to inaccurate estimate of water content (Hamed et al. 2003). On the other hand, soil resistivity boxes are relatively cost effective and simple to conduct. The standard method for electrical conductivity tests of soils is specified in ASTM G 57 (ASTM 2006). For laboratory experimentation, soil is filled in a rectangular soil box. Four electrodes, i.e., a pair of outer electrodes as the current electrodes and a pair of inner pin-shaped electrodes as the potential electrodes, are employed.

As an alternative to use a standard soil box, some measurement systems have been reported in the literature. A cylinder with two electrodes arranged horizontally or vertically was designed by McCarter (1984) and Rinaldi and Cuestas (2002). In this device, a pair of end plate electrodes was used as both the current and potential electrodes. Another measurement device given in the literature consisted of a circular cell that incorporates eight holes at 45° intervals for the insertion of electrodes (Rhoades et al. 1976; Kalinski and Kelly 1993; Auerswald et al. 2001). Measurements were obtained eight times around the circular cell, moving each set of four adjacent electrodes, known as a Wenner array, and the average of the resistances was taken. Abu-Hassanein et al. (1996) developed a four-electrode cell with dimensions of the compaction mold described in ASTM D 698 (ASTM 2007). More recently, multi-electrode cells with several circumferential electrodes were fabricated to investigate the electrical anisotropy of soils (McCarter and Desmazes 1997; Bryson and Bathe 2009). The aforementioned measurement systems, however, have some limitations: 1) it is difficult to achieve uniform compaction of soil, followed by the variation of soil density in the box, and 2) it may result in poor contacts at the

soil-electrode interface from insertion of electrodes. To compensate for these uncertainties in measurement, a circular two-electrode cell in conjunction with a specially designed compaction apparatus was developed in Scholte et al. (2002), which was adopted in this study.

The objective of this study is to present the results of the electrical conductivity measurement on compacted kaolin clay at different porosities, dry unit weights, amount of water and pore water salinities, and to demonstrate the characteristic electrical responses with respect to these parameters. The experimental results are also analyzed to compare the existing prediction models of electrical conductivity of saturated and unsaturated soils, together with computing the empirical constants in these models.

2.2 Background

2.2.1 Influencing Factors on Soil Electrical Conductivity

Several researchers (Jackson et al. 1978; Abu-Hassanein et al. 1996; Rinaldi and Cuestas 2002) have shown that the electrical conductivity of a soil-water system is related to inherent factors such as the particle size, shape, gradation, orientation and mineralogical composition, and to more variable factors including the porosity, pore water, temperature, concentration and type of electrolytes, and frequency of the electrical field for the measurement.

Three parameters used to define the amount of water in bulk soil are: the gravimetric water content w (the weight ratio of water to solid), the degree of saturation S (the volumetric ratio of water to void) and the volumetric water content θ (the volumetric ratio of water to bulk soil).

The parameters are correlated in soil phase relations:

$$\theta = w \frac{\gamma_d}{\gamma_w} = Sn \quad (2.1)$$

where γ_w is the unit weight of water, γ_d is the dry unit weight of soil, and n is the soil porosity given as

$$n = 1 - \frac{\gamma_d}{G_s \gamma_w} \quad (2.2)$$

where G_s is the specific gravity of soil solid. Note that the volumetric water content is equal to soil porosity when the soil is fully saturated.

The electrical conductivity of soils is comprised of three components, i.e., the pore water electrical conductivity, surface electrical conductivity and solid electrical conductivity. The pore water contributes to the electrical conductivity through electromigration of dissolved ions, which is dependent upon the salinity (ionic strength), temperature and the frequency imposed to ions. It is noteworthy that the term salinity represents the overall effect of dissolved ionic species such as Na^+ , K^+ , Ca^{2+} , Mg^{2+} , Cl^- , CO_3^- , HCO_3^- , SO_4^- , etc in an aqueous solution (Hamed et al. 2003). The pore water electrical conductivity, therefore, is a reliable indicator to assess the concentration of soluble salts in soils (U.S. Salinity Laboratory Staff 1954). The second component of soil electrical conductivity, i.e., the surface electrical conductivity, is attributed to migration of absorbed counterions on the surface of soil solids. The surface electrical conductivity dominates over the electrical conductivity of solids in soils with low salinities, and is influenced by the soil fabric (which refers to the arrangement of grains of all size ranges, shapes and associated pores) as well as by organic matters (Auerswald et al. 2001). The third component of soil electrical conductivity, i.e., the solid electrical conductivity, is typically much lower than the surface electrical conductivity and hence can be neglected.

2.2.2 Electrical Conductivity Models for Soil

Archie (1942) established a simple one-conductance model accounting only for the contribution of water phase in completely saturated soils. The bulk soil electrical conductivity of a fully water-saturated soil κ_0 is related to the pore water electrical conductivity κ_w as a function of soil porosity n , according to

$$\kappa_0 = n^m \kappa_w \quad (2.3)$$

where m is the constant termed the cementation exponent, which increases with increasing the soil cementation. According to Abu-Hassanein et al. (2001), the cementation exponent is affected by compaction and anisotropy, as well as fabric.

Winsauer et al. (1952) modified Archie model by introducing a tortuosity factor c , yielding

$$\kappa_0 = cn^m \kappa_w \quad (2.4)$$

The c and m may be considered to be covariant because both are not independent parameters. It is commonly accepted that the increase in soil density by compaction leads to increasing the tortuosity factor (Salem 2001).

Since soil pore water flows through similar paths as the electric current, both the hydraulic and electrical conductivities of soils may be thought to be linked by a single parameter, the tortuosity τ which is defined as the ratio of the effective length of a flow path to the straight length of a porous media. Based on this concept, the theoretical relationship between the tortuosity and normalized electrical conductivity κ_w / κ_0 (known as the formation factor F) was derived by Walsh and Brace (1984):

$$\tau = \sqrt{n \frac{\kappa_w}{\kappa_0}} \quad (2.5)$$

As the degree of saturation S decreases, the bulk soil electrical conductivity will decrease, because some of the pore space formerly occupied by water is replaced by air of low electrical conductivity. The electrical conductivity of unsaturated soil κ_b is related to that of fully saturated soil κ_0 (Keller and Frischknecht 1966) by:

$$\kappa_b = \kappa_0 S^p \quad (2.6)$$

where p is the saturation exponent. It should be noted that Eq. (2.6) was developed for porous media having fixed pore structure that has no blockage to continuous flow.

On the other hand, the electrical conductivity of unsaturated soils can be characterized in terms of the volumetric water content θ . Rhoades et al. (1976) proposed a two-conductance model which is most widely used in soil science. The predominant conductance is through the pore water, and the contribution of soil solids takes place along the continuous films of exchangeable cations that reside on the surface of charged solid particles. Accordingly, the soil electrical conductivity can be regarded as being analogous to two electric conductors in parallel, expressed by

$$\kappa_b = (a\theta^2 + b\theta)\kappa_w + \kappa_s \quad (2.7)$$

where κ_s is the surface electrical conductivity, a and b are empirical constants, and other parameters have been defined before. Hamed et al. (2003) reported that values of a and b lie in the range of -14.0 to 9.7 and -6 to 14.2, respectively.

Shah and Singh (2005) suggested a generalized form of Archie model for unsaturated soils, in which surface conductance effect was neglected, as a function of the volumetric water content θ with two constants α and β :

$$\kappa_b = \alpha \kappa_w \theta^\beta \quad (2.8)$$

They believed that the empirical constants determined by the measured electrical conductivity will implicitly reflect the influence of the soil solid conductance. The values of α and β are in the range of 0.33 to 15.85 and 0.74 to 3.92, respectively.

2.3 Experimental Investigation

2.3.1 Materials and Equipments

A commercially processed kaolin clay was used in this study. The index properties of the kaolin clay are summarized in Table 2.1. The soil was oven dried at 105 °C because no water may be initially present before mixing with electrolytes. The electrolytes of three ionic strengths were employed to create pore water with different electrical conductivities: solutions of sodium chloride (NaCl) at molar concentrations of 0.03, 0.1 and 0.2 mol/L. The NaCl solutions were made by dissolving NaCl in deionized water (electrical conductivity of < 1 S/m). A predetermined weight of the dried clay was mixed with a NaCl solution of known weight to obtain the desired gravimetric water content, and then stored in sealed containers for 24 hours.

A circular two-electrode cell in conjunction with a compaction apparatus is shown in Figure 2.1. The circular two-electrode cell consists of an outer electrode and an inner electrode, made of stainless steel. The cell houses an annular soil sample with 50 mm outer diameter, 21.6 mm inner diameter and 35 mm thickness. The compaction apparatus was designed to achieve uniform

compaction and to eliminate gaps between the soil sample and cell. The apparatus comprises top and bottom plates held together by connecting bolts. The bottom plate has an inset ring on which the base of the outside electrode is located. The inside electrode placed on the bottom plate is secured on a threaded rod to ensure its location on the center of the outside electrode during compaction. The top plate has a circular opening and an inset ring of the same size as the inside diameter of the outer electrode. The plate is used to hold the outside electrode in place during compaction. The compaction is carried out through a standard Proctor hammer through an annular ram that has slightly smaller diameter than the cell. An extension sleeve is added to the center electrode as a guide for the ram. The soil sample is compacted in two layers. For better continuity at the interface between the compacted two layers, the base of ram is fitted with small prominent points that provide additional kneading action when the soil sample is compacted. After compaction, the excess soil is trimmed off using the top edge of the outer electrode as a guide.

An AC source is connected in series to a test specimen and a 50 Ω resistor, generating a radial electrical field through the soil sample compacted in the annular space of the cell, as illustrated in Figure 2.2. The voltage across the soil sample between the inner and outer electrodes is measured using a digital multimeter, and then the current is calculated indirectly by measuring the voltage across the 50 Ω resistor. The electrical conductivity of the soil compacted in the cell can be determined by knowing the dimensions of the cell, applied voltage V and current I (Scholte et al. 2002):

$$\kappa_b = \frac{\left(\ln \frac{r_i}{r_o} \right) I}{2\pi t_s V} \quad (2.9)$$

where r_o and r_i are radii of outer and inner electrode, t_s is the soil sample thickness. In this study, the electrical conductivity measurement on the soil sample was made under the frequency of 60 Hz. It is based on the experimental evidence discussed in Abu-Hassanein et al. (1996), indicating that this frequency is high enough to have negligible effects of electrode polarization.

2.3.2 Experimental Method

The soil cured was compacted directly into the circular two-electrode cell, according to the equipment setup described above. The density of the soil sample was controlled by blow counts of the hammer (i.e., compaction energy). Figure 2.3 displays the uniformly compacted soil samples with gravimetric water contents of 10 and 30%, showing that good contacts were attained between soil and electrodes. Following compaction, the electrical conductivity of the soil sample was measured. The electrical measurement on all samples was performed at the temperature of 19 ± 1 °C. Within this range, the temperature dependency of electrical conductivity is quite small and negligible. After measurement, the weight of soil sample was precisely measured for calculation of the bulk unit weight, and afterwards a small portion of soil was taken from the top and bottom of the cell to confirm the corresponding desired gravimetric water content of the sample. The porosity, degree of saturation and volumetric water content of the soil samples were calculated by using Eqs. (2.1) and (2.2).

The pore water electrical conductivity of the kaolin clays mixed with three NaCl solutions was determined following the standard method described in U.S. Salinity Laboratory Staff (1954). At each NaCl concentration, seven saturated pastes, mixed with clay-to-solution weight ratios of 0.1 to 1.5, were prepared. The pastes were mechanically agitated for one hour and then centrifuged at 5,000 rpm for 15 minutes. Lastly, the electrical conductivities of decanted

solutions were measured using a hand-held electrical conductivity probe. The results of electrical conductivity measurement on a total of 24 solutions tested including pure NaCl solutions are depicted in Figure 2.4. The electrical conductivity of decanted solution increases slightly as the clay-to-solution weight ratio increases. It is attributed to dissolving some of free and absorbed ions in kaolin clay into the solution. The electrical conductivities of the decanted solutions obtained from pastes with the clay-to-solution weight ratio of 1.5 were considered to be the pore water electrical conductivities of three saline kaolin clays: 0.289, 1.084, and 2.050 S/m (see Table 2.2). These values are within the possible salinity range of in-situ soils (Rhoades et al. 1976; Shah and Singh 2005).

2.4 Results and Discussion

A summary of experimental results for all soil samples tested is presented in Table 2.2. The data interpretation was focused on the relationships of the bulk soil electrical conductivity with the soil porosity, dry unit weight, pore water salinity, and amount of water (gravimetric water content, degree of saturation and volumetric water content). The relations are of fundamental importance to site characterization and other engineering applications (Arulanandan and Muraleetharan 1988; Kaya and Fang 1997).

2.4.1 Effect of Soil Porosity: Saturated Samples

The relationship between the soil porosity and formation factor for saturated soil samples (Nos. 13-15, 28-31, 45-47, see Table 2.2) is shown in Figure 2.5. It should be noted that soil samples with the degree of saturation above 0.99 are considered to be fully saturated owing to the limitation of the test methodology used. The soil porosity lies within the range of about 0.53 to 0.60, which is consistent with results reported by Kezdi (1974), i.e., soil porosity typically

varies from 0.45 to 0.70 for silty clays. The formation factor decreases as the soil porosity increases, indicating that at a given pore water salinity, the bulk soil electrical conductivity of saturated kaolin clay increases with increasing the porosity. This is due to the fact that conduction in saturated soil is dominated by pore water content. On the other hand, Figure 2.5 shows the somewhat scatter of experimental data about a best fit curve but which is systematic. It may be attributed to the effect of surface conductance depending on soil salinity, leading to difference in the formation factor. According to Archie model, i.e., Eq. (2.3), the cementation exponent calculated from the regression analysis is determined to be 2.14 with $R^2 = 0.53$. Based on Winsauer model, i.e., Eq. (2.4), the cementation exponent and tortuosity factor are analyzed to be 1.86 and 0.85 with $R^2 = 0.54$. These values are comparable to those reported in literature (see Table 2.3).

For more than 60 years, the relation between the formation factor and soil porosity has been extensively studied for natural geomaterials (i.e., soils and rocks) obtained from offshore and onshore areas as well as artificial materials such as ploydisperse glass spheres and fused glass beads. Of these materials, the electrical responses of soils were reviewed, and the summary of the empirical constants in Eqs. (2.3) and (2.4) for various soils is given in Table 2.3, together with the number of data available for each of them. The values of the constants were obtained directly from the literature or calculated from the reported data of formation factor as a function of soil porosity. It is revealed that practically the cementation exponent in Archie model falls within the limits of 1.27 and 2.29 for soils, although Wyllie and Gregory (1953) pointed out that it can theoretically range from one to infinity. For Winsauer model, the cementation exponent and tortuosity factor are in the ranges of 0.45 to 1.52 and 0.86 to 2.49, respectively.

This study includes the quantification of the empirical constants in both Archie and Winsauer models based on a number of measurements on the formation factor with respect to soil porosity. Figure 2.6 illustrates the general relationships between the formation factor and soil porosity for reported data considered in Table 2.3. Over a wide range of soil porosities (0.2 – 0.9), the formation factor decreases from 16.0 to 1.5 with increasing the porosity. The experimental data of this study are comparatively in good agreement with reported data. In Figure 2.6, the dotted line represents Archie model ($m = 1.65$ with $R^2 = 0.65$), and the solid line corresponds to Winsauer model ($c = 0.71$ and $m = 1.27$ with $R^2 = 0.73$). The two general relations can enhance the understanding of electrical conduction characteristics of soils over a wide porosity range as well as predicting the soil porosity with known formation factor.

From the experimental results of kaolin clay, the tortuosity is determined according to Eq. (2.5). Figure 2.7 shows that the tortuosity decreases with increasing soil porosity at a given soil salinity. Similar observation is investigated in the literature (Salem and Chilingarian 2000). The result provides evidence to support the hypothesis that in case of lower porosity, both the hydraulic flow and electric current can be forced to take a longer and more tortuous path that leads to increasing resistance and higher tortuosity.

2.4.2 Effect of Gravimetric Water Content

The relationships between the bulk soil electrical conductivity, dry unit weight and gravimetric water content at three soil pore water salinities are depicted in Figure 2.8. In each case, a distinct relation between the bulk soil electrical conductivity and dry unit weight of soil is noted. The figure indicates that the bulk soil electrical conductivity is sensitive to the gravimetric water content and dry unit weight. The bulk soil electrical conductivity increases as the

gravimetric water content increases, as would be expected. Moreover, increasing the gravimetric water content causes the steeper slope of the bulk soil electrical conductivity versus dry unit weight curve, associated with that particular gravimetric water content. This means that the effect of soil unit weight on the bulk soil electrical conductivity becomes more important at the higher gravimetric water content. On the other hand, it is observed under the same gravimetric water content that the bulk soil electrical conductivity increases with increasing the dry unit weight. This is attributed to the fact that, with the increase in the dry unit weight, the volumetric water content increases as well, which results in a higher bulk soil electrical conductivity. From these results, it can be inferred that the soil gravimetric water content is not the sole influencing factor to the bulk soil electrical conductivity even if the pore water salinity is kept constant. This is parallel to the fact that conduction of current in soil is controlled by the volumetric fraction of constituents (especially, the volumetric water content) in a soil. However, the observation on soil electrical behavior with respect to the dry unit weight of soil at constant gravimetric water content is still significant because this is the case for a compacted earth fill where water is uniformly distributed in the soil but not compaction energy.

2.4.3 Effect of Degree of Saturation

The variation of the bulk soil electrical conductivity against the degree of saturation under various pore water salinities is presented in Figure 2.9. It is seen that as the degree of saturation decreases, the bulk soil electrical conductivity decreases. This is due to the fact that the continuous film of soil pore water over soil solid surfaces becomes thinner and the conducting channels become considerably tortuous. On the other hand, the bulk soil electrical conductivity increases when the pore water salinity increases. This behavior is generally observed in particulate-type materials in which water (for instance) phase is distributed within a matrix

(Rinaldi and Cuestas 2002). Figure 2.9 displays that for a given soil salinity, a unique relationship between the bulk soil electrical conductivity and degree of saturation exists, which is independent of the soil unit weight. However, at 100% saturation, considerable scattering of data is observed, especially at higher pore water salinity. It is attributed that the volumetric water content at 100% saturated soil can be varied with different porosities (see Eq. (2.1)) that produces different bulk soil electrical conductivities. Furthermore, the surface conductance that depends on soil salinity and water content may affect the bulk soil electrical conductivity.

Eq. (2.6) in combination with Eqs. (2.3) and (2.4), which relates the electrical conductivity and degree of saturation, is fit to the experimental data. The results of the regression analysis are summarized in Table 2.4. The correlation coefficient R^2 is greater than 0.95 for the data. The saturation exponents are consistent with those reported in literature (Schwartz and Kimminau 1987), i.e., in the range between 1.0 and 2.5. The relationship between the normalized electrical conductivity κ_b / κ_w and degree of saturation is illustrated in Figure 2.10 with a fitting curve as a function of only the degree of saturation.

2.4.4 Effect of Volumetric Water Content

The influences of the soil volumetric water content and pore water salinity on the bulk soil electrical conductivity are examined. As plotted in Figure 2.11, the experimental results indicate that the bulk soil electrical conductivity increases with increasing the volumetric water content. On the other hand, it is observed that the electrical behaviors are sensitive to the pore water salinity.

The surface electrical conductivity can be theoretically determined by extrapolating the fitting line between the bulk soil electrical conductivity and volumetric water content. However,

better determination of surface electrical conductivity can be obtained by arbitrarily selecting the values (20, 30, 40 and 50%) of volumetric water content and estimating bulk soil electrical conductivities corresponding with different pore water salinities at the same volumetric water content (Kalinski and Kelly 1993). This is illustrated in Figure 2.12, in which the surface electrical conductivities are estimated as the intercepts of linear regression lines. The results reveal that the surface electrical conductivity ranges from 0.007 S/m to 0.027 S/m, which are comparable to that of clayey soils in work of Shang et al. (1993) and Hamed et al. (2003). It means that the surface electrical conductivity is not constant but depends on the amount of water in soils.

The best relationship between the normalized electrical conductivity $(\kappa_b - \kappa_s) / \kappa_w$ and soil volumetric water content is obtained by Eq. (2.7) using the surface electrical conductivity of $\kappa_s = 0.011$ S/m, and is illustrated in Figure 2.13. The relation ($R^2 = 0.99$) can be expressed as

$$\kappa_b = (1.19\theta^2 - 0.18\theta) \kappa_w + 0.011 \quad (2.10)$$

It is shown in the figure that Eq. (2.10) gives good estimates of electrical behavior for kaolin clay investigated despite using a fixed value of κ_s . Kalinski and Kelly (1993) and Hamed et al. (2003) have also noted that the Rhoades model provides accurate approximations of soil electrical conductivity for a wide range of soils.

In order to estimate the parameters in Eq. (2.8), which is the generalized Archie model as a function of the volumetric water content, the relationship between the normalized electrical conductivity κ_b / κ_w and volumetric water content is established and is plotted in Figure 2.14. The regression equation has the form of ($R^2 = 0.95$)

$$\kappa_b / \kappa_w = 0.79 \theta^{1.91} \quad (2.11)$$

In this figure, the model proposed by Shah and Singh (2005) shows its limitations for kaolin clay tested due to neglecting the surface conductance effect, although they assumed that this effect will be appropriately included in the model using two empirical constants.

2.5 Conclusions

The electrical conductivity of kaolin clay was measured using a circular two-electrode cell in conjunction with a specially designed compaction apparatus. The influences of porosity, dry unit weight, amount of water in a soil (gravimetric water content, degree of saturation and volumetric water content) and pore water salinity on the soil electrical conductivity were investigated. The following conclusions can be drawn from this study:

1. The formation factors of saturated kaolin clay follow both the Archie model and Winsauer models.
2. Based on the experimental data reported and measured for saturated soils, the two general relationships according to both the Archie and Winsauer models are established, which are useful for understanding electrical conduction characteristics of soils over a wide porosity range. With known formation factor, the soil porosity can be estimated, which forms a background against actual soil porosity.
3. The tortuosity calculated from the measured formation factor decreases with increasing the soil porosity. Estimate of the tortuosity, reflecting the complexities of soil fabric, enables one to comprehend the mechanisms of hydraulic flow and electrical current.
4. In unsaturated kaolin clay, the prediction models for the soil electrical conductivity are evaluated with calculated the empirical constants in these models (Table 2.4, and Eqs.

(2.10) and (2.11)). Among the models analyzed, the Rhoades model is shown to be the best fit for the kaolin clay investigated comparing to other models.

References

- Abu-Hassanein, Z.S., Benson, C.H., and Blotz, L.R. (1996). "Electrical resistivity of compacted clays." *Journal of Geotechnical Engineering*, 122(5), 397-406.
- Archie, G.E. (1942). "The electrical resistivity log as an aid in determining some reservoir characteristics." *Transactions of the American Institute of Mining, Metallurgical and Petroleum Engineers*, 146, 54-62.
- Arulanandan, K., and Muraleetharan, K.K. (1988). "Level ground soil-liquefaction analysis using in situ properties: ." *Journal of Geotechnical Engineering*, 114(7), 753-770.
- ASTM. (2006). "Standard test method for field measurement of soil resistivity using the Wenner four-electrode method." *G 57-06*, West Conshohocken, Pa.
- ASTM. (2007). "Standard test method for laboratory compaction characteristics of soil using standard effort." *D 689-07*, West Conshohocken, Pa.
- Auerswald, K., Simon, S., and Stanjek, H. (2001). "Influence of soil properties on electrical conductivity under humid water regimes." *Soil Science*, 166(6), 382-392.
- Bennett, R.H., Li, H., Lambert, D.N., Fischer, K.M., and Walter, D.J. (1990). "In situ porosity and permeability of selected carbonate sediment: Great Bahama Bank Part 1: measurement." *Marine Georesources and Geotechnology*, 9(1), 1-28.
- Biella, G., Lozej, A., and Tabaco, L. (1983). "Experimental study of some hydrogeophysical properties of unconsolidated porous media." *Ground Water*, 21(6), 741-751.
- Boyce, R.E. (1968). "Electrical resistivity of modern marine sediments from the Bering Sea." *Journal of Geophysical Research*, 73(14), 4759-4766.
- Bryson, L.S., and Bathe, A. (2009). "Determination of selected geotechnical properties of soil using electrical conductivity testing." *Geotechnical Testing Journal*, 32(3), 252-261.

- Erchul, R.A., and Gluarte, R.C. (1982). "Electrical resistivity used to measure liquefaction of sand." *Journal of Geotechnical Engineering*, 108(GT5), 778-782.
- Friedman, S.P., and Robinson, D.A. (2002). "Particle shape characterization using angle of repose measurements for predicting the effective permittivity and electrical conductivity of saturated granular media." *Water Resources Research*, 38(11), 1236-1235.
- Gorman, T., and Kelly, W.E. (1990). "Electrical-hydraulic properties of unsaturated Ottawa sands." *Journal of Hydrology*, 118(1-4), 1-18.
- Hamed, Y., Persson, M., and Berndtsson, R. (2003). "Soil solution electrical conductivity measurements using different dielectric techniques." *Soil Science Society of America Journal*, 67, 1071-1078.
- Hulbert, M.H., Bennett, R.H., and Lambert, D.N. (1982). "Seabed geotechnical parameters from electrical conductivity measurements." *Geo-Marine Letters*, 2(3-4), 219-222.
- Jackson, P.D. (1975). "An electrical resistivity method for evaluating the in-situ porosity of clean marine sands." *Marine Geotechnology*, 1(2), 91-115.
- Jackson, P.D., Smith, D.T., and Stanford, P.N. (1978). "Resistivity-porosity-particle shape relationships for marine sands." *Geophysics*, 43(6), 1250-1268.
- Jones, P.H., and Buford, T.B. (1951). "Electric logging applied to ground-water exploration." *Geophysics*, 16(1), 115-139.
- Kachanoski, R.G., Rringle, E., and Ward, A. (1992). "Field measurement of solute travel times using time domain reflectometry." *Soil Science Society of America Journal*, 56, 47-52.
- Kalinski, R.J., and Kelly, W.E. (1993). "Estimating water content of soils from electrical resistivity." *Geotechnical Testing Journal*, 16(3), 323-329.
- Kalinski, R.J., and Kelly, W.E. (1994). "Electrical-resistivity measurements for evaluating compacted-soil liners." *Journal of Geotechnical Engineering*, 120(2), 451-457.
- Kaya, A., and Fang, H. (1997). "Identification of contaminated soils by dielectric constant and electrical conductivity." *Journal of Geotechnical Engineering*, 123(2), 169-177.

- Keller, G.V., and Frischknecht, F.L. (1966). *Electrical methods in geophysical prospecting*, Pergamon Press, New York.
- Kezdi, A. (1974). *Handbook of soil mechanics*, Vol. 1, Elsevier, Amsterdam.
- Kim, D.C., and Manghnani, M.H. (1992). "Influence of diagenesis on the electrical resistivity and the formation factor of deep-sea carbonate sediments." *Geo-Marine Letters*, 12(1), 14-18.
- Lavoie, D., Mozely, E., Corwin, R., Lamber, D., and Valent, P. (1988). "The use of a towed, direct-current, electrical resistivity array for the classification of marine sediments." *Oceans 88 Conference*, Baltimore, 397-404.
- Lovell, M.A. (1985). "Thermal conductivity and permeability assessment by electrical resistivity measurement in marine sediments." *Marine Geotechnology*, 6(2), 205-240.
- McCarter, W.J. (1984). "The electrical resistivity characteristics of compacted clays." *Geotechnique*, 34(2), 263-267.
- McCarter, W.J., and Desmazes, P. (1997). "Soil characterization using electrical measurements." *Geotechnique*, 47(1), 179-183.
- Mohamedelhassan, E., and Shang, J.Q. (2003). "Electrokinetics-generated pore fluid and ionic transport in an offshore calcareous soil." *Canadian Geotechnical Journal*, 40(6), 1185-1199.
- Nadler, A., and Frenkel, H. (1980). "Determination of soil solution electrical conductivity from bulk soil electrical conductivity measurements by the four-electrode method." *Soil Science Society of America Journal*, 44, 1216-1221.
- Nichol, C., Beckie, R., and Smith, L. (2002). "Evaluation of uncoated and coated time domain reflectometry probes for high electrical conductivity system." *Soil Science Society of America Journal*, 66, 1454-1465.
- Rhoades, J.D., Manteghi, N.A., Shouse, P.J., and Alves, W.J. (1989). "Soil electrical conductivity and soil salinity: new formulations and calibrations." *Soil Science Society of America Journal*, 53, 433-439.

- Rhoades, J.D., Raats, R.A.C., and Prather, R.J. (1976). "Effects of liquid-phase electrical conductivity, water content, and surface conductivity on bulk soil electrical conductivity." *Soil Science Society of America Journal*, 40, 651-655.
- Rinaldi, V.A., and Cuestas, G.A. (2002). "Ohmic conductivity of a compacted silty clay." *Journal of Geotechnical and Geoenvironmental Engineering*, 128(10), 824-835.
- Rittirong, A., Douglas, R.S., Shang, J.Q., and Lee, E.C. (2008). "Electrokinetic improvement of soft clay using electrical vertical drains." *Geosynthetics International*, 15(5), 369-381.
- Salem, H.S. (2001). "Determination of porosity, formation resistivity factor, Archie cementation factor, and pore geometry factor for a glacial aquifer." *Energy Sources Part A*, 23(6), 589-596.
- Salem, H.S., and Chilingarian, G.V. (2000). "Influence of porosity and direction of flow on tortuosity in unconsolidated porous media." *Energy Sources Part A*, 22(3), 207-213.
- Scholte, J.W., Shang, J.Q., and Rowe, R.K. (2002). "Improved complex permittivity measurement and data processing technique for soil-water systems." *Geotechnical Testing Journal*, 25(2), 187-198.
- Schwartz, L.M., and Kimminau, S. (1987). "Analysis of electrical conduction in the grain consolidation model." *Geophysics*, 52(10), 1402-1411.
- Shah, P.H., and Singh, D.N. (2005). "Generalized Archie's law for estimation of soil electrical conductivity." *Journal of ASTM International*, 2(5), 1-20.
- Shang, J.Q., Lo, K.Y., and Incullet, I.I. (1993). "Polarization and conduction of clay-water-electrolyte systems." *Journal of Geotechnical Engineering*, 121(3), 243-248.
- Shang, J.Q., Tang, Q.H., and Xu, Y.Q. (2009). "Consolidation of marine clay using electrical vertical drains." *Geomechanics and Engineering*, 1(4), 275-289.
- U.S. Salinity Laboratory Staff (1954). *Diagnosis and improvement of saline and alkali soils*, USDA Handbook 60, U.S. Government Print Office, Washington, D.C.

- Vanclooster, M., Mallants, D., Vanderborght, J., Diels, J., Feyen, J., and van Orshoven, J. (1995). "Monitoring solute transport in a multi-layered sandy lysimeter using time domain reflectometry." *Soil Science Society of America Journal*, 59, 337-344.
- Walsh, J.B., and Brace, W.F. (1984). "The effect pressure on porosity and the transport properties of rock." *Journal of Geophysical Research*, 89(B11), 9425-9431.
- Wheatcroft, R.A. (2002). "In situ measurements of near-surface porosity in shallow-water marine sands." *IEEE Journal of Oceanic Engineering*, 27(3), 561-570.
- Winsauer, W.O., Shearin, H.M., Masson, P.H., and Williams, M. (1952). "Resistivity of brine-saturated sands in relation to pore geometry." *American Association of Petroleum Geologists Bulletin*, 36(2), 253-277.
- Wyllie, M.R.J., and Gregory, A.R. (1953). "Formation factors of unconsolidated porous media: Influence of particle shape and effect of cementation." *Transactions of the American Institute of Mining, Metallurgical and Petroleum Engineering*, 198, 103-110.

Table 2.1 Index properties of kaolin clay tested

Parameters	Kaolin clay
Soil classification (USCS)	CH
Specific gravity (-)	2.61
Liquid limit (%)	73
Plastic limit (%)	39
Plasticity index (%)	34
% Finer sieve # 200	97.6
Clay (< 0.002 mm) (%)	15.9
Maximum dry unit weight (kN/m ³)	14.1
Optimum gravimetric water content (%)	28.7
Void ratio at optimum gravimetric water content (-)	0.80
Cation exchange capacity (CEC) (meq/100g)	5.82

Table 2.2 Summary of soil sample properties

Sample	w (%)	γ_d (kN/m ³)	n (-)	S (%)	θ (-)	κ_w (S/m)	κ_b (mS/m)
1	9.2	10.3	0.597	16.2	0.097	0.289	5.1
2	9.4	11.3	0.557	19.5	0.109	0.289	7.0
3	9.3	12.9	0.496	24.7	0.122	0.289	8.2
4	20.2	10.3	0.598	35.4	0.212	0.289	13.9
5	20.1	11.1	0.567	40.1	0.227	0.289	15.0
6	20.4	11.9	0.536	46.1	0.247	0.289	18.6
7	30.3	9.9	0.612	50.1	0.307	0.289	23.9
8	30.3	10.7	0.581	57.1	0.332	0.289	30.1
9	30.4	11.6	0.549	65.3	0.358	0.289	36.4
10	37.6	12.5	0.513	93.1	0.478	0.289	66.9
11	37.7	12.7	0.504	97.0	0.488	0.289	70.3
12	37.8	12.8	0.501	98.2	0.492	0.289	72.4
13	45.9	11.6	0.547	99.2	0.543	0.289	84.2
14	50.8	11.0	0.571	99.7	0.569	0.289	92.5
15	55.9	10.4	0.594	99.7	0.593	0.289	101.6
16	7.6	11.0	0.570	15.0	0.085	1.084	7.2
17	7.8	11.5	0.550	16.7	0.092	1.084	11.0
18	7.6	12.8	0.499	19.9	0.099	1.084	13.8
19	18.8	10.4	0.596	33.3	0.198	1.084	27.0
20	18.9	11.3	0.558	39.0	0.218	1.084	37.4
21	18.7	12.7	0.504	48.0	0.242	1.084	47.2
22	27.2	10.6	0.585	50.4	0.295	1.084	61.5
23	27.2	11.6	0.547	58.7	0.321	1.084	79.9
24	27.4	12.2	0.523	65.2	0.341	1.084	97.8
25	39.8	12.3	0.520	95.8	0.498	1.084	239.8
26	39.7	12.4	0.516	97.3	0.502	1.084	249.7
27	39.9	12.4	0.515	98.3	0.506	1.084	260.5
28	42.9	12.1	0.528	100.1	0.529	1.084	283.4
29	44.7	11.8	0.541	99.2	0.537	1.084	288.2
30	48.0	11.4	0.556	99.9	0.556	1.084	313.3
31	49.9	11.1	0.568	99.2	0.563	1.084	336.4
32	9.4	10.1	0.606	15.9	0.097	2.050	11.0
33	9.4	10.8	0.577	18.0	0.104	2.050	15.6
34	9.3	12.8	0.502	24.1	0.121	2.050	23.5
35	18.7	11.0	0.569	36.9	0.210	2.050	50.0
36	18.5	11.8	0.540	41.1	0.222	2.050	62.1
37	18.6	12.1	0.526	43.8	0.230	2.050	68.4
38	18.5	12.9	0.496	49.1	0.243	2.050	82.9
39	30.3	11.5	0.552	64.2	0.354	2.050	167.7
40	30.2	12.3	0.520	72.7	0.378	2.050	201.5
41	30.4	12.7	0.502	78.6	0.395	2.050	236.2
42	39.6	12.1	0.527	92.7	0.489	2.050	366.1
43	39.5	12.3	0.518	95.7	0.496	2.050	383.8
44	39.5	12.5	0.513	97.9	0.502	2.050	400.5
45	45.4	11.7	0.544	99.4	0.541	2.050	511.5
46	49.0	11.2	0.563	99.2	0.559	2.050	561.8
47	57.2	10.2	0.600	99.6	0.598	2.050	596.9

Table 2.3 Cementation exponent (m) and tortuosity factor (c) for various soils

Site	Medium	No. of Samples	Porosity n	Archie model	Winsauer model		References
				m	m	c	
Onshore	Aquifer sands	62	0.25 - 0.50	1.48	0.78	1.24	Jones and Buford (1951)
Offshore	Sandy soils	42	0.58 - 0.87	2.29	0.77	1.45	Boyce (1968)
Offshore	Marine sands	42	0.38 - 0.48	1.54	0.82	1.31	Jackson (1975)
Offshore	Marine sands	35	0.33 - 0.50	1.45	0.61	0.91	Jackson et al. (1978)
Offshore	Sandy soils	19	0.49 - 0.72	1.98	0.94	1.86	Hulbert et al. (1982)
Onshore	Sands	44	0.23 - 0.45	1.54	0.87	1.42	Biella et al. (1983)
Offshore	Marine clays	26	0.52 - 0.71	1.94	0.78	1.42	Lovell (1985)
Offshore	Marine sediment	13	0.27 - 0.77	1.76	0.77	1.45	Lavoie et al. (1988)
Onshore	Ottawa sands	8	0.36 - 0.42	1.63	0.52	0.91	Gorman and Kelly (1990)
Offshore	Carbonated sands	29	0.30 - 0.61	1.47	0.62	0.86	Bennett et al. (1990)
Offshore	Weathered chalk	41	0.26 - 0.55	2.00	0.45	1.07	Kim and Manghnani (1992)
Offshore	Calcareous ooze	35	0.52 - 0.72	2.14	0.96	2.07	Kim and Manghnani (1992)
Onshore	Glacial aquifer	19	0.25 - 0.51	2.07	0.80	1.87	Salem (2001)
Offshore	Carbonate sands	6	0.37 - 0.50	1.27	0.71	0.88	Wheatcroft (2002)
Onshore	Loess	8	0.33 - 0.49	2.04	1.52	2.49	Rinaldi and Cuestas (2002)
Onshore	Tuff grains	4	0.60 - 0.64	1.66	0.82	1.23	Friedman and Robinson (2002)
Onshore	Quartz sands	7	0.40 - 0.44	1.45	0.74	1.11	Friedman and Robinson (2002)
Onshore	Kaolin clay	7	0.53 - 0.60	2.14	0.85	1.86	This study

Table 2.4 Calculated values of the empirical constants using Eq. (2.6)

Expression	No. of samples	c	m	p	R^2
$\kappa_b / \kappa_w = n^m S^p$ from Archie model	47	-	2.27	1.93	0.99
$\kappa_b / \kappa_w = cn^m S^p$ from Winsauer model	47	0.62	1.52	1.90	0.95



(a) Disassembled compaction cell and standard Proctor hammer



(b) Assembled compaction cell

Figure 2.1 Circular two-electrode cell and compaction apparatus

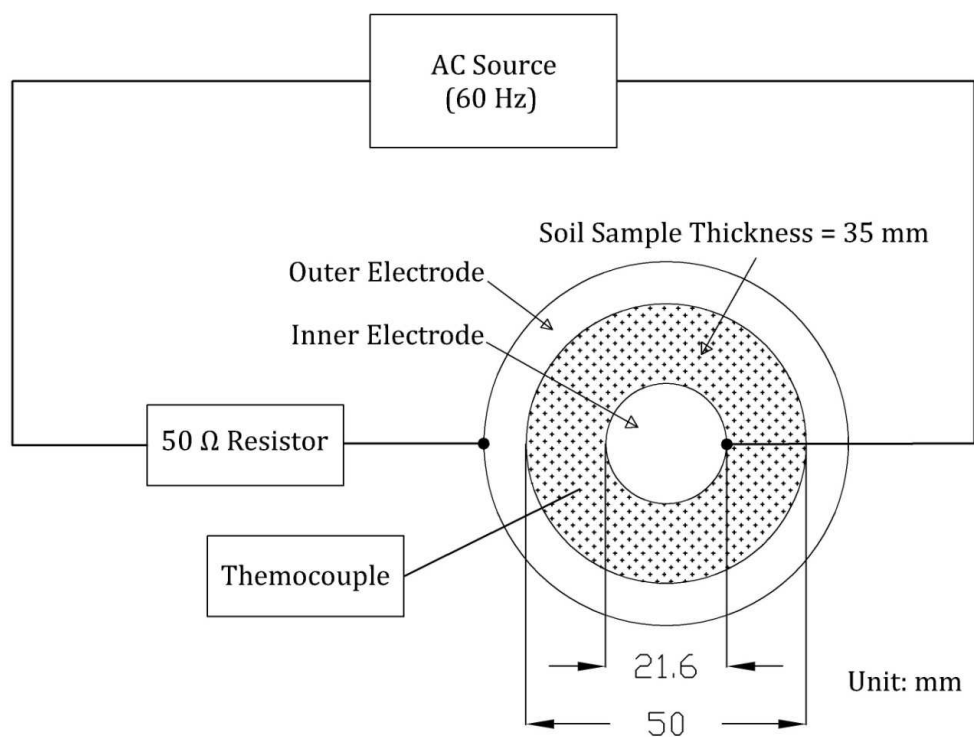
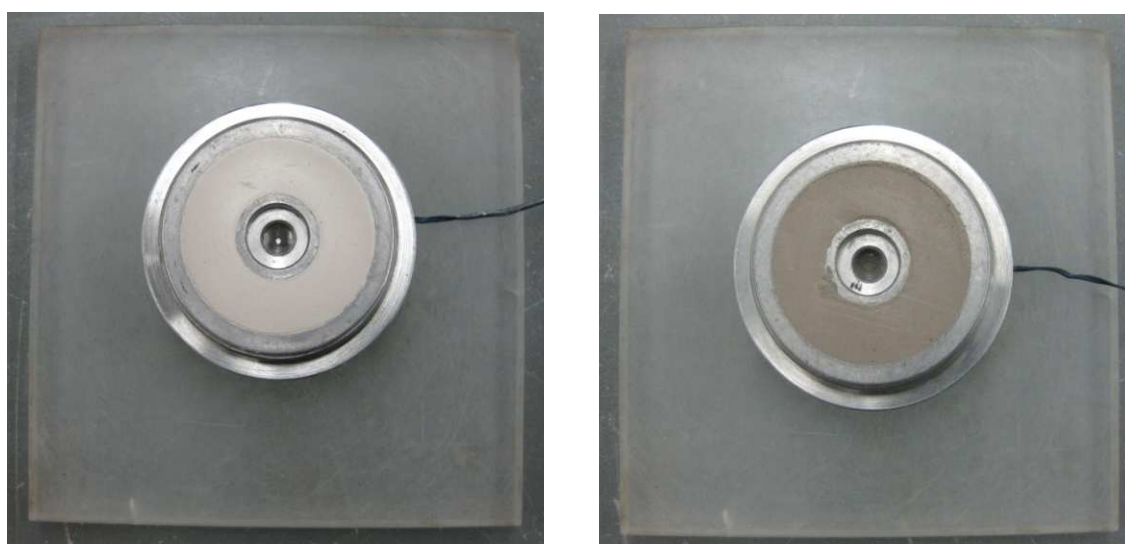


Figure 2.2 Schematic of the electrical conductivity measurement system



(a) 10% gravimetric water content

(b) 30% gravimetric water content

Figure 2.3 Compacted annular soil samples in the cell

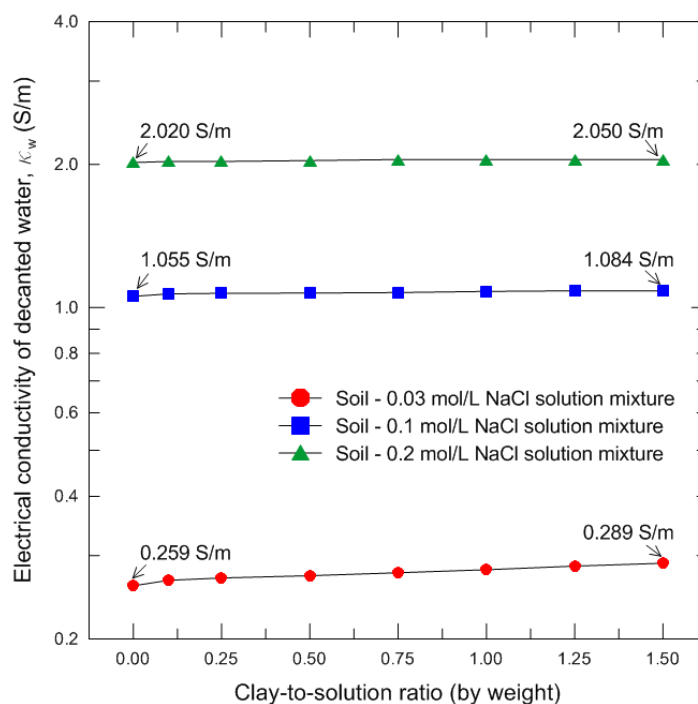


Figure 2.4 Variation of electrical conductivity against clay-to-solution ratio for decanted solutions

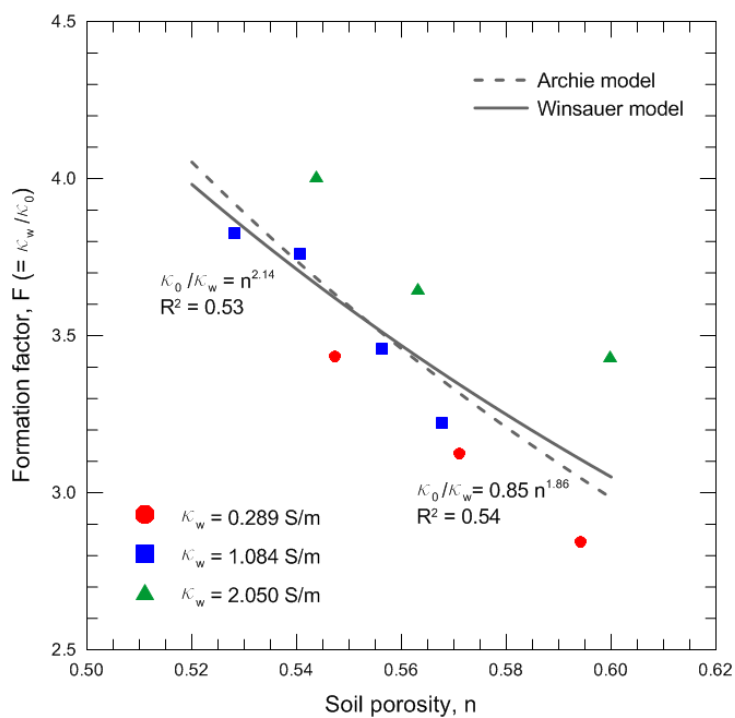


Figure 2.5 Formation factor of saturated samples with different salinities against soil porosity

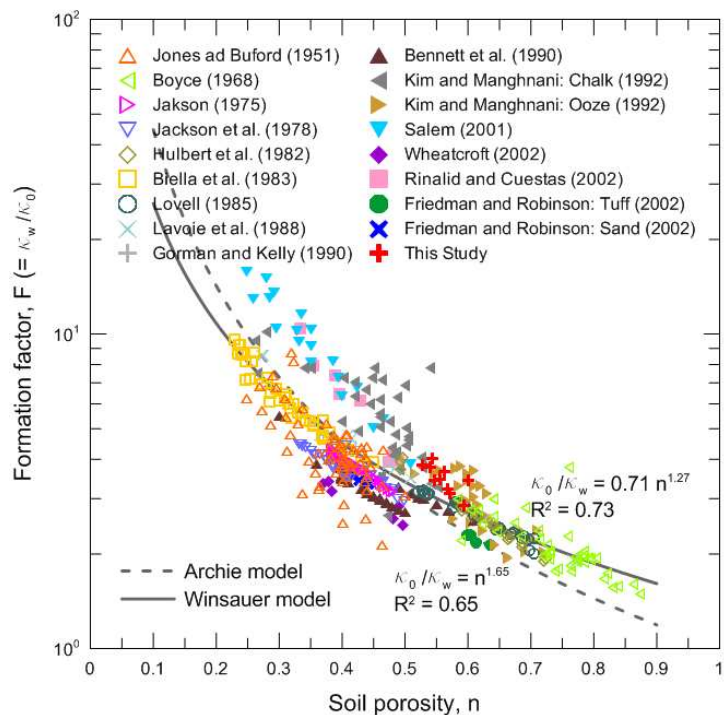


Figure 2.6 General relationships between formation factor and soil porosity for measured and reported data

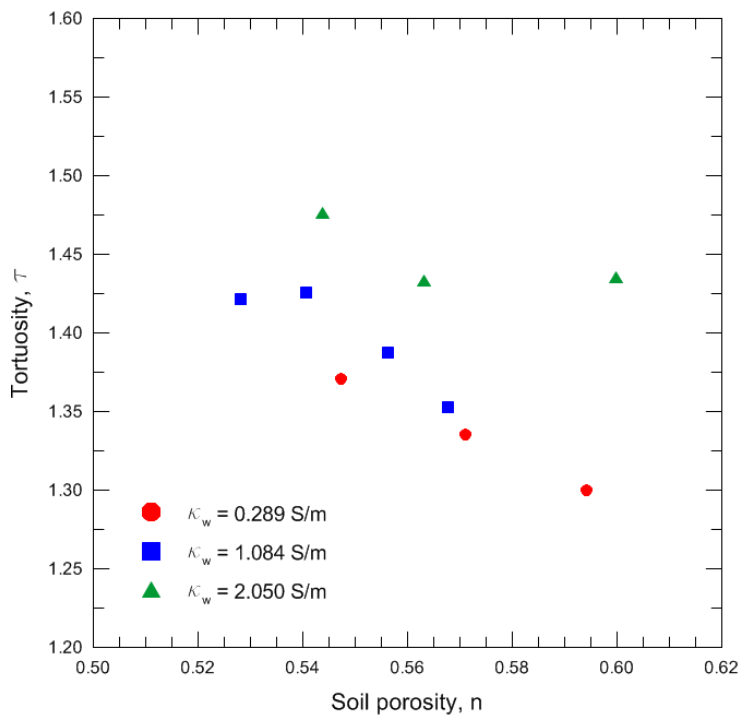
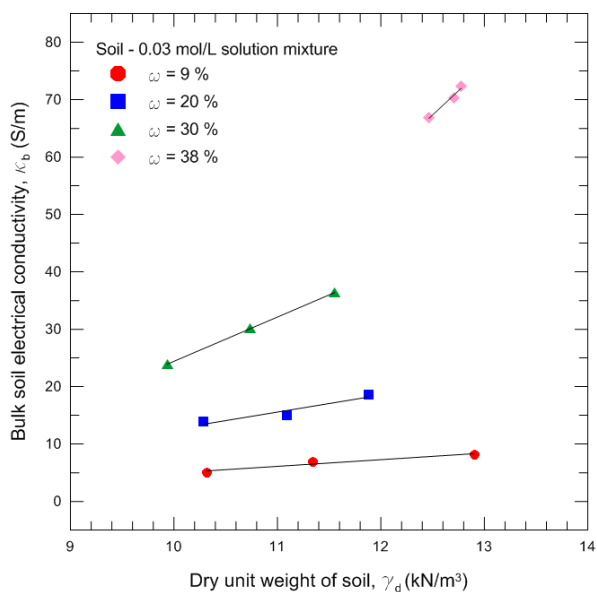
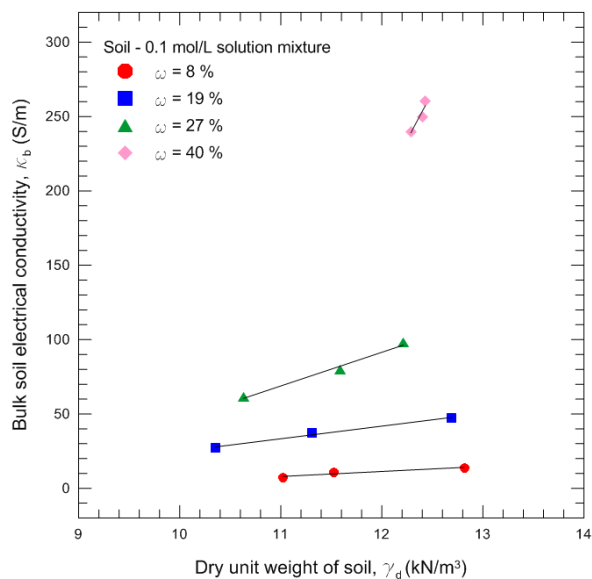


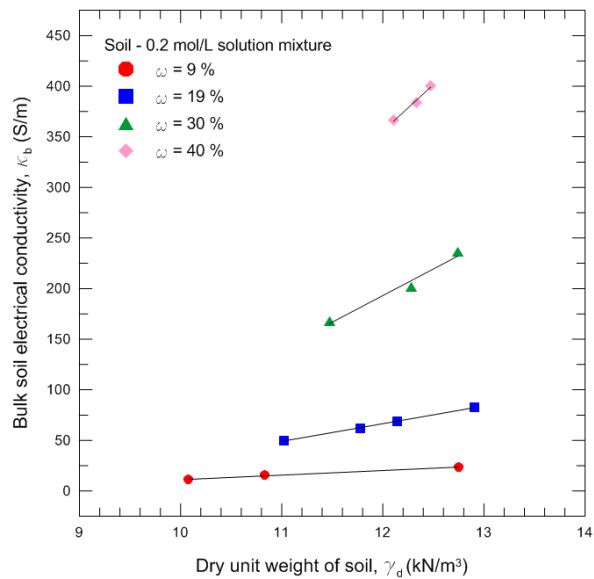
Figure 2.7 Tortuosity of saturated samples with different salinities against soil porosity



(a)



(b)



(c)

Figure 2.8 Influence of gravimetric water content and dry unit weight on bulk soil electrical conductivity

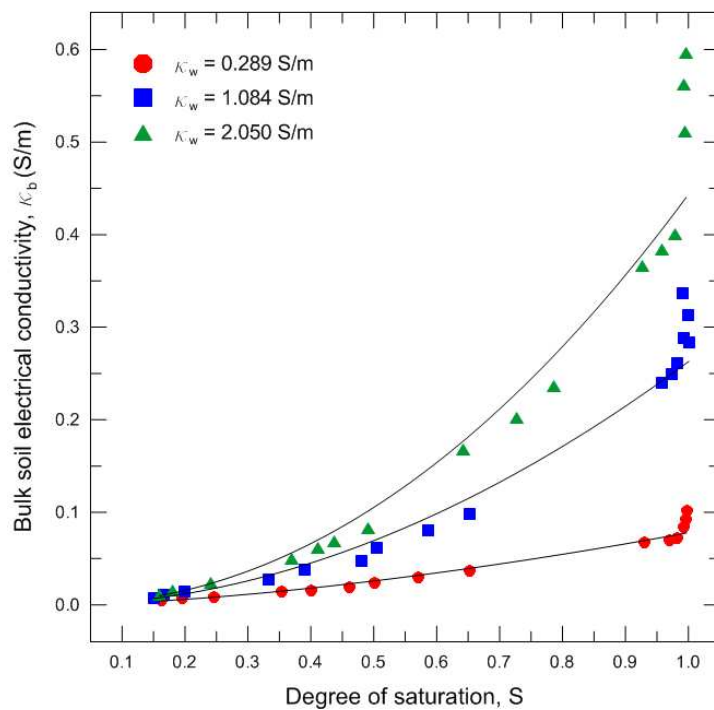


Figure 2.9 Influence of degree of saturation and salinity on bulk soil electrical conductivity

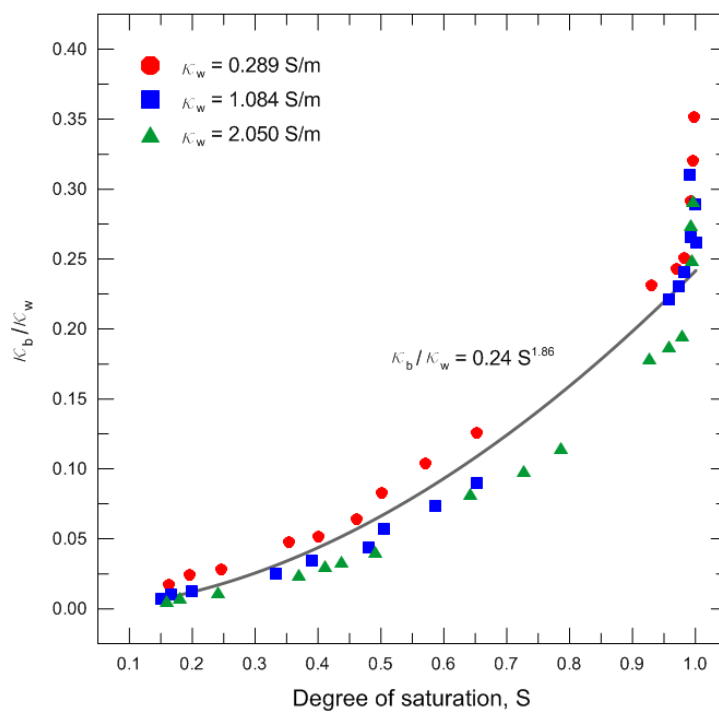


Figure 2.10 Relationship between κ_b / κ_w and degree of saturation

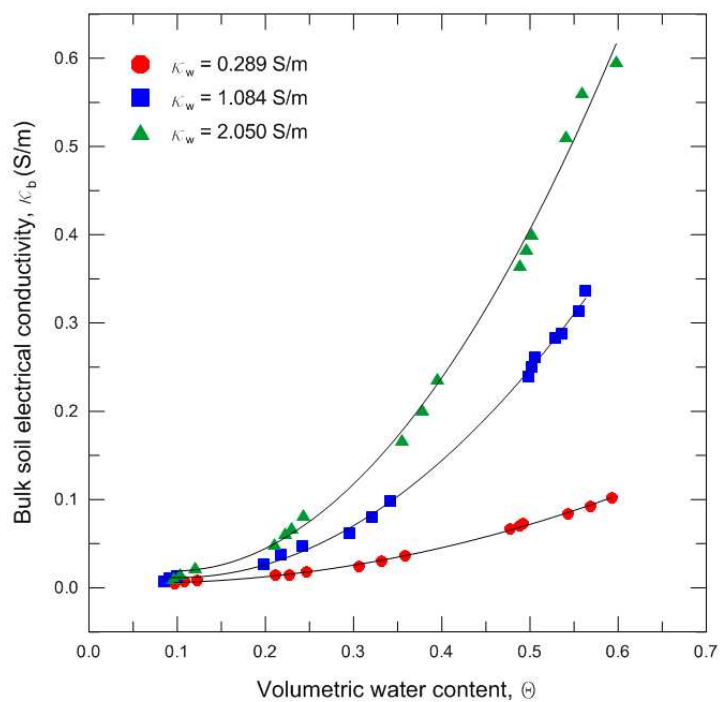


Figure 2.11 Influence of volumetric water content and salinity on bulk soil electrical conductivity

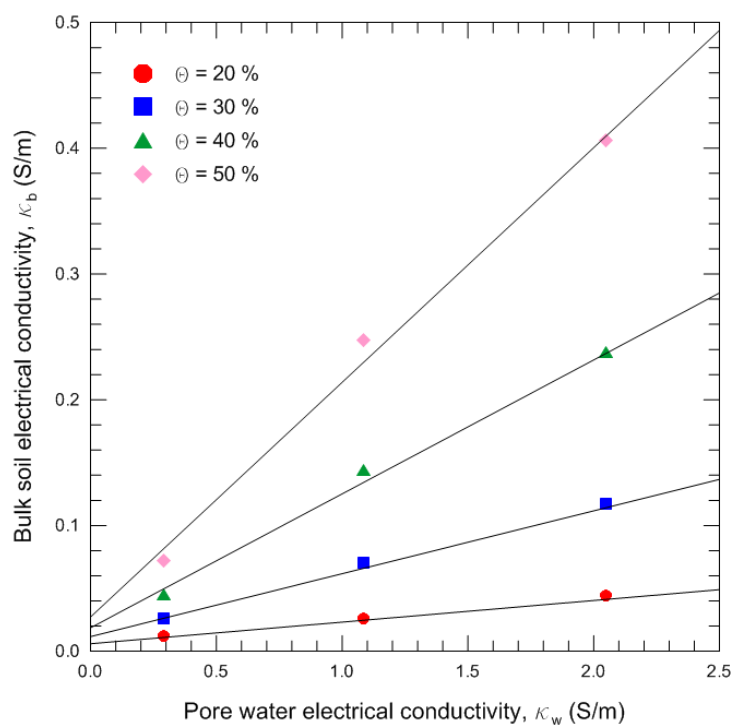


Figure 2.12 Variation of bulk soil electrical conductivity against salinity for different volumetric water contents

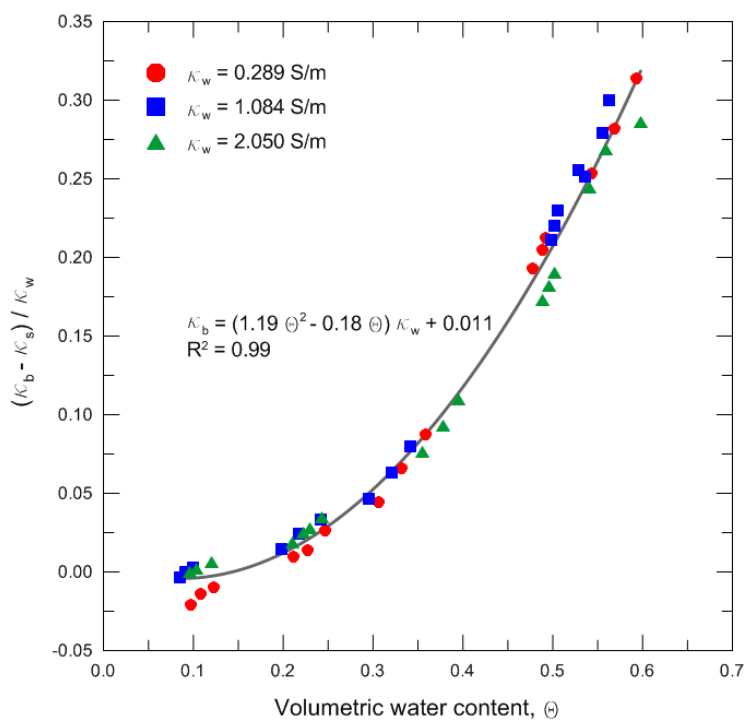


Figure 2.13 Relationship between $(\kappa_b - \kappa_s) / \kappa_w$ and volumetric water content

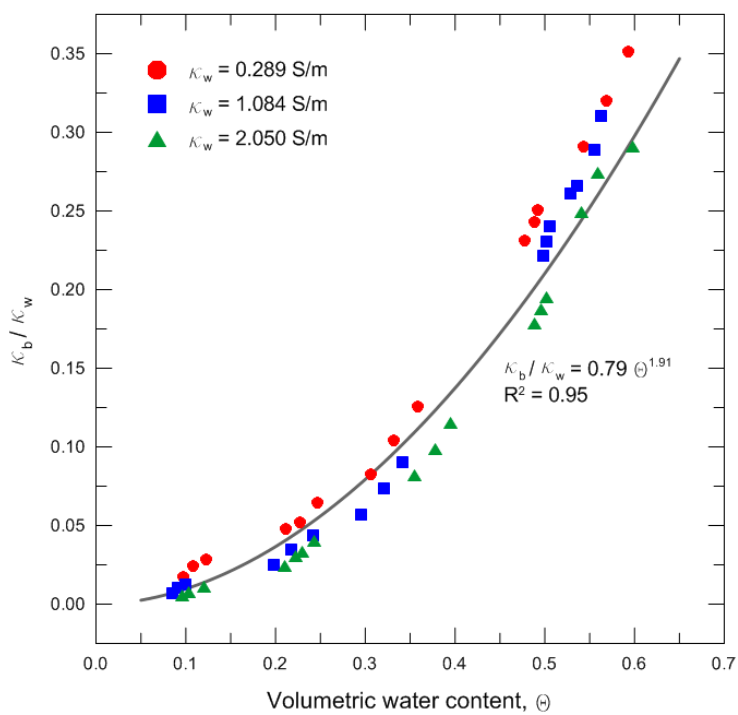


Figure 2.14 Relationship between κ_b / κ_w and volumetric water content

CHAPTER 3

THERMAL PROPERTIES OF DRY MIXTURES OF MINE TAILINGS AND TIRE CRUMBS

3.1 Introduction

In geotechnical engineering practice, geomaterials, including natural soil, crushed rock and tailings from mining activities, and cement concrete, are commonly used as fills of earthworks. On the other hand, waste and by-product materials such as scrap tire, coal fly/bottom ash, sewage sludge ash, rice husk ash, etc, are often applied to enhance the physical and chemical properties of the fill materials. These materials are often required to have specific thermal properties depending on their applications. For instance, good insulating fills are needed for oil and gas pipelines and underground storage tanks of liquefied natural gas (LNG). In contrast, geothermal heat pumps and high-voltage power cables require fill materials to dissipate heat readily. Hence, suitable selection of fill materials is very important for energy savings.

In the mining industry, substantial mining tailings are generated worldwide after extraction of valuable metals and minerals from ore body. The mine tailings are the finely ground rocks, and can be either reactive (generating acid mine drainage, AMD hereafter) or non-reactive, depending on the mineralogical composition. Recently, the utilization of mine wastes by modifying the physical and chemical properties of mine tailings has been practiced, for example, as the backfill of cemented tailings (Ercikdi et al. 2010) and as the raw material of building bricks (Yellishetty et al. 2008). These applications have advantages from technical, economic and environmental perspectives. Nevertheless, most mine tailings have traditionally been disposed on site in the form of impoundments. The surface impoundments of high water content

tailings allow for their consolidation and desiccation. The impoundments may be in water or dry, depending on the disposal history and site conditions. Some tailings may be applied as construction materials on the mine site for infrastructures when natural soils are not available in ample quantity near the site and underwater disposal is not essential to control AMD (Bussiere 2007). Moreover, the use of such mine tailings can be beneficial for the reduction in tailings accumulation and costs associated with constructing and reclaiming tailings dykes and other infrastructures on the mine site.

More than one billion scrap tires are produced each year worldwide, and the handling of these scrap tires has become a serious environment problem over past decades. As a possible alternative for their disposal, the scrap tires are used in civil engineering applications. The scrap tires are usually grinded to particles. According to ASTM D 6270 (ASTM 2008), they are classified into three distinct groups in particle sizes: tire shreds (50 to 305 mm), tire chips (12 to 50 mm) and particulate rubber (less than 12 mm), often known as tire crumbs (Edinçliler et al. 2010). The rubber tire particles are lightweight and durable, and display favorable drainage characteristic, good thermal insulation and high energy absorption. They are also comparatively cost effective when used as fills compared to other materials. Owing to these advantages, tire particles can be applied alone or mixed with other geomaterials as backfills of embankments, retaining walls, bridge abutments, leachate collection layers in landfills, subgrade thermal insulators and vibration attenuation media (Humphrey et al. 1997; Tweedie et al. 1998; Aydilek et al. 2006; Tandon et al. 2007; Hazarika et al. 2008).

Studies on tire particles and soil-tire particle mixtures have been carried out extensively, including characterization of mechanical properties such as the strength, compressibility, compactivity and permeability, as related to the size and shape of tire particles, soil type and

mixing ratio (Hudson et al. 2007; Ozkul and Baykal 2007; Wartman et al. 2007; Tanchaisawat et al. 2010; Edincliler et al. 2010). Meanwhile, a variety of field and laboratory studies for evaluating toxicity of leachates from scrap tires have been conducted (McIsaac and Rowe 2005; Sheehan et al. 2006; Tandon et al. 2007). A comprehensive overview on the environmental impacts of scrap tires is given in ASTM D 6270 (ASTM 2008). However, the thermal properties of scrap tires and their mixtures with geomaterials, which are important in the design as insulation fills, have not been addressed in detail in the literature. For instance, in the work of Humphrey et al. (1997), the thermal conductivity of tire chips was back-calculated by using one dimensional heat flow theory and measured temperature profile of an in-situ three-layer (soil-tire chip-soil) system under steady state conditions. Therefore, more information on thermal properties of tire particles and their mixtures with geomaterials will be beneficial for practical applications.

3.2 Objective and Scope

This study is directed to the beneficial use of tire particles as lightweight fill materials with improved thermal insulation. Tailings from a mining site and tire crumbs were selected for the study for reasons discussed in the previous section. The thermal properties and packing densities of mine tailings mixed with tire crumbs in dry state were measured to investigate the roles of tire particles inclusion in amending the thermal and packing behaviors of mineral aggregates. The mixture samples were prepared in the laboratory by controlling the mixing ratio of the two materials and packing methods. The results of thermal conductivity and volumetric heat capacity measurements on the mixtures are presented to demonstrate their correlations with the volumetric mixing ratio of tire crumbs as well as the porosity of the mixtures.

The scope of the study includes a review of concepts from particle packing characteristics relevant to mixtures of mine tailings and tire crumbs, which will enhance the understanding of the thermal responses of the mixtures. Methods are addressed to estimate the loosest and densest packing behaviors of the mixtures from the theory and from experimental investigations, respectively. Based on the experimental results, a multiple linear regression model for predicting the thermal conductivity of the mixtures is established as a function of two variables, i.e., the volumetric mixing ratio of tire crumbs and porosity. The volumetric heat capacity diagram is presented, which enables the volumetric heat capacity to be determined for the mixtures at known porosity and volumetric mixing ratio of tire crumbs.

3.3 Heat Transfer in Geomaterials

Heat transfer takes place through conduction, convection and radiation. Of the three mechanisms, conduction prevails in solids and is the predominant mechanism for heat transfer in most geomaterials (Farouki 1986). The thermal properties of a geomaterial are affected by the volumetric fractions of its constituents (air, water, minerals and organic matter). The thermal properties of constituents of geomaterials vary in a broad range, as shown in Table 3.1. Furthermore, the fabric of geomaterials, which refers to the arrangement of particles of all size ranges, shapes and associated pores (Mitchell and Soga 2005), has an effect on their thermal properties (Carson et al. 2003; Cote and Konrad 2005).

The thermal conductivity λ (W/mK) is defined as the heat flux under a unit temperature gradient under steady state, one dimensional conditions, as stated in the Fourier's law:

$$\lambda = -\frac{q}{dT/dx} \quad (3.1)$$

where q (W/m^2) is the heat flux which is the amount of thermal energy transferred per unit time in the x (m) direction per unit area perpendicular to the transfer direction, and T (K) is the temperature. A high thermal conductivity signifies that heat easily propagates through a material. Several researchers (Farouki 1986; Brandon and Mitchell 1989) have pointed out that the thermal conductivity of geomaterials varies with temperature and pore fluid salinity, as well as the thermal conductivities and volumetric fractions of constituents.

The volumetric heat capacity C_v ($\text{J}/\text{m}^3\text{K}$) is the amount of heat required to change a unit temperature per unit volume of material:

$$C_v = \frac{dQ}{dT} \quad (3.2)$$

where Q (J/m^3) is the thermal energy per a unit volume and T (K) is the temperature. A high volumetric heat capacity implies that a material has high capacity to store thermal energy. De Vries (1963) suggested that the volumetric heat capacity of a geomaterial can be estimated as the arithmetic mean of the volumetric heat capacity C_i of each constituent in the geomaterial, using the volumetric fraction V_i as weight:

$$C_v = \sum_i V_i C_i = V_a C_a + V_w C_w + V_s C_s \quad (3.3)$$

where C and V denote the volumetric heat capacity and volumetric fraction of each constituent: air (a), water (w), and soil solid (s), respectively. Note that the solid constituents include various minerals and organic matter, which are not separated. When a dry mixture of mine tailings and tire crumbs is considered, Eq. (3.3) can be rewritten as

$$C_v = V_a C_a + V_m C_m + V_t C_t \quad (3.4)$$

where C_m and C_t are the volumetric heat capacities, and V_m and V_t are the volumetric fractions of mine tailings and tire crumbs, respectively. Eq. (3.4) can be expressed in terms of the porosity and volumetric mixing ratio of tire crumbs in the mixture R_{mV} :

$$C_v = nC_a + (1-n)(C_m - R_{mV}C_m + R_{mV}C_t) \quad (3.5)$$

where n is the porosity of the mixture and R_{mV} is the volumetric mixing ratio of tire crumbs in the mixture.

3.4 Particle Packing Characteristics

The term of packing may be defined as any manner of arrangement of solid units, in which each constituent unit is supported and held in place in the Earth's gravitational field by tangent contact with its neighbors (Graton and Fraser 1935). The term *packing* is sometimes used interchangeably with the term *fabric* that describes the geomaterial particles and aggregates arrangement in soil mechanics. To comprehend the packing behaviors of particulate material mixtures, numerous theoretical and experimental studies have been performed. In general, the purposes of these studies are to minimize the void or maximize the density of the mixtures in ceramic, construction, food and polymer industries. In this section, a literature review on particle packing theories is presented in order to interpret the thermal behaviors of mine tailings and tire crumbs mixtures.

The porosity n , void ratio e and bulk unit weight γ_b , which are strongly related to the packing of granular materials, are correlated in the volume-weight phase relationships defined in soil mechanics:

$$n = \frac{e}{1+e} = 1 - \frac{\gamma_b}{G_s \gamma_w} \quad (3.6)$$

where G_s is the specific gravity of a mixture and γ_w is the unit weight of water. In addition, the arrangement of the packing is indirectly characterized by means of the coordination number N (defined as the average number of contact points that each particle has with surrounding particles).

The packings of uniform spheres provide insight for understanding the packing behaviors of granular materials. The regular packing arrangements of uniform spheres can be theoretically calculated using geometry. The porosity of uniform spheres ranges from a low of 0.260 for cubic packing to a higher of 0.476 for rhombohedral packing, and the corresponding coordination number is in the range of 6 to 12 (White and Walton 1937). However, random packings are more realistic to particulate materials. McGeary (1961) revealed that for packings of uniform spheres from 41 μm to 3 mm in size, the minimum porosity representing dense random packing lies within the range of 0.375 to 0.405. German (1986) summarized the reported porosities for randomly packed uniform spheres, and noted that the porosity for dense random packing varies from 0.333 to 0.390 with an average of 0.362, whereas the porosity of loose random packing of uniform spheres ranges from 0.375 to 0.440 with an average of 0.408. Murphy (1982) compiled the coordination number data from the literature and proposed an empirical relationship between the coordination number N and porosity n in a randomly packed assembly of uniform spheres, namely,

$$N = 27.03n^2 - 44.54n + 21.80 \quad (3.7)$$

Although this relation holds for $0.2 \leq n \leq 0.6$, it is obvious that the decrease in the porosity of random sphere packs increases the coordinate number, both being the result of denser packing.

The packing of granular materials is controlled by intrinsic factors such as the shape, size and gradation of particles, as well as by external factors such as the container wall effect and packing method. These factors, thus, have influences on the thermal properties of the mixtures.

Irregular particles tend to form looser packing than equivalent spheres. The porosity of natural sands with the same average particle size increases with decreasing the roundness and sphericity, resulting in lower coordinate number as well as lower stiffness (Cho et al. 2006). The greater the surface roughness is, the lower the packing density (Shinohara 1984). On the other hand, it was observed that the increase in the porosity with increasing particle irregularity leads to the decrease in the thermal conductivity (Carson et al. 2003; Yun and Santamarina 2008).

Fine particles likely exhibit looser packing than those of coarse particles due to surface effects. When the particle sizes approach to less than 50 μm , interparticle forces become prominent because of the increase in the specific surface area of particles (Samley 1970). The factors such as frictional forces and bridging between fine particles contribute to the formation of loose or honeycomb structures with high pore space (Lade et al. 1998). Also, cementation between particles causes agglomeration and particles clusters, yielding high porosity (Fedors and Landel 1979). Norris (1977) pointed out that finer sands are generally more irregular and as a result, have higher porosity than coarse sands. Normally, the porosity of coarse-grained soils is within the range of 0.23 to 0.50, while fine-grained soils can have porosities greater than 0.50 (Budhu 2007). Meanwhile, it was shown that the thermal conductivity decreases as soil particles decrease in size (Tavman 1996; Smits et al. 2010).

Mixtures of non-uniform particles display a tendency to be denser than those of the same sizes since finer particles may occupy the voids between coarser particles. Panayiotopoulos (1989) noted that the influence of particle size distribution on packing efficiency is greater than those of particle size and shape. As the particle size ratio (i.e., the ratio of coarse particle to fine particle) increases, the coordination number of coarse particles increases (Suzuki and Oshima 1983). On the other hand, it was found that the thermal conductivity of well-graded soils is greater than that of poor-graded soils (Brandon and Mitchell 1989; Cote and Konrad 2005).

The container wall effect is defined as the packing of particles being disrupted by the smooth wall of container, which leads to higher porosity near the wall. In a similar manner, the coarse particles dispersed or isolated within the fine particles may prevent truly random packing of fine particles at the interfaces of coarse and fine particles. The container wall effect on packing is less pronounced with rough walls and irregular particles. When the distance from the wall is at least ten times the particle size, the randomness of particles becomes constant (McGeary 1961). Meanwhile, the densest and loosest random packings are affected by packing procedures. In other words, the minimum and maximum porosities of a mixture depend on the methods employed for their determination (Lade et al. 1998), which may be estimated by procedures declared in ASTM D 4253 and D 4254 (ASTM 2006a, b). Additionally, other methods have been adopted by some researchers (Messing and Onada 1978; Al-Jarallah and Tons 1981).

For a mixture containing particles of two sizes, it can be idealized as a binary mixture, and its porosity variation against the volumetric mixing ratio of coarse particles to the total solids is illustrated in Figure 3.1, where porosities at $R_{mV} = 0$ and 1 correspond to random packings of fine and coarse particles, respectively. The porosity decreases with an increase in the volumetric

mixing ratio of coarse particles until it reaches a threshold value. This threshold value represents an optimal packing for a binary mixture, which is a point where the behavior of the mixture changes from fine-dominated to coarse-dominated. The trend is overturned with further increases in the volumetric mixing ratio of coarse particles. When the particle size ratio approaches infinity, the voids of the coarse particles are larger enough to allow for the random packing of fine particles, the porosity n_{opt} and volumetric mixing ratio R_{mV-opt} at the optimal packing can be obtained from the following equations, respectively (Lade et al. 1998):

$$n_{opt} = n_c n_f \quad (3.8)$$

$$R_{mV-opt} = 1 - \frac{1}{e_f} \left(\frac{n_f}{1/e_c + n_f/e_f} \right) \quad (3.9)$$

where n and e denote the porosity and void ratio of each particle in mixtures: coarse (c) and fine (f), respectively. The theoretical packing curve, i.e., the porosity behavior of mixtures n_{mix} in Figure 3.1, is expressed as

$$n_{mix} = \frac{e_f(1 - R_{mV})}{1 + e_f(1 - R_{mV})} \quad \text{for } R_{mV} \leq R_{mV-opt} \quad (3.10)$$

$$n_{mix} = \frac{R_{mV}(e_c + 1) - 1}{R_{mV}(e_c + 1)} \quad \text{for } R_{mV} \geq R_{mV-opt} \quad (3.11)$$

It is clear from these equations that the optimal packing point in binary mixtures is not unique because it relies on the packing characteristics of the host materials.

3.5 Experimental Study

To study the thermal and packing behaviors of mine tailings, tire crumbs and their mixtures, an experimental program was designed and carried out. A description of materials, apparatus, sample preparation and methodology is provided in this section, followed by discussion of experimental results and statistical analysis.

3.5.1 Materials

The materials used in this study are mine tailings and tire crumbs. Mine tailings were recovered from the Musselwhite mine, a gold mine located 500 km north of Thunder Bay, Ontario, Canada. Tire crumbs were supplied by a tire recycling facility located in Ontario. The index properties of two materials were determined following the recommended procedures by American Society of Testing and Materials (ASTM), and summarized in Table 3.2.

The specific gravity of mine tailings is 3.37, which is greater than that of typical soils owing to predominant amphibole minerals of high specific gravity (Wang et al. 2006), and the specific gravity of tire crumbs is measured as 1.19, which is comparable to those reported in ASTM D 6270 (ASTM 2008). The Atterberg limit tests on tailings particles finer than 75 μm revealed that the mine tailings are non-plastic. Scanning electron microscope (SEM) images of mine tailings and tire crumbs are displayed in Figure 3.2. For mine tailings (Figure 3.2(a)), particles are angular to subangular in shape, and typically consist of large bulky particles, platy particles and flocks (agglomeration of clay-sized particles). As shown in Figure 3.2(b), the tire crumbs are angulated and roughened as they are produced through the mill process.

The particle size distributions of the mine tailings and tire crumbs are shown in Figure 3.3. In Figure 3.3(a), the shaded area indicates the typical grading of Canadian hard rock tailings as

presented by Bussiere (2007). The mine tailings are made up of a wide range (0.42 to 138 μm) of particle sizes, characterized as a silt, with 9.4% sand, 83.2% silt and 7.4% clay ($< 2 \mu\text{m}$) sized particles. The size of tire crumbs ranges from 0.069 mm to 0.85 mm, as shown in Figure 3.3(b). On the other hand, the textures of both the mine tailings and tire crumbs are quantified as the effective D_{10} and median D_{50} particle sizes, together with the coefficient of uniformity C_u and the coefficient of curvature C_c , as given in Table 3.2. Their textures can be further specified by using other statistical measures such as mode D_m , mean \bar{D} , standard deviation σ , skewness Sk and kurtosis K (see Appendix A for the definition and statistical meaning of the measures) that are used to characterize the properties of geomaterials. As an example, Carrier (2003) pointed out that the \bar{D} size of particles best represents the particle size for the estimation of the coefficient of permeability of a soil than the D_{10} size of particle. It is also noteworthy that the D_{50} almost never displays the same value as the \bar{D} since the particle size probability density functions are likely to be skewed. Accordingly, the statistical measures of the mine tailings and tire crumbs were computed and are listed in Table 3.3. Based on the descriptive terminology of shapes suggested by Blott and Pye (2001), the mine tailings are poorly sorted ($\sigma = 3.596$), with fine skewed (indicating an excess of fines, $Sk = -0.981$) and mesokurtic ($K = 3.469$) distribution, whereas tire crumbs is moderately well sorted ($\sigma = 1.557$), with fine skewed ($Sk = -1.043$) and leptokurtic ($K = 3.810$) distribution, as comparing to the log-normal distribution. As shown in Figure 3.3(a), meanwhile, the particle size distribution of mine tailings used is characterized as the tertiary mode, which is attributed to the fact that ore has been artificially ground to a targeted particle size for liberating gold from the rock.

Wang et al. (2006) have studied the mineralogical and geochemical properties of the mine tailings used in this study. According to their results, the mine tailings contain 3% reactive minerals (i.e., pyrrhotite) and the remainder is composed of amphibole, quartz, mica or illite, and chlorite. The amount of pyrrhotite is small, comparing to that of other sulphide-containing mine tailings reported in the literature (e.g., 80% pyrrhotite: Amaratunga 1995; 49% pyrite: Ercikdi et al. 2010). This means that the mine tailings tested has low reactivity. Moreover, the mine tailings contain 1.2% carbonate, in the form of calcite and dolomite, which provide a pH buffer capacity. On the other hand, the pH of the mine tailings is measured as 8.4, which is slightly alkaline. This is mainly due to the addition of lime during the milling process and the presence of carbonates. Up to date, AMD has not been generated on the mine site.

3.5.2 Apparatus

In this study, all measurements of thermal properties were conducted using a thermal property analyzer (Model KD2 Pro, Decagon Devices Inc.). The methodology of the measurement is based on the transient line heat source theory (Bristow et al. 1998). This apparatus reproduces thermal properties of reference materials with $\pm 5\%$ accuracy within the temperature range of - 50 to 150 °C. The KD2 Pro analyzer comprises a hand-held unit and a sensor. The sensor has two-parallel probes of 1.3 mm diameter and 30 mm length at a spacing of 6 mm, which is inserted into the sample under testing. One of probes contains a heater and the other, a thermistor. A heat pulse is applied to the heater and, the temperature is simultaneously recorded at the thermistor. The thermal properties of the sample are automatically determined from the temperature response with time. A single measurement takes about 2 minutes including the temperature equilibrium period prior to heating and cooling.

3.5.3 Sample Preparation

In this study, samples tested include mine tailings, tire crumbs, and seven mixtures of the tailings and tire particles. The thermal conductivity and volumetric heat capacity of mixtures were measured and compared with those of pure mine tailings and pure tire crumbs. Nine samples with the rubber-to-tailings weight ratios of 0.0, 0.1, 0.2, 0.3, 0.4, 0.5, 0.6, 0.8 and 1.0 were prepared. The weight ratio was used instead of the volumetric ratio, because preparing samples is more readily performed using weight measurement. The weight mixing ratios were converted to the volumetric mixing ratios for evaluating packing and thermal behaviors of the samples in the analysis related to the volumetric terms. The volumetric mixing ratio of tire crumbs in the mixture R_{mV} can be calculated from the weight mixing ratio R_{mW} , knowing the specific gravities of tire crumbs G_{st} , and mine tailings G_{sm} , by using the following equation (Youwai and Bergado 2003):

$$R_{mV} = \frac{R_{mW}}{G_{st}} \left(\frac{1 - R_{mW}}{G_{sm}} + \frac{R_{mW}}{G_{st}} \right)^{-1} \quad (3.12)$$

It is intuitively recognized that the mixtures will form different fabrics under different particle sizes and shapes, which will influence the thermal properties of the mixtures, as discussed in the previous section.

3.5.4 Methodology

The tire crumbs and tailings at predetermined weight ratio were placed in a mechanical mixer and mixed until the samples were visually homogenous. The mixture was then packed following three different procedures: loosest packing, intermediate packing and densest packing.

A standard Proctor mold of volume 943.7 cm^3 (101.6 mm diameter and 116.4 mm height), as described in ASTM D 698 (ASTM 2007), was used as the container. No surcharge and compaction were applied in the sample preparation to avoid crushing tailings particles and compression of tire particles.

A mixture with loosest random packing was achieved following the Method A specified by ASTM D 4254 standard (ASTM 2006b), in which a funnel was used to pour the mixture into the container. A mixture with the densest random packing was attained using an electromagnetic vibrating table (Model VP-51-D1, FMC tech.). A mixture with the intermediate packing was prepared following the same procedures for the densest packing, but the time and amplitude of vibration were attenuated. For each rubber-tailings weight ratio, one to three samples were prepared with various degrees of intermediate packing.

After packing, the extension collar on the mold was removed and the excess material was carefully trimmed off. The weight of the sample was measured for calculation of the bulk unit weight and porosity from Eq. (3.6). Lastly, the volumetric fractions of constituents in the sample (air, mine tailings and tire crumbs) were computed using Eq. (3.12) with the known porosity.

After the sample was prepared and its properties were measured, the KD2 Pro analyzer was vertically inserted into the sample. A total of three measurements, taken from 50 mm from the mold wall, were made and the average value and standard deviation were calculated. All measurements were carried out at the room temperature of $20 \text{ }^\circ\text{C}$, with deviation less than $\pm 0.5 \text{ }^\circ\text{C}$.

3.6 Results and Discussion

A summary of results for all samples tested is tabulated in Table 3.4. One can notice that the measured bulk unit weight and porosity already capture the effects of the particle sizes, shapes and gradation as well as the container wall effect. In this section, the experiment results are presented and discussed to highlight the roles of coarse-grained tire particles inclusion in modifying the thermal and packing characteristics of fine-grained tailings.

3.6.1 Packing Behaviors of Mixtures

The minimum and maximum bulk unit weights (γ_{\min} and γ_{\max}) of the mixtures are plotted against the volumetric mixing ratio of tire crumbs, as shown in Figure 3.4, in which the bulk unit weights corresponding to samples with intermediate packing are not included. The variation of the maximum bulk unit weight with the volumetric mixing ratio of the lightweight tire crumbs is greater than that of the minimum bulk unit weight. On the other hand, the results indicate that the inclusion of the lightweight tire crumbs decreases the bulk unit weight regardless of the packing density, and the trend is non-linear, which is due to the change in the amount of air-entrainment as influenced by the volume of tire crumbs in the mixture.

The minimum and maximum porosities (n_{\min} and n_{\max}) of the mixtures against the volumetric mixing ratio of tire crumbs are shown in Figure 3.5, to compare with bulk unit weights in Figure 3.4. Again, the porosities corresponding to intermediate packing are not presented in this plot. The porosity change in Figure 3.5 represents the changes of air fraction in mixtures. The porosity of the mixtures decreases as packing density increases, while the variations of porosity are similar irrespective of packing states. As the volumetric mixing ratio of tire crumbs increases from 0 to 0.55, both the minimum and maximum porosities of the mixtures

decrease gradually. As the volumetric mixing ratio of tire crumbs further increase from 0.55 to 1, the limit porosities of the mixtures increase significantly. This trend supports the fact that the decrease in the bulk unit weight of the mixtures with the increased portion of tire crumbs is caused not only by the reduced mixture weight, but also by the changes in entrained air in the mixture. The porosity of mine tailings ranges from 0.44 to 0.60, which is in the range of typical fine-grained soils, whereas the porosity of tire crumbs varies from 0.63 to 0.68, which are relatively large comparing to geomaterials. This may be attributed to the angular shape and rough surface of the tire particles. The observation shows the evidence that the porosity of materials is associated with the combined effect of particle size, shape and gradation.

The binary packing theory, modeled as Eqs. (3.8)-(3.11), is applied to the measured porosities of the mixtures of mine tailings and tire crumbs, as shown in Figure 3.5. Based on particle size statistics of the two materials given in Table 3.3, the particle size ratios of the mode D_{m_t}/D_{m_m} and the median D_{50_t}/D_{50_m} (where the subscript t and m denote the tire crumbs and mine tailings, respectively) are computed to be 9.3 and 17.5, respectively. In addition, the particle size ratio of the mean with standard deviation $(\bar{D}_t \pm \sigma_t)/(\bar{D}_m \pm \sigma_m)$ is determined to be between about 20 and 30. The results demonstrate that the fitted curves of measured porosities are consistent with the theoretical packing curves: the porosity of the mixtures is less than the porosities of pure materials. However, the optimal packings of two limit porosities, i.e., minimum and maximum porosities, do not exhibit a distinctive point as derived from the ideal binary mixture shown in Figure 3.1. This is probably due to the fact that for mixtures with tire crumbs content less than the optimal packing value, tire particles do not float within the tailings particles matrix without the interference of random tailings packs. For mixtures with tire crumbs content higher than the optimal packing value, tailings particles could not migrate into the pore

space between tire particles without frictional resistance that leads to disconnected tire particles. Similar smooth packing trends for mixtures containing construction aggregates of two different sizes have been observed in the literature (Al-Jarallah and Tons 1981, Lade et al. 1998, Jones et al. 2002). In their works, the median particle size ratio is in the range of about 2 to 30. Polito (1999) analyzed the packing for mixtures of 37 sands and 5 non-plastic silts, and concluded that the volumetric mixing ratio of sands at the optimal packing point was within the range of 0.55 to 0.75. In contrast, for the irregular shaped tire crumbs and tailings mixtures, it is found that the optimal packing is located at a lower volumetric mixing ratio of tire crumbs, i.e., in the range of 0.50 to 0.60.

The relationship between the minimum and maximum porosities of the mixtures is shown in Figure 3.6. The result reveals that the maximum porosity increases with an increase in the minimum porosity. The data regression equation has the form of ($R^2 = 0.85$)

$$n_{\max} = 0.48 n_{\min} + 0.36 \quad (3.13)$$

Based on this relation, the packing method used in this study can be employed to prepare mixtures with minimum and maximum porosities. The correlation can also be used to estimate the minimum porosity from the maximum porosity and vice versa, for rubberized geomaterials.

The porosity range, i.e., $n_{\max} - n_{\min}$ (or the void ratio range, i.e., $e_{\max} - e_{\min}$) is used as an index property of granular geomaterials that reflects their fabrics (Cubrinovski and Ishihara 2000). Figure 3.7 shows the porosity range versus the volumetric mixing ratio of tire crumbs. The values of $n_{\max} - n_{\min}$ slightly increases with the increasing volumetric mixing ratio of tire crumbs first, then it begins to decrease noticeably with a further increase in the volumetric mixing ratio, finally it decrease steadily. This indicates that a transition region exists, ranging

from $R_{mV} = 0.55$ to 0.75. In this region, both the mine tailings portion and tire crumbs portion in the mixtures govern the porosity of the mixtures, beyond this range, the mixture fabric transits from a rigid (i.e., a mine tailings supported fabric) to a soft (i.e., a tire crumbs supported fabric) granular skeleton. Meanwhile, it is shown that there is little porosity change in packing of pure tire crumbs, which is expected since the vibration has limited effect on densification of lightweight and highly compressible materials.

These observations can provide insight to the optimal mixing design of geomaterials mixed with recycled tire particles, which represent rigid-soft mixtures. Furthermore, the results suggest that factors such as the particle sizes, shapes and gradation may control the packing characteristics of the mixtures. The effect of these features to the thermal behavior of the mixtures will be discussed in the following section.

3.6.2 Thermal Behaviors of Mixtures

The relationships between the thermal conductivity and volumetric mixing ratio of tire crumbs for the densest and loosest random packings are shown in Figure 3.8. It is no surprise to see that the thermal conductivities of the mixtures with the densest packing are greater than those with the loosest packing, as the thermal conductivity of solids is higher than that of air. It is of interest to note from Figure 3.8 that the trends of thermal conductivity curves at two different packing states are similar. For the densest packing, the thermal conductivity values reduce from 0.248 W/mK for mine tailings to 0.080 W/mK for tire crumbs, while for the loosest packing, the values decrease from 0.140 to 0.073 W/mK. The mixture containing 65.4% of tire crumbs by volume (40% by weight) has a reduction of thermal conductivity of about 50% comparing to the mine tailings without the addition of tire crumbs. More importantly, the thermal conductivities of

the two packing states follow a similar trend compared to packing behaviors as presented in Figure 3.4. This finding substantiates the fact that the thermal conductivity of granular geomaterials is correlated to the inherent thermal properties of constituents as well as the volumetric fractions of constituents and arrangement of particles in the mixtures.

The relationships between the volumetric heat capacity and volumetric mixing ratio of tire crumbs for the densest and loosest random packings are shown in Figure 3.9. The volumetric heat capacity of the densest packing mixtures is larger than that of the loosest packing mixtures. On the other hand, as the volumetric mixing ratio of tire crumbs increases, the volumetric heat capacity initially increases slightly and then dramatically decreases for both packings. It is also noted that the trend of variation of the volumetric heat capacity versus the volumetric mixing ratio of tire crumbs is similar to that of the porosity versus the volumetric mixing ratio of tire crumbs, as indicated in Figure 3.5. This embodies that the volumetric heat capacity of the mixtures is more affected by the volumetric fraction of air than by that of solid phases. This is attributable to the fact that the volumetric heat capacity of air is three orders of magnitude lower than that of most solids, including tailings and tire particles.

Figure 3.10 shows the relationships between the thermal conductivity and porosity for all experimental data tested in this study, including samples with intermediate packings. The thermal conductivity of mine tailings decreases with increasing porosity and ranges from 0.248 to 0.140 W/mK for porosities between 0.44 and 0.60. Meanwhile, the thermal conductivity of tire crumbs varies from 0.080 to 0.073 W/mK for porosities ranging from 0.63 to 0.68. The measured thermal conductivities of the mixtures of the two materials are located within the upper and lower bounds with respect to the mine tailings and tire crumbs, respectively. This plot also shows that as the weight mixing ratio of tire crumbs increases, the thermal conductivity

decreases. Hence, the thermal insulation effect of recycled tire crumbs can be utilized in engineering applications.

The thermal conductivities of dry geomaterials including crushed rocks, gravels, sands, silts and clays, as related to their porosities have been studied by many researchers (Kersten 1949; Gangadhara Rao and Singh 1999; Corte et al. 2009). Figure 3.11 shows comparison of the measured values of the thermal conductivity of mine tailings and tire crumbs and those of other materials reported in the literature. The thermal conductivity of mine tailings is within the typical range of sands and clays, whereas the thermal conductivity of tire crumbs is lower than that of typical geomaterials. The plot also explains that the thermal conductivity of geomaterials is sensitive to the fabric as well as the thermal conductivity of their constituents. For instance, the thermal conductivity of crushed rocks is scattered and differs from that of natural gravels despite their similar grain sizes (> 20 mm).

Figure 3.12 shows the relationships between the volumetric heat capacity and porosity for all experimental data obtained in this study. The volumetric heat capacity of the mixtures decreases with increasing porosity. The volumetric heat capacity of mine tailings ranges from 1.677 to 1.217 MJ/m³K for porosities between 0.44 and 0.60. On the other hand, the thermal conductivity of dry tire crumbs varies from 0.901 to 0.811 MJ/m³K for porosities ranging from 0.63 to 0.68. These two trends are the upper and lower bounds of the mixtures of mine tailings and tire crumbs, respectively. Figure 3.12 also demonstrates that the rate of volumetric heat capacity changes against the porosity decreases with increasing weight mixing ratios of tire crumbs in the mixtures.

From Figures 3.10-3.12, one may recognize that the thermal properties of mine tailings and tire crumbs mixtures strongly depend on the packings of the mixtures as represented by porosity. Consequently, the porosity plays a critical role in heat transfer of the dry mixtures, and can be considered to be a secondary factor that captures the primary factors, i.e., the particle sizes, shapes and gradation as well as the particle characteristics of host materials. Especially, given the mechanism of thermal contacts at the particle-scale, the increase in thermal conductivity with decreasing porosity may reflect the improvement of particle contacts in the mixtures.

3.7 Statistical Analysis

In the above section, the results of thermal properties and packing tests were interpreted to explore the correlation between thermal and packing behaviors of the mine tailings and crumb tires mixtures. In this section, the results of statistical analysis on the average thermal properties in Table 3.4 are presented and discussed.

Regression analysis was used for statistical evaluation. The general multiple linear regression model can be formulated in the following equation:

$$Y = \beta_0 + \beta_1 X_1 + \beta_2 X_2 + \dots + \beta_i X_i + \beta_n X_n + \varepsilon \quad (3.14)$$

where β_i is the regression coefficient, X_i is the independent variables, Y is the dependent variable, and ε is a random error term.

In this study, the multiple linear regression analyses were performed in two phases: to build a prediction model for the thermal conductivity, and to develop an analysis chart for the volumetric heat capacity. In the first phase, the multiple linear regression analysis was carried out to establish the relationship of the average thermal conductivity of mine tailings, tire crumbs

and their mixtures as related to the volumetric mixing ratio of tire crumbs R_{mV} and porosity n . In the second phase, the volumetric heat capacity values of mine tailings and tire crumbs (i.e., C_m and C_t) were first computed by using multiple linear regression analysis (without accounting for intercept term, β_0) applied to Eq. (3.4) with other known variables (i.e., C_v, C_a, V_a, V_m and V_t), and then the calculated values are applied to Eq. (3.5) to produce a volumetric heat capacity diagram of the mixtures as a function of the volumetric mixing ratio of tire crumbs R_{mV} and porosity n .

3.7.1 Regression Model for Thermal Conductivity

A multivariate regression model is developed at a significance level of 5% to relate the thermal conductivity λ , and the volumetric mixing ratio of tire crumbs R_{mV} and porosity n :

$$\lambda = 0.368 - 0.079R_{mV} - 0.353n \quad (3.15)$$

Eq. (3.15) states that the form of the regression model is consistent with the trends of test results observed in Figure 3.10. That is, the thermal conductivity decreases with increasing volumetric mixing ratio of tire crumbs and increasing porosity.

The statistical properties from the regression analysis are summarized in Table 3.5. The coefficient of determination R^2 is 0.908, which indicates a strong correlation between the thermal conductivity and the two variables (i.e., R_{mV} and n). However, a large R^2 value does not necessarily guarantee accurate prediction, and therefore the F - value test is also used to assess the regression model. By definition, the F - value is the ratio of the mean squares of regression (MSR) and mean squares of error (MSE) if the hypothesis of the test is all regression coefficients being zero (Montgomery et al. 2004). When the F - value of the regression model is

larger than the critical F - value that is the upper limit of the F ratio, the model is feasible at a given probability and degree of freedom. The F - value is calculated to be 182.5, much greater than the critical F - value at the probability of 95%, i.e., 3.3, suggesting that the regression model is highly significant.

The standard residual of predicted thermal conductivity, defined as $r_s = r/SE$, where r_s = standard residual, r = residuals, and SE = standard error, is shown in Figure 3.13. The SE of thermal conductivity regression model is 0.014, and the 95% confidence band is ± 2.03 . This plot demonstrates that the majority of the standard residuals fall in the 95% confidence bandwidth of 4.05. The standard residuals are evenly distributed with regard to the predicted values of thermal conductivity, indicating the regression model is strongly significant for the estimate of thermal conductivity.

Additionally, even if the regression model is statistically significant in terms of R^2 , F - value and standard residuals, implying the model is applicable, it does not guarantee that the model is in any way optimal. It could be, for example, that one variable is dominating the regression equations while another variable in the equation is irrelevant. Thus, the significance of the regression coefficients of the variables in the empirical model was examined via Student's t - test, which is designed to evaluate the hypothesis of a particular regression coefficient being zero at an arbitrary probability. The significance of any regression coefficient can be assessed by comparing the t - statistic of the regression coefficient (defined as the ratio of the regression coefficient β_i , and its standard error SE , i.e., $|t-stat| = |\beta_i / SE(\beta_i)|$) and the Student's t distribution. In other words, if the value of t - statistic for any of the regression coefficients is less than the Student's t distribution at the probability of 95%, i.e., 1.69, it can be concluded that

the data do not provide convincing evidence that the coefficient is different from zero. The results of Student's t test reveal that the intercept, volumetric mixing ratio of tire crumbs and porosity are significant at the probability of 95% in the regression model, as shown in Table 3.5. Comparing to the values of t -statistic obtained, the porosity is slightly more significant than the volumetric mixing ratio of tire crumbs.

As a result, the multiple linear regression model to relate the volumetric mixing ratio of tire crumbs R_{mV} and porosity n is highly significant as indicated by a series of statistical analyses. A practical application of the empirical model is to predict the thermal conductivity if the volumetric mixing ratio of tire crumbs and porosity of a mixture are known. Also, it can be applied to estimate conditions to attain a desired thermal conductivity. Although the model was built with limited data, it provides a viable insight to the understanding of the thermal conductivity behaviors of rubberized geomaterials in dry condition.

3.7.2 Analysis Chart for Volumetric Heat Capacity

With known volumetric fractions of constituents (i.e., air, mine tailings and tire crumbs) and volumetric heat capacities of air and mixtures, the volumetric heat capacities of mine tailings and tire crumbs mixtures were determined by using the multiple linear regression analysis applied to Eq. (3.4). The volumetric heat capacity values of the mine tailings and the tire crumbs are found to be 2.889 and 2.461 MJ/m³K, respectively. The resulting values of statistical properties are coefficient of determination $R^2 = 0.999$ with standard error $SE = 0.033$ and F -value = 32,829.6. These volumetric heat capacity values were used to Eq. (3.5) that correlates the volumetric heat capacity of mixtures C_v , volumetric mixing ratio of tire crumbs R_{mV} , and porosity n . Figure 3.14 shows an analysis chart for estimating the volumetric heat capacity of mixtures at known

porosity and volumetric mixing ratio of tire crumbs. The curves represent the porosity range of 0.3 - 0.7, as indicated in Figure 3.12. The volumetric heat capacity decreases with increasing volumetric mixing ratio of tire crumbs at a given porosity. Meanwhile, the volumetric heat capacity decreases with increasing air fraction in mixtures at a given volumetric mixing ratio of tire crumbs. These trends are consistent with the results shown in Figure 3.12. From a practical perspective, the analysis chart may prove useful for reasonable predictions of the volumetric heat capacity from easily available mixture properties, i.e., the volumetric mixing ratio of tire crumbs and porosity only.

3.8 Summary and Conclusions

The objective of this study was to investigate the thermal and packing behaviors of mine tailings and tire crumbs mixtures, which has potential applications in utilizing recycled tire particles as lightweight fill materials with enhanced thermal insulation. The study included a detailed literature review on particle packing characteristics of spherical and granular materials, which serves to improve the understanding of the packing of mine tailings and tire crumbs mixtures that associate with their thermal properties. In the experimental program, the thermal and packing properties of dry mixtures of mine tailings and tire crumbs with different mixing ratios were measured to investigate the roles of tire particles inclusion on the thermal and packing behaviors of mineral aggregates, as well as to examine their relationships with the porosity. The following conclusions can be made based on the results of this study:

1. The factors affecting the packing and thermal properties of geomaterials include the particle size, shape and gradation as well as the container wall effect and packing method.

2. The bulk unit weights of the loosest and densest packed mixtures decreased non-linearly with increasing volumetric mixing ratios of tire crumbs in the mixtures, and the variations of their thermal conductivities were similar to the convex-shaped variations of bulk unit weights.
3. The minimum and maximum porosities of the mixtures against the volumetric mixing ratio of tire crumbs showed the smooth concave-shaped variation, not the sharp V-shaped variation derived from the ideal binary mixture. As increased the volumetric mixing ratios of tire crumbs in the mixtures, the volumetric heat capacity values of the mixtures corresponding to the densest and loosest packings initially increased slightly and then decreased considerably, similar to the trend of porosity variation.
4. At the volumetric mixing ratios of tire crumbs of 0.55 to 0.75, the mixtures demonstrated transitional fabrics, i.e., the structure changed from a tailings controlled rigid fabric and a rubber particles controlled soft fabric.
5. The porosity plays a preponderant role in heat transfer of the dry mixtures: both the thermal conductivity and the volumetric heat capacity increased linearly with decreasing porosity.
6. A multiple linear regression model was developed to estimate the thermal conductivity of the mine tailings and tire crumbs mixtures as related to the volumetric mixing ratio of tire crumbs and porosity. A series of statistical analyses revealed that the regression model is highly significant.
7. An analysis chart was established that enables the volumetric heat capacity of the mine tailings and tire crumbs mixtures to be determined at the known porosity and volumetric mixing ratio of tire crumbs in the mixtures.

It is believed that the findings and interpretation methods presented in this study will be beneficial for the understanding of the thermal characteristics of rubberized geomaterials in dry condition.

References

- Al-Jarallah, M., and Tons, E. (1981). "Void content prediction in two-size aggregate mixes." *Journal of Testing and Evaluation*, 9(1), 3-10.
- Amaratunga, L.M. (1995). "Cold-bond agglomeration of reactive pyrrhotite tailings for backfill using low cost binders: Gypsum β -Hemihydrate and cement." *Minerals Engineering*, 8(12), 1455-1465.
- ASTM. (2006a). "Standard test methods for maximum index density and unit weight of soils using a vibration table" *D4253-06*, West Conshohocken, Pa.
- ASTM. (2006b). "Standard test methods for minimum index density and unit weight of soils and calculation of relative density." *D4254-06*, West Conshohocken, Pa.
- ASTM. (2007). "Standard test methods for laboratory compaction characteristics of soil using standard effort [12,400 ft-lb/ft³ (600 kN-m/m³)]." *D698-07*, West Conshohocken, Pa.
- ASTM. (2008). "Standard practice for use of scrap tires in civil engineering applications." *D6270-08*, West Conshohocken, Pa.
- Aydilek, A.H., Madden, E.T., and Demirkan, M.M. (2006). "Field evaluation of a leachate collection system constructed with scrap tires." *Journal of Geotechnical and Geoenvironmental Engineering*, 132(8), 990-1000.
- Balland, V., and Arp, P.A. (2005). "Modelling soil thermal conductivities over a wide range of conditions." *Journal of Environmental Engineering Science*, 4(6), 549-558.
- Blott, S.J., and Pye, K. (2001). "GRADISTAT: a grain size distribution and statistics package for the analysis of unconsolidated sediments." *Earth Surface Processes and Landforms*, 26(11), 1237-1248.

- Brandon, T.L., and Mitchell, J.K. (1989). "Factors influencing thermal resistivity of sands." *Journal of Geotechnical Engineering*, 115(12), 1683-1698.
- Bristow, K.L. (1998). "Measurement of thermal properties and water content of unsaturated sandy soil using dual-probe heat-pulse probes." *Agricultural and Forest Meteorology*, 89(2), 75-84.
- Budhu, M. (2007). *Soil mechanics and foundations*, 2nd ed., John Wiley & Sons, New Jersey.
- Bussiere, B. (2007). "Colloquium 2004: hydrogeotechnical properties of hard rock tailings from metal mines and emerging geoenvironmental disposal approaches." *Canadian Geotechnical Journal*, 44(9), 1019-1052.
- Carrier III, W.D. (2003). "Goodbye, Hanzen; hello, Kozeny-Carman." *Journal of Geotechnical and Geoenvironmental Engineering*, 129(11), 1054-1056.
- Carson, J.K., Lovatt, S.J., Tanner, D.J., and Cleland, A.C. (2003). "An analysis of the influence of material structure on the effective thermal conductivity of theoretical porous materials using finite element simulations." *International Journal of Refrigeration*, 26(8), 873-880.
- Cho, G., Dodds, J., and Santamarina, J.C. (2006). "Particle shape effects on packing density, stiffness, and strength: natural and crushed sands." *Journal of Geotechnical and Geoenvironmental Engineering*, 132(5), 591-602.
- Cortes, D.D., Martin, A.I., Yun, T.S., Francisca, F.M., Santamarina, J.C., and Ruppel, C. (2009). "Thermal conductivity of hydrate-bearing sediments." *Journal of Geophysical Research*, 114, B11103.
- Cote, J., and Konrad, J. (2005). "A generalized thermal conductivity model for soils and construction materials." *Canadian Geotechnical Journal*, 42(2), 443-458.
- Cubrinovski, M., and Ishihara, K. (2000). "Flow potential of sandy soils with different grain compositions." *Soils and Foundations*, 40(4), 103-119.
- De Vries, D.A. (1963). "Thermal properties of soils." *Physics of Plant Environment* edited by W.R. van Wijk, North-Holland Publishing Company, Amsterdam, 210-235.

- Edinçliler, A., Baykal, G., and Saygili, A. (2010). "Influence of different processing techniques on the mechanical properties of used tires in embankment construction." *Waste Management*, 30(6), 1073-1080.
- Ercikdi, B., Cihangir, F., Kesimal, A., Deveci, H., and Alp, I. (2010). "Utilization of water-reducing admixtures in cemented paste backfill of sulphide-rich mill tailings." *Journal of Hazardous Materials*, 179(1-3), 940-946.
- Farouki, O.T. (1986). *Thermal properties of soils*, Series on Rock and Soil Mechanics Vol. 11, Trans Tech Publications, Clausthal-Zellerfeld.
- Fedors, R.F., and Landel, R.F. (1979). "Effect of surface adsorption and agglomeration on the packing of particles." *Powder Technology*, 23(2), 219-223.
- Gangadhara Rao, M.V.B.B., and Singh, D.N. (1999). "A generalized relationship to estimate thermal resistivity of soils." *Canadian Geotechnical Journal*, 36(4), 767-773.
- German, R.M. (1989). *Particle packing characteristics*, Metal Power Industries Federation, Princeton.
- Graton, L.C., and Fraser, H.J. (1935). "Systematic packing of spheres: with particular relation to porosity and permeability." *Journal of Geology*, 43(8), 785-909.
- Hazarika, H., Kohama, E., and Sugano, T. (2008). "Underwater shake table tests on waterfront structures protected with tire chip cushion." *Journal of Geotechnical and Geoenvironmental Engineering*, 134(12), 1706-1719.
- Hudson, A.P., Beavon, R.P., Powrie, W., and Parkes, D. (2007). "Hydraulic conductivity of tyres in landfill drainage systems." *Proceedings of Institution of Civil Engineers: Waste and Resource Management*, 160(WR2), 63-70.
- Humphrey, D.N., Chen, L.H., and Eaton, R.A. (1997). "Laboratory and field measurement of the thermal conductivity of tire chips for use as subgrade insulation." *Preprint No. 971289*, Transportation Research Board, Washington, D.C.

- Jones, M.R., Zheng, L., and Newlands, M.D. (2002). "Comparison of particle packing models for proportioning concrete constituents for minimum voids ratio." *Materials and Structures*, 35(5), 301-309.
- Kersten, M.S. (1949). *Laboratory research for the determination of the thermal properties of soils*, Research Laboratory Investigation. Engineering Experiment Station, Technical Report 23, University of Minnesota, Minneapolis.
- Krishnaiah, S., and Singh, D.N. (2006). "Determination of thermal properties of some supplementary cementing materials used in cement and concrete." *Construction and Building Materials*, 20(3), 193-198.
- Lade, P.V., Liggió, C.D., and Yamamuro, J.A. (1998). "Effects of non-plastic fines on minimum and maximum void ratios of sand." *Geotechnical Testing Journal*, 21(4), 336-347.
- Madsen, F.T. (1998). "Clay mineralogical investigations related to nuclear waste disposal." *Clay Minerals*, 33(1), 109-129.
- McGeary, R.K. (1961). "Mechanical packing of spherical particles." *Journal of the American Ceramic Society*, 44(10), 513-522.
- Mclsaac, R., and Rowe, R.K. (2005). "Change in leachate chemistry and porosity as leachate permeates through tire shreds and gravel." *Canadian Geotechnical Journal*, 42(4), 1173-1188.
- Messing, G.L., and Onada, G.Y. (1978). "Inhomogeneity - packing density relations in binary powders - experimental studies." *Journal of the American Ceramic Society*, 61(7-8), 363-366.
- Midttomme, K., and Roaldset, E. (1998). "The effect of grain size on thermal conductivity of quartz sands and silts." *Petroleum Geoscience*, 4(2), 165-172.
- Mitchell, J.K., and Soga, K. (2005). *Fundamentals of soil behavior*, 3rd ed., John Wiley & Sons, New Jersey.

- Montgomery, D.C., Runger, G.C., and Hubele, N.F. (2004). *Engineering statistics*, 3rd ed., John Wiley & Sons, New York.
- Murphy, W.F. (1982). "Effects of microstructure and pore fluids on the acoustic properties of granular sedimentary materials." PhD Thesis, Stanford University, Stanford.
- Naidu, A.D., and Singh, D.N. (2004). "Field probe for measuring thermal resistivity of soils." *Journal of Geotechnical and Geoenvironmental Engineering*, 130(2), 213-216.
- Norris, G. (1977). "The drained shear strength of uniform quartz sand as related to particle size and natural variation in particle shape and surface roughness." PhD Thesis, The University of California, Berkeley.
- Ould-Lahoucine, C., Sakashita, H., and Kumada, T. (2002). "Measurement of thermal conductivity of buffer materials and evaluation of existing correlations predicting it." *Nuclear Engineering and Design*, 216(1-3), 1-11.
- Ozkul, Z.H., and Baykal, G. (2007). "Shear behavior of compacted rubber fiber-clay composite in drained and undrained loading." *Journal of Geotechnical and Geoenvironmental Engineering*, 133(7), 767-781.
- Panayiotopoulos, K.P. (1989). "Packing of sands - a review." *Soil and Tillage Research*, 13(2), 101-121.
- Polito, C.P. (1999). "The effect of nonplastic and plastic fines on the liquefaction of sandy soils." PhD Thesis, Virginia Polytechnic Institute and State University, Blacksburg.
- Samley, I. (1970). "Cohesion of soil particles and the intrinsic resistance of simple soil system to wind erosion." *European Journal of Soil Science*, 21(1), 154-161.
- Sheehan, P.J., Warmerdam, J.M., Ogle, S., Humphrey, D.N., and Patenaude, S.M. (2006). "Evaluating the risk to aquatic ecosystems posed by leachate from tire shred fill in road using toxicity tests, toxicity identification evaluations, and groundwater modeling." *Environmental Toxicology and Chemistry*, 25(2), 400-411.

- Shinohara, K. (1984). "Rheological property of particulate solids." *Handbook of Powder Science and Technology* edited by M.E. Fayed, and L. Otten., Van Nostrand Reinhold Co., New York, 129-169.
- Smits, K.M., Sakaki, T., Limsuway, A., and Illangasekare, T.H. (2010). "Thermal conductivity of sands under varying moisture and porosity in drainage-wetting cycles." *Vadose Zone Journal*, 9(1), 172-180.
- Suzuki, M., and Oshima, T. (1983). "Estimation of the co-ordination number in a multi-component mixture of spheres." *Powder Technology*, 35(2), 159-166.
- Tanchaisawat, T., Bergado, D.T., Voottipruex, P., and Shehzad, K. (2008). "Interaction between geogrid reinforcement and tire chip-sand lightweight backfill." *Geotextiles and Geomembranes*, 28(1), 119-127.
- Tandon, V., Velazco, D.A., Nazarian, S., and Picornell, M. (2007). "Performance monitoring of embankment containing tire chips: case study." *Journal of Performance Constructed Facilities*, 21(3), 207-214.
- Tavman, I.H. (1996). "Effective thermal conductivity of granular porous materials." *International Communication in Heat and Mass Transfer*, 23(2), 169-176.
- Tweedie, J.J., Humphrey, D.N., and Sandford, T.C. (1998). "Tire shreds as lightweight retaining wall backfill: active condition." *Journal of Geotechnical and Geoenvironmental Engineering*, 124(11), 1061-1070.
- Wang, H.L., Shang, J.Q., Kovac, V., and Ho, K.S. (2006). "Utilization of Atikokan coal fly ash in acid rock drainage control from Musselwhite Mine tailings." *Canadian Geotechnical Journal*, 43(3), 229-243.
- Wartman, J., Natale, M.F., and Strenk, P.M. (2007). "Immediate and time-dependent compression of tire derived aggregate." *Journal of Geotechnical and Geoenvironmental Engineering*, 133(3), 245-256.
- White, H.E., and Walton, S.F. (1937). "Particle packing and particle shape." *Journal of the American Ceramic Society*, 20(1-12), 155-166.

- Yellishetty, M., Karpe, V., Reddy, E.H., Syubhash, K.N., and Ranjith, P.G. (2008). "Reuse of iron ore mineral wastes in civil engineering constructions: a case study." *Resources, Conservation and Recycling*, 52(11), 1283-1289.
- Youwai, S. and Bergado, D.T. (2003). "Strength and deformation characteristics of shredded rubber tire-sand mixtures." *Canadian Geotechnical Journal*, 40(2), 254-264.
- Yun, T.S., and Santamarina, J.C. (2008). "Fundamental study of thermal conduction in dry soils." *Granular Matter*, 10(3), 197-207.

Table 3.1 Densities and thermal properties of basic geomaterial constituents

Material	Particle density ρ (g/cm ³)	Thermal conductivity λ (W/mK)	Volumetric heat capacity C_v (MJ/m ³ K)
Air	0.00125 ^a	0.025 to 0.026 ^a (283 K)	1.25×10^{-3} ^a
Water	1 ^a	0.57 to 0.58 ^a (283 K)	4.18 ^a
Quartz	2.66 ^{a,b}	8.8 ^a (283 K)	2.01 ^a 2.13 ^b
Other minerals	2.65 ^{a,b}	2.0 ^{a†} (298 K) 3.5 ^{a‡} (298 K)	2.01 ^a 2.39 ^b
Organic matter	1.3 ^a	0.25 ^a (-)	2.51 ^a

[†] and [‡]: values are for feldspar and mica, and amphibolite, respectively.

^a Balland and Arp (2005)

^b Bristow (1998)

Table 3.2 Index properties of mine tailings and tire crumbs

Properties	Mine tailings	Tire crumbs
Specific gravity, G_s	3.374	1.190
Optimum water content, w_{opt} (%)	13.5	-
Maximum dry unit weight, $\gamma_{d \max}$ (kN/m ³)	19.5	-
Effective size, D_{10} (μm)	2.8	237.1
Median size, D_{50} (μm)	25.6	448.1
Coefficient of uniformity, C_u	11.43	2.08
Coefficient of curvature, C_c	1.61	0.96

Table 3.3 Particle size statistics of mine tailings and tire crumbs

Sample statistics	Mine tailings	Tire crumbs
Mode, D_m (μm)	45.7	425.0
Mean, \bar{D} (μm)	18.5	444.4
Standard deviation, σ (μm)	3.596	1.557
Skewness, Sk (μm)	-0.981	-1.043
Kurtosis, K (μm)	3.469	3.810

Table 3.4 Summary of packings and thermal properties of the mixtures tested

No.	Weight mixing ratio of tire crumbs R_{mW} (-)	Volumetric mixing ratio of tire crumbs R_{mV} (-)	Bulk unit weight γ_b (kN/m ³)	Porosity n (-)	Thermal conductivity λ (W/mK)	Volumetric heat capacity C_v (MJ/m ³ K)
1	0	0	13.3	0.60	0.140 (0.003) [†]	1.217 (0.003) [†]
2	0	0	14.8	0.55	0.166 (0.002)	1.287 (0.008)
3	0	0	16.2	0.51	0.204 (0.003)	1.452 (0.012)
4	0	0	17.1	0.48	0.226 (0.005)	1.574 (0.014)
5	0	0	18.7	0.44	0.248 (0.002)	1.677 (0.029)
6	0.1	0.240	12.8	0.54	0.138 (0.003)	1.259 (0.014)
7	0.1	0.240	13.9	0.50	0.155 (0.002)	1.312 (0.008)
8	0.1	0.240	15.2	0.46	0.189 (0.003)	1.501 (0.007)
9	0.1	0.240	16.8	0.40	0.218 (0.004)	1.617 (0.026)
10	0.1	0.240	17.7	0.37	0.245 (0.003)	1.728 (0.018)
11	0.2	0.415	11.2	0.54	0.127 (0.005)	1.272 (0.041)
12	0.2	0.415	12.5	0.48	0.146 (0.003)	1.362 (0.017)
13	0.2	0.415	13.4	0.45	0.164 (0.005)	1.447 (0.023)
14	0.2	0.415	14.5	0.40	0.186 (0.009)	1.642 (0.036)
15	0.2	0.415	15.4	0.36	0.220 (0.004)	1.731 (0.010)
16	0.3	0.549	10.2	0.52	0.123 (0.002)	1.255 (0.006)
17	0.3	0.549	10.9	0.49	0.139 (0.005)	1.325 (0.014)
18	0.3	0.549	11.9	0.44	0.166 (0.003)	1.491 (0.021)
19	0.3	0.549	12.6	0.41	0.176 (0.004)	1.542 (0.028)
20	0.3	0.549	13.6	0.36	0.209 (0.003)	1.711 (0.012)
21	0.4	0.654	8.7	0.55	0.114 (0.002)	1.181 (0.008)
22	0.4	0.654	9.4	0.51	0.127 (0.002)	1.278 (0.014)
23	0.4	0.654	9.9	0.48	0.131 (0.002)	1.304 (0.017)
24	0.4	0.654	10.4	0.46	0.145 (0.001)	1.397 (0.005)
25	0.4	0.654	11.1	0.42	0.165 (0.008)	1.532 (0.005)
26	0.5	0.739	7.5	0.56	0.113 (0.002)	1.157 (0.017)
27	0.5	0.739	7.8	0.55	0.118 (0.003)	1.191 (0.021)
28	0.5	0.739	8.3	0.52	0.121 (0.002)	1.207 (0.017)
29	0.5	0.739	8.5	0.51	0.131 (0.002)	1.294 (0.008)
30	0.5	0.739	9.1	0.47	0.138 (0.002)	1.354 (0.008)
31	0.6	0.810	6.8	0.57	0.104 (0.003)	1.131 (0.011)
32	0.6	0.810	7.2	0.54	0.110 (0.003)	1.194 (0.007)
33	0.6	0.810	7.6	0.52	0.117 (0.001)	1.240 (0.010)
34	0.6	0.810	8.0	0.49	0.126 (0.003)	1.307 (0.014)
35	0.8	0.919	5.2	0.62	0.089 (0.000)	0.987 (0.006)
36	0.8	0.919	5.6	0.58	0.097 (0.001)	1.061 (0.005)
37	0.8	0.919	6.0	0.55	0.104 (0.002)	1.124 (0.017)
38	1	1	3.8	0.68	0.073 (0.001)	0.811 (0.010)
39	1	1	4.0	0.66	0.076 (0.002)	0.855 (0.016)
40	1	1	4.3	0.63	0.080 (0.001)	0.901 (0.011)

[†] Standard deviation

Table 3.5 Summary of multiple linear regression analysis result

Observations	40		
R - squared	0.908		
Standard error	0.014		
F - value	182.5		
	Coefficients	Standard error	t - statistic
Intercept	0.368	0.015	24.007
R_{mV}	-0.079	0.008	-9.424
n	-0.353	0.033	-10.697

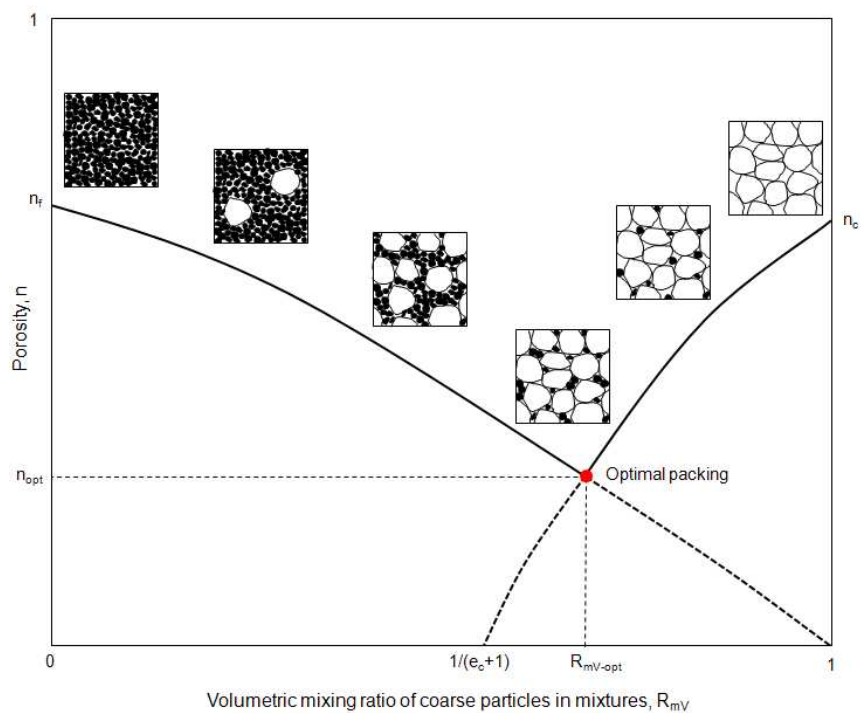


Figure 3.1 Porosity in binary packing against volumetric mixing ratio of coarse particles in mixtures (modified from Lade et al. (1998))

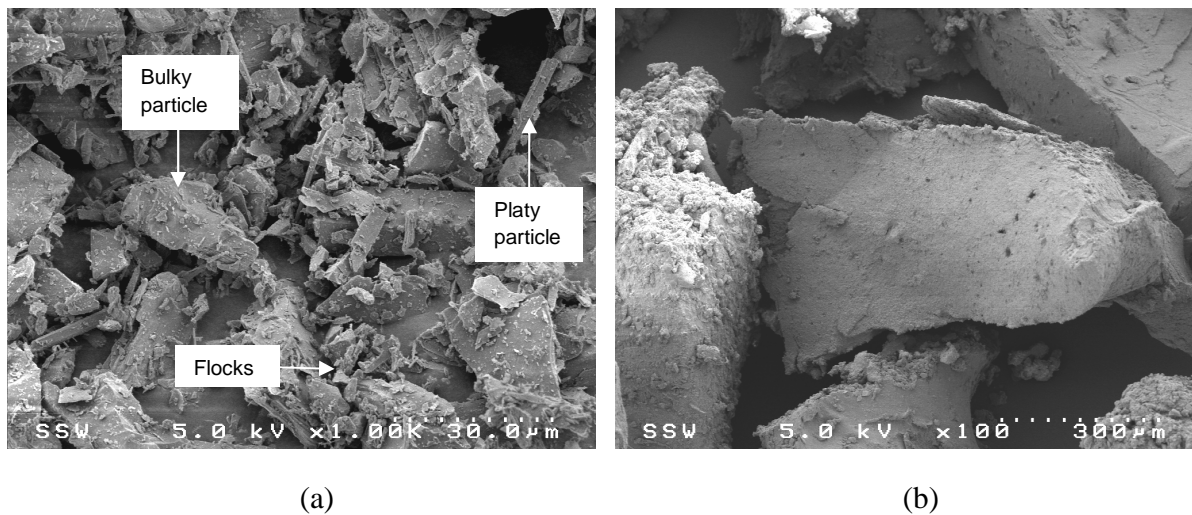
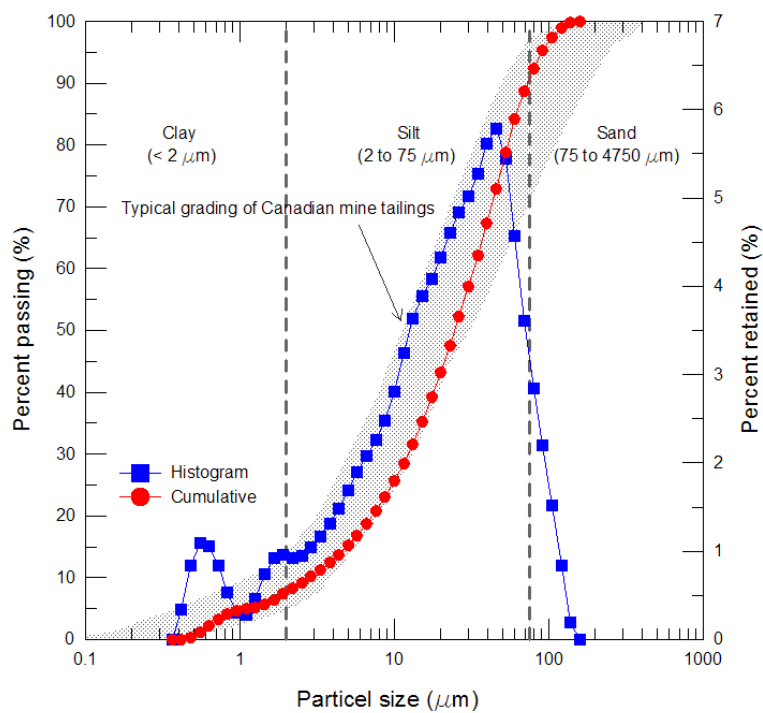
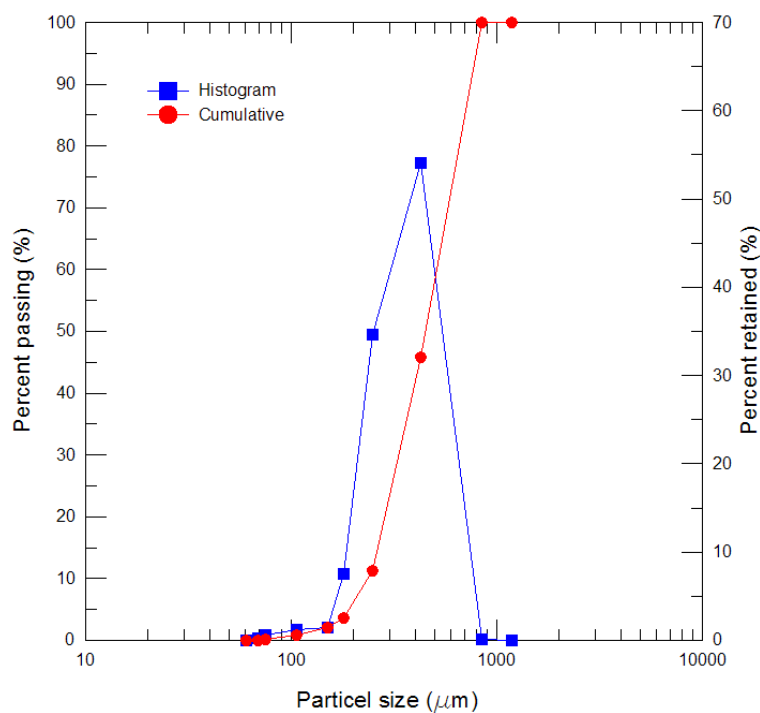


Figure 3.2 SEM images: (a) mine tailings; (b) tire crumbs



(a)



(b)

Figure 3.3 Particle size distribution curves: (a) mine tailings; (b) tire crumbs

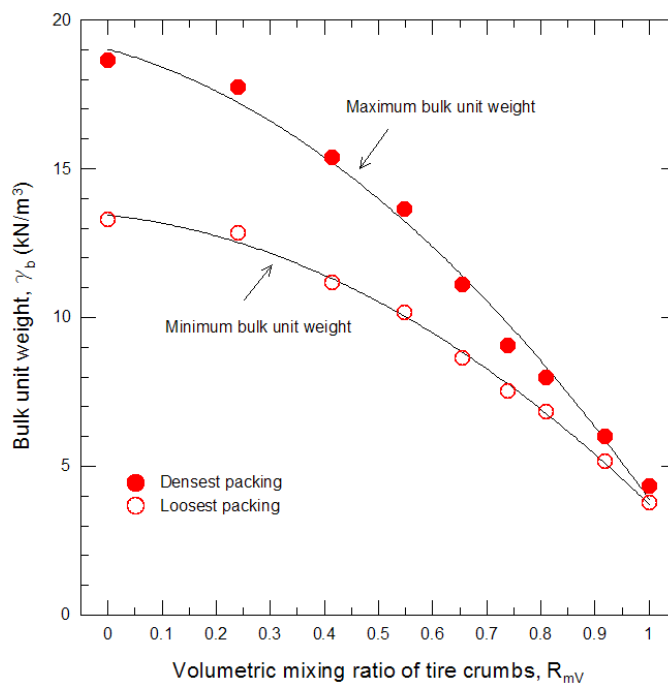


Figure 3.4 Variations of minimum and maximum bulk unit weights for mixtures of mine tailings and tire crumbs

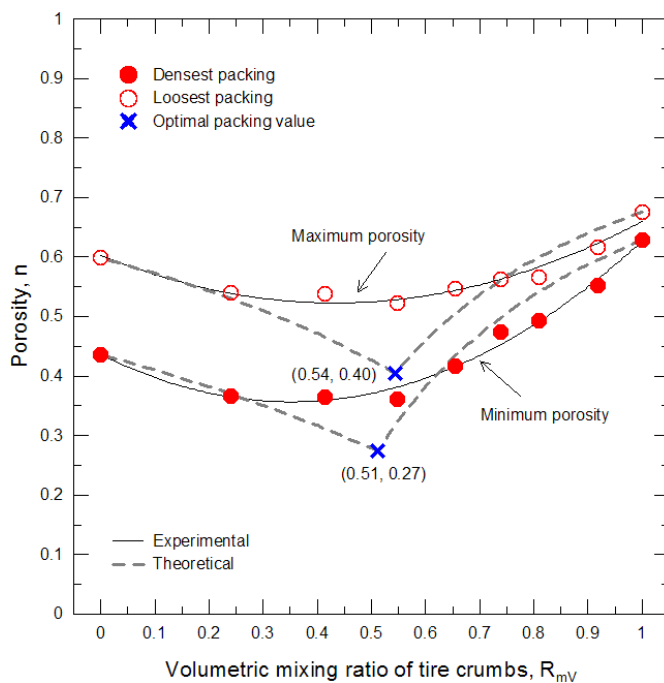


Figure 3.5 Variations of minimum and maximum porosities for mixtures of mine tailings and tire crumbs

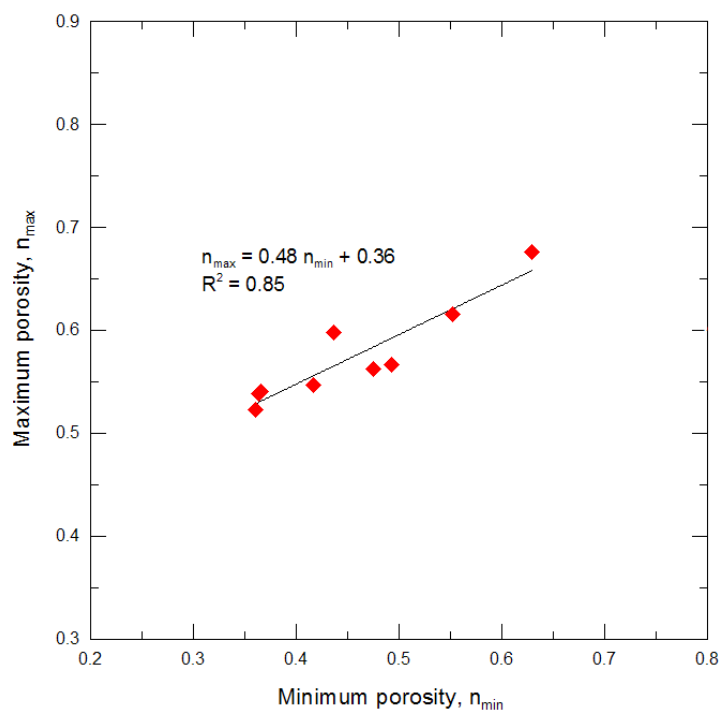


Figure 3.6 Correlation between minimum and maximum porosities

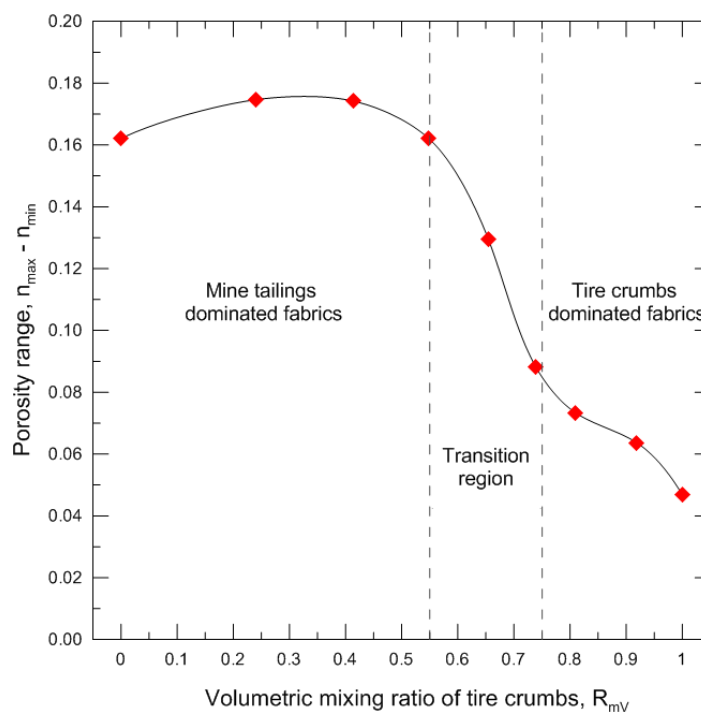


Figure 3.7 Change in porosity ranges for mixtures of mine tailings and tire crumbs

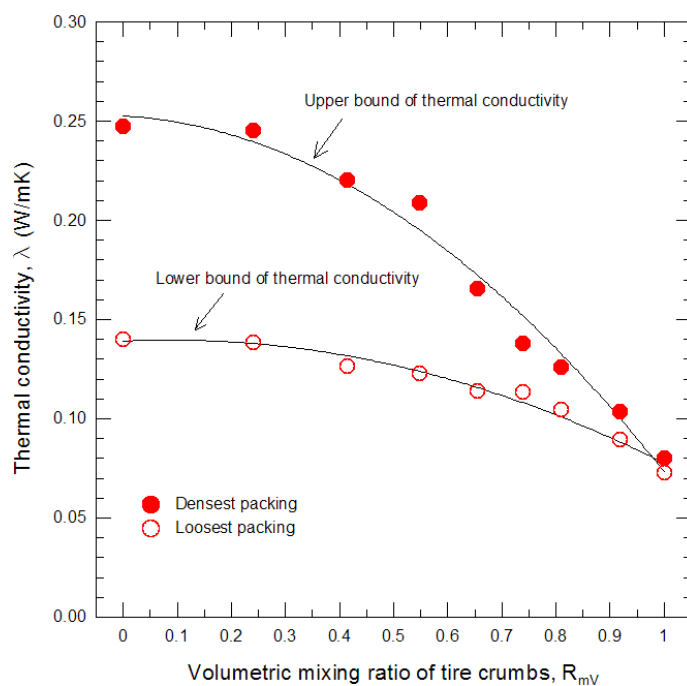


Figure 3.8 Relationships between thermal conductivity and volumetric mixing ratio of tire crumbs for loosest and densest packings for mine tailings and tire crumbs mixtures

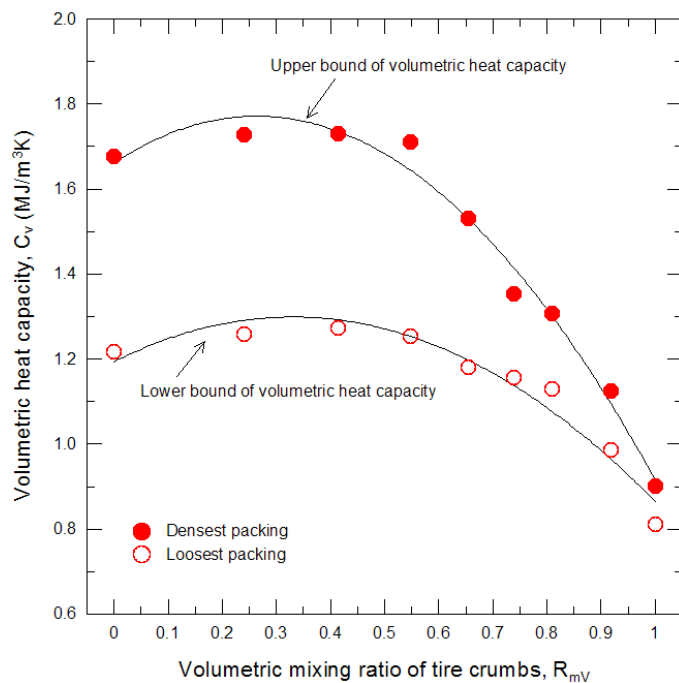


Figure 3.9 Relationships between volumetric heat capacity and volumetric mixing ratio of tire crumbs for loosest and densest packings for mine tailings and tire crumbs mixtures

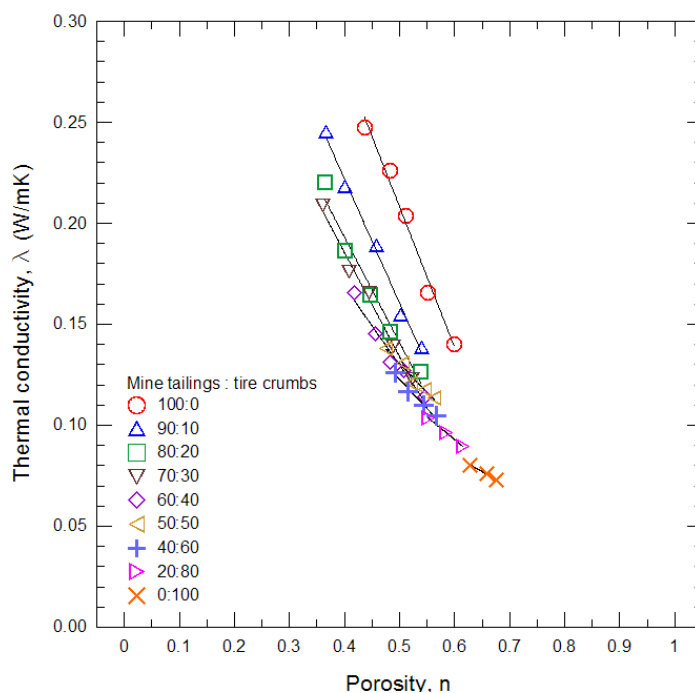


Figure 3.10 Effect of weight mixing ratio of mine tailings and tire crumbs mixtures on thermal conductivity

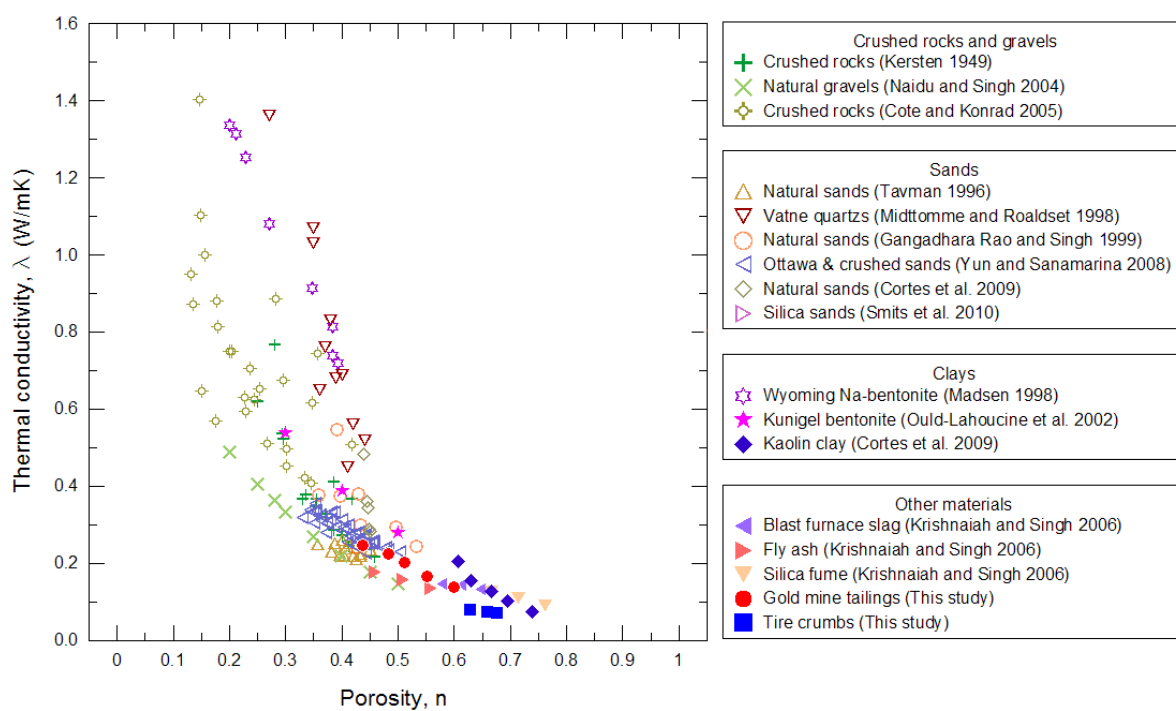


Figure 3.11 Thermal conductivity of various dry geomaterials

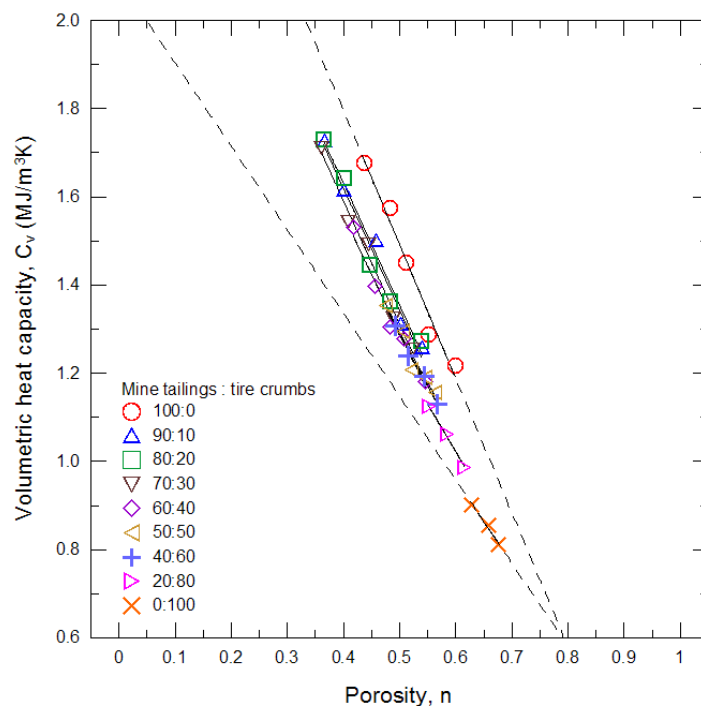


Figure 3.12 Effect of weight mixing ratio of mine tailings and tire crumbs mixtures on volumetric heat capacity

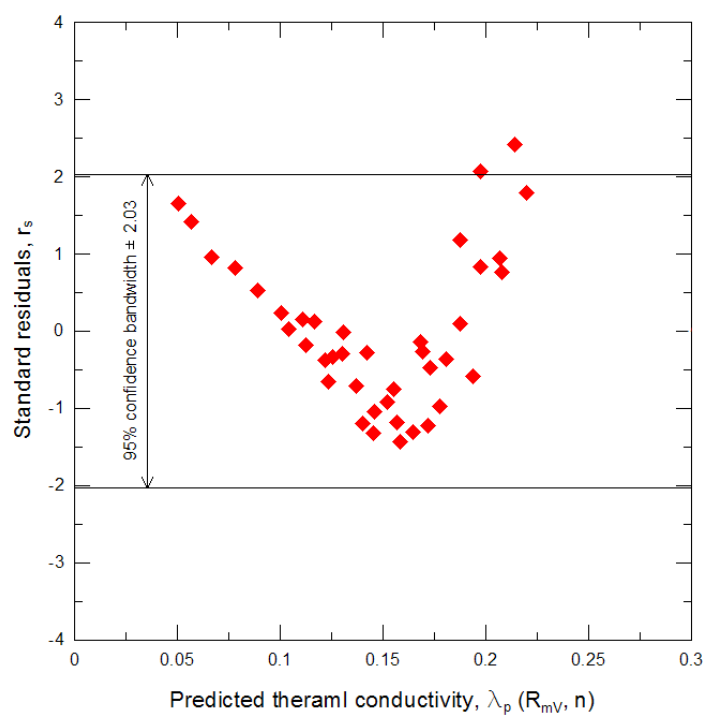


Figure 3.13 Standard residuals of a regression model with two variables

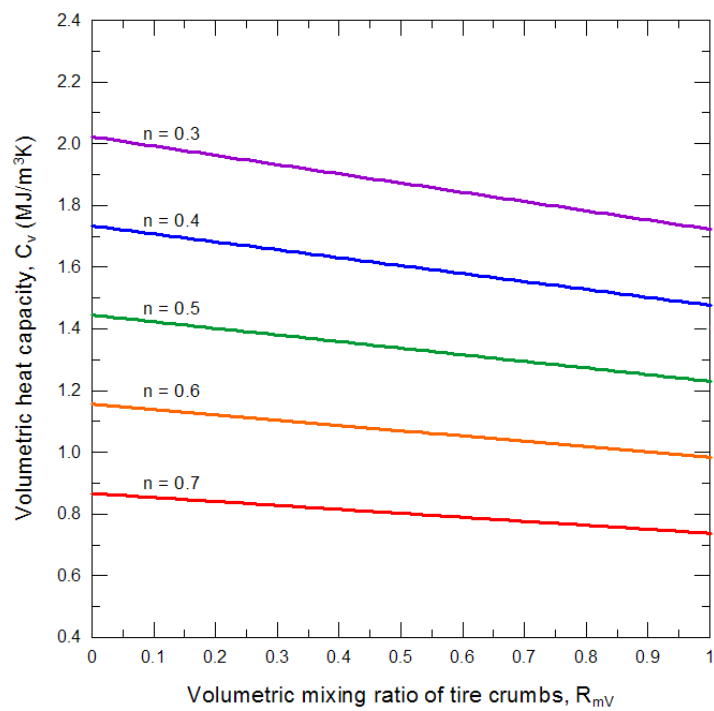


Figure 3.14 Change of volumetric heat capacity at different volumetric mixing ratios of tire crumbs and porosities

CHAPTER 4

THERMAL CONDUCTIVITY OF COMPACTED MIXTURES OF MINE TAILINGS AND TIRE CRUMBS

4.1 Introduction

Geomaterials mostly consist of mineral solids, water and air at various proportions. The study on heat transfer through geomaterials is important in geoenvironmental applications such as oil and gas pipelines, high-power electric cables, radioactive waste disposal facilities, ground heat exchangers, etc. Thermal transport takes place through conduction, convection and radiation, in which conduction is most predominant in granular materials and is quantified by the thermal conductivity.

The thermal conductivity of a geomaterial is strongly dependent on the volumetric fractions of its constituents. The thermal conductivities of basic geomaterial constituents vary across several orders of magnitude, for example, mineral solids (order of 10 W/mK), water (order of 1 W/mK) and air (order of 0.01 W/mK). Numerous studies have been reported on the thermal conductivity of geomaterials as influenced by the properties associated to their constituents, i.e., dry density, water content, degree of saturation, water vapors and ices, water flow, electrolyte type and concentration, and mineralogical compositions (Horai 1971; Steiner and Komle 1991; Abu-Hamdeh and Reeder 2000; Tarnawski et al. 2000; Bachmann et al. 2001; Ochsner et al. 2001; Yun et al. 2011). Moreover, the structure of geomaterials has a significant impact on their thermal conductivity. The term of structure refers to the combined effects of fabric (the geometrical configuration of solid particles of all size ranges, shapes and surface roughness) and bonding (the inter-particulate forces that hold particle together, including cementation,

electrostatic, electromagnetic and other forces) (Mitchell and Soga 2005). Woodsinde and Messmer (1961) pointed out that the cementation of particles is an effective process to increase the thermal conductivity of geomaterials. Narsilio et al. (2010) found that the improved extent/quality of contacts between inter-particles leads to better thermal conduction.

Reusing solid wastes in civil engineering applications can be beneficial to reduce greenhouse gas emissions. The solid wastes that have potential to be recycled for use as construction materials include scrap tires and mine tailings. Waste rubber tires exhibit low density, high durability, good thermal insulation, high energy absorption as well as relatively low cost. The scrap tires are grinded to particles of various sizes for practical purposes. According to ASTM D 6270 (ASTM 2008), granulated rubber is defined as particulate rubber composed of mainly non-spherical particles, normally less than 12 mm in size, that is commonly known as tire crumbs (Edinçliler et al. 2010). On the other hand, tailings from mining activities are ground rock particles from which valuable metals and minerals are extracted. Mine tailings are conventionally disposed on site and often used as fill material where natural soils are not available or abundant, provided that the generation of acid mine drainage (AMD) is prohibited. In combination, tire particles and mine tailings may be utilized in construction as fills. Chapter 3 examined the thermal characteristics of dry mixtures of low reactivity mine tailings and tire crumbs, suggesting their potential beneficial use as reduced weight fill materials with enhanced thermal insulation. A prediction model for the thermal conductivity and an analysis chart for estimating the volumetric heat capacity for mine tailings and tire crumbs mixtures in dry state were presented.

This paper is the continuation of the work presented in Chapter 3. Thermal conductivity measurements were performed on wet mixtures of mine tailings and tire crumbs. Forty

specimens were compacted under various water contents, mixing ratios, compactive efforts and tire crumbs sizes in the laboratory. Experimental results were presented to illustrate the general relations of thermal conductivity with the influencing factors. The thermal conductivity anisotropy of the compacted mixtures was also observed. Statistical data analysis was conducted to identify the significance of these influencing factors. A stepwise multiple linear regression analysis was also carried out to establish an empirical model for predicting the thermal conductivity of the compacted mine tailings and tire crumbs mixtures.

4.2 Experimental Design

To study the thermal conductivity characteristics of compacted mixtures of mine tailings and tire crumbs, an experimental program was designed and performed. The materials, specimen preparation, and devices and methodology are described in this section.

4.2.1 Materials

In this study, mine tailings and tire crumbs are the host materials used to produce the mixtures. Distilled water with the temperature of about 20 °C was used in compaction of the mixtures. The physical properties of the mine tailings and tire crumbs are summarized in Table 4.1, whereas Figure 4.1 shows the particle size distributions.

The dry mine tailings were recovered from the Musselwhite mine located in northern Ontario, Canada. The specific gravity of mine tailings is 3.37, which is greater than that of most soils. The Atterberg limit tests on tailings particles finer than 75 μm indicated that the mine tailings are non-plastic. The tailings comprise a wide range of particle sizes (0.42 to 138 μm), which is in the typical grading range of Canadian hard rock tailings (Bussiere 2007). The detailed mineralogical properties of the tailings tested in this study have been reported by Wang

et al. (2006). According to their results, the mine tailings contain relatively low percentage of sulphide minerals (i.e., 3% pyrrhotite by mass), comparing to that of other sulphide-containing mine tailings published in the literature (e.g., 80% pyrrhotite: Amaratunga 1995, 54% pyrite: Ouellet et al. 2006). On the other hand, the pH of the mine tailings is measured as 8.4, which is near neutral. This is mainly due to the addition of lime during the milling process and the presence of carbonates. Hence, the tailings exhibit relatively low reactivity.

The tire crumbs of two particle sizes were supplied by a tire recycling facility located in Ontario. Both tire crumbs contain no steel wires. The small tire crumbs contain a small amount of fiber dust. The specific gravities of small and large tire crumbs are measured as 1.19 and 1.16, respectively, which are comparable to those of tire derived aggregates reported in ASTM D 6270 (ASTM 2008). The particle sizes of small tire crumbs vary from 0.069 to 1.18 mm with the median particle size of 0.46 mm, whereas the particle sizes for large tire crumbs range from 0.25 to 4.75 mm with the median particle size of 2.1 mm. Based on the coefficients of uniformity and curvature (C_u and C_c), both tire crumbs can be characterized as poorly graded materials.

4.2.2 Specimen Preparation

The mixing ratio of tire crumbs in the mixtures, R_m , is based on the dry mass of solids and defined as

$$R_m = \frac{m_{TC}}{m_{MT} + m_{TC}} \quad (4.1)$$

where m_{TC} is the mass of tire crumbs and m_{MT} is the mass of mine tailings. Initially, six dry mixtures of mine tailings and tire crumbs were prepared: five with the mixing ratios of 0.0, 0.1,

0.2, 0.3 and 0.4 for small tire crumbs, and one with 0.2 for large tire crumbs. Each mixture was thoroughly mixed in a mechanical mixer.

After the preparation of a dry mixture, a predetermined mass of the mixture was mixed with distilled water of known mass to obtain the desired gravimetric water content. For each mixture, five molding water contents of 5 to 25% with an increment of 5% were used. After mixing with water, the mixture was compacted into a cylindrical mold of volume 943.7 cm^3 (101.6 mm diameter and 116.4 mm height) in accordance with the standard Proctor compaction procedures of ASTM D 698 (ASTM 2007). In the case of mixtures with small tire crumbs with a mixing ratio of 0.2, two specimens were also prepared with the modified Proctor in ASTM D 1577 (ASTM 2009) and reduced Proctor suggested by Daniel and Benson (1990). The reduced Proctor procedure is identical to the standard Proctor procedure but the number of blows per layer is reduced from 25 to 15. These compactive efforts were designed to simulate the compaction states generally encountered in the field. To minimize the variability in the compactive effort applied to each mixture, an automatic compaction equipment was utilized. Following compaction, the excess mixture was trimmed off from the mold, then the mass of the specimen in the mold was measured to determine the bulk density and dry density.

In this study, 40 specimens were tested and their identifications are presented in Table 4.2, with the mnemonic abbreviation noted below the table. For example, TC0.2-SP-S-W15 represents a specimen with the 0.2 mixing ratio of small tire crumbs and 15% water content, compacted under standard Proctor energy.

4.2.3 Devices and Methodology

All thermal conductivity measurements were made using a KD2 Pro thermal property analyzer. It consists of a handheld controller and a sensor. The sensor has two-parallel stainless-steel probes of 1.3 mm diameter and 30 mm length at a spacing 6 mm, which is inserted into subject medium. One of probes contains a heating element to generate a heat pulse into the medium between the probes and the other contains a thermocouple to measure the heat transported from the medium. The thermal conductivity of the medium is automatically determined from the temperature evolution with time based on the transient line heat source theory reported by Kluitenberg et al. (1995). This device reproduces thermal conductivity of reference materials with $\pm 5\%$ accuracy within the temperature range of - 50 to 150 °C and a single measurement approximately takes 2 minutes.

For the thermal conductivity measurement, the compacted mixture of mine tailings and tire crumbs was extruded from the mold using a hydraulic jack. Figure 4.2 shows a uniformly compacted specimen with the mixing ratio of small tire crumbs of 0.2 and the water contents of 15%, i.e., specimen TC0.2-SP-S-W15. In order to explore the anisotropy of the thermal conductivity, the direction of measurement on the specimen was controlled: 1) the thermal conductivity perpendicular to the principal axis of the cylinder (representing the horizontal thermal conductivity) was measured by inserting the sensor perpendicular to the orientation of compaction; 2) the thermal conductivity along the principal axis of the cylinder (representing the vertical thermal conductivity) was measured by inserting the sensor parallel to the orientation of compaction. At top and bottom layers of the compacted specimen, respectively, two sets of horizontal and vertical thermal conductivities were tested with eight readings taken in each

specimen. The thermal conductivity measurements were carried out at the room temperature of 20 ± 0.5 °C.

4.3 Methods of Data Analysis

Based on the results of thermal conductivity measurement on compacted mine tailings and tire crumbs mixtures, statistical analyses were performed as follows: 1) the mean, median and standard deviation of four readings corresponding to the “horizontal” and “vertical” thermal conductivities (λ_h and λ_v) were calculated; 2) the same statistical estimates of eight readings from all horizontal and vertical thermal conductivities measured from each specimen were computed and represented as the “overall” thermal conductivity λ . The summary of the thermal conductivity measurement and statistical data is presented in Table 4.2.

To observe the trends of thermal conductivity against the effects of the influencing factors (i.e., water content, mixing ratio, compactive effort and tire crumbs size) of the compacted mixtures, the means of horizontal, vertical and overall thermal conductivities and their standard deviations were plotted with respect to the influencing factors. Analysis of variance (ANOVA) was then carried out to assess, in quantitative terms, the relative contributions of the influencing factors on the thermal conductivity of compacted mixtures. Stepwise multiple linear regression analysis was also employed to predict the thermal conductivity of the compacted mixtures. These statistical analyses were conducted by using 320 raw data (= 40 specimens \times 8 test points).

4.4 Results and Discussion

4.4.1 Compaction Characteristics

Figure 4.3 shows the changes in maximum dry density, $\rho_{d \max}$, and optimum water content, w_{opt} , with the mixing ratio of small tire crumbs. The maximum dry density ranges from 1.99 to 1.23 g/cm³, while the optimum water content varies from 12.7 to 17.3%. The maximum dry density decreases with the increase in the mixing ratio of tire crumbs. This is due to the reduced specific gravity of the mixtures with higher fraction of tire crumbs. On the other hand, the optimum water content slightly decreases first, then increases with increasing mixing ratio of tire crumbs. This can be interpreted as that with the increase of tire crumbs, more water is required to re-orientate solid particles during compaction. Similar compaction behavior was reported for mixtures of soils and tire particles in the literature (Cetin et al. 2006; Christ and Park 2010). Moreover, the significant increase of optimum water content is observed in the mixing ratios of tire crumbs $R_m > 0.3$. In this case, the compacted mixtures transit from a rigid mine tailings dominated fabric to a soft tire crumbs dominated fabric, based on the packing mechanism on a binary mixture of particles of different sizes (Lade et al. 1998).

4.4.2 Thermal Conductivity Characteristics

Figures 4.4-4.6 show the bulk density, ρ_b , and thermal conductivity, λ , of the compacted specimens of mine tailings and tire crumbs mixture versus the water content, as related to the mixing ratio of tire crumbs, compactive effort and tire crumbs size, respectively.

Figure 4.4 illustrates the variations of bulk density and thermal conductivity for the compacted mixtures with different mixing ratios of small tire crumbs. The bulk density of the

specimens decreases with increasing mixing ratio of tire crumbs for a given water content. For example, the bulk densities are 2.28, 2.02, 1.81, 1.61 and 1.41 g/cm³, respectively, when the mixing ratio of tire crumbs are 0, 0.1, 0.2, 0.3 and 0.4 at a water content of 15%. The bulk density decreases by 38% when the mixing ratio of tire crumbs is increased from 0 to 0.4 at a water content of 15%. Furthermore, at a given water content, the thermal conductivity of the specimens decreases with increasing mixing ratio of tire crumbs. For instance, the thermal conductivities are 1.610, 1.195, 0.925, 0.742 and 0.543 W/mK, respectively, when the mixing ratio of tire crumbs are 0, 0.1, 0.2, 0.3 and 0.4 at a water content of 15%. The thermal conductivity decreases by 66% when the mixing ratio of tire crumbs is increased from 0 to 0.4 at a water content of 15%. The reduction of both the bulk density and thermal conductivity is mainly due to the low density and low thermal conductivity of tire rubber particles. However, it should be noted that the air content of the specimens increases with increasing mixing ratio of tire crumbs, which adds to the decrease in bulk density and thermal conductivity to a minor extent. This is attributed to the fact that the angular shape and rough surface of rubber particles that are produced through the mill process have a tendency to entrap air. It is inferred from these results that recycled tire crumbs have potential applications as lightweight fill materials with improved thermal insulation.

Figure 4.5 highlights the effect of compactive effort on the bulk density and thermal conductivity of compacted mixtures of small tire crumbs with the mixing ratio of 0.2. The highest values of bulk density and thermal conductivity of the specimens are attained at the modified Proctor, followed by the standard Proctor and the reduced Proctor. As seen in Figure 4.5, at a constant water content of 15%, specimens with bulk densities of 1.83, 1.81 and 1.70 g/cm³ corresponding to modified, standard and reduced Proctors have thermal conductivities of

0.957, 0.925 and 0.807 W/mK, respectively. The increase in the thermal conductivity with the increase of compactive effort is probably because the higher compactive effort induces better contact between neighboring solid particles for heat transfer.

Figure 4.6 compares the bulk densities and thermal conductivities of the compacted mixtures with the same mixing ratio of tire crumbs but different tire crumbs sizes. As shown in Figures 4.6(a) and 4.6(b), the specimens with small tire crumbs have the lower bulk density and thermal conductivity than those mixed with large tire crumbs. Quantitatively, the bulk densities of the specimens with small tire crumbs are 2 to 6% less than those of large tire crumbs and the thermal conductivities are 3 to 12% lower. The differences in both the bulk density and thermal conductivity of the specimens with different tire crumbs size are highly related to the air content in their matrix since air has much lower density/thermal conductivity than water and solids: the increase in the air content with decreasing tire crumbs size leads to lower bulk density and thermal conductivity. It is confirmed in Figure 4.6(c), in which the volumetric air content θ_a (the volumetric ratio of air to the total volume of a compacted mixture) is determined by

$$\theta_a = 1 - w\rho_d - \frac{\rho_d}{G_s} \quad (4.2)$$

where w is the water content, ρ_d is the dry density of the mixture and G_s is the specific gravity of the mixture. As seen in Figure 4.6, the volumetric air content of specimens with small tire crumbs is more than that of specimens with large tire crumbs under all water contents. This is likely due to the fact that small tire crumbs exhibit higher specific surface that results in higher air-entrainment in their rough surface than large tire crumbs. Given the conduction mechanism at the microscale, the increase in the air content with decreasing tire crumbs size attenuates the thermal bridge between solid particles and contributes to the decrease in heat conduction.

In general, it is observed in Figures 4.4-4.6 that the changes of bulk density and thermal conductivity with the water content display a similar trend: at a given compactive effort, the bulk density and thermal conductivity increase with increasing water content, until the maximum bulk density and maximum thermal conductivity are reached. Then, both the bulk density and thermal conductivity slightly decrease with further increase in the water content. This trend can be explained as follows: as water is added to a mine tailings and tire crumbs mixture, it replaces the air, provoking increased bulk density as well as forms a thin film around the tailings solids and rubber particles, acting as a thermal bridge for heat transfer; as the water content increases, the pore air is replaced by water and solids, causing significant increases in the bulk density and thermal conductivity; however, beyond a certain water content, the water takes up the space that would have been occupied by the solids with little change of air volume near saturation, resulting in slight reduction of bulk density and thermal conductivity (see Figure 4.6). It is also found that a maximum thermal conductivity tends to occur at the optimal water content corresponding to the maximum bulk density, indicating the closest arrangement of solid particles. Similar observations were obtained for fine-grained soils by Salomone and Kovacs (1983, 1984) who used the term “critical water content” that is correlated to the optimum water content. Thus, it can be demonstrated that the influence of water content on the thermal conductivity of the compacted mine tailings and tire crumbs mixtures is more prominent when the water content is less than the critical water content. On the other hand, the impact is minor when the water content is higher than the critical water content. The critical water content is dependent on the mixing ratio of tire crumbs, compactive effort and tire crumbs size, which is essentially associated to the gradation, size, shape, surface roughness of the materials. Meanwhile, it is worth noting that the thermal conductivity difference that is attributable to varying water

contents leads to the difference in microstructures formed during compaction. For instance, Delage et al. (1996) investigated the impacts of water content change on the fabric of compacted soils and pointed out that compaction on the dry side induces aggregate-dominated fabric whereas the wet side causes matrix-dominated fabric without apparent aggregates.

Figure 4.7 shows the thermal conductivity, λ , versus bulk density, ρ_b , of all specimens. The thermal conductivity increases with increasing bulk density with a linear correlation ($R^2 = 0.93$). Therefore, one may recognize that the bulk density is a key property in heat transfer of compacted geomaterials.

4.4.3 Anisotropy of Thermal Conductivity

Compacted geomaterials may form anisotropic fabrics attributed to the pore structure and particle orientation. The fabric anisotropy often induces the anisotropy of engineering properties (Mitchell and Soga 2005). In particular, the anisotropy of thermal conductivity of compacted geomaterials may be significant in heat transfer.

The horizontal thermal conductivity, λ_h , versus vertical thermal conductivity, λ_v , for all specimens are plotted in Figure 4.8(a). The thermal conductivity of the compacted mine tailings and tire crumbs mixtures shows to be slightly anisotropic: the horizontal thermal conductivities are higher than the vertical thermal conductivities with a difference less than 15%. The anisotropy ratio η of thermal conductivity can be expressed as

$$\eta = \frac{\lambda_h}{\lambda_v} \quad (4.3)$$

The linear regression of data in Figure 4.8(a) yields an anisotropy ratio of 1.05 ($R^2 = 0.99$). The anisotropy may, in part, be due to the pore orientation as well as mineral and rubber bedding. Meanwhile, the role of water content in the thermal conductivity anisotropy of the compacted mine tailings and small tire crumbs mixture is illustrated in Figures 4.8(b) and 4.8(c). The anisotropy impact is more evident at lower water contents, regardless of the mixing ratio of tire crumbs, compactive effort and tire crumbs size. In general, there is no significant effect of the mixing ratio of tire crumbs on the thermal conductivity anisotropy. Anisotropy is also independent of the compactive effort and tire crumbs sizes considered in this study. This observation on the influence of water content to the thermal conductivity anisotropy of the compacted mixtures is consistent with the understanding of the microstructure of compacted geomaterials, discussed previously.

4.5 Statistical Analyses

The experimental results on compacted mixtures of mine tailings and tire crumbs have been presented in Figures 4.4-4.6 to demonstrate the correlations of the thermal conductivity as related to the compositional and compaction factors. In this section, the statistical significance of these data is analyzed. An ANOVA study was conducted by the general linear modeling procedure of a statistical analysis software (SAS). Statistical significance was established when the calculated F values exceeded the critical F values for a significance level of 5% (Montgomery et al. 2004). The calculated F values, defined as the ratio of the between-samples sum of squares to the error sum of squares, estimate the random error. The critical F value is the upper limit of the F ratio and can be found in statistical references. The p value is the tail probability for a given distribution, which will be less than 0.05 whenever the calculated F value is greater than the

critical F value, which is an indicator of the statistical significance in relation to the contribution of a given variable.

A four-factor ANOVA was carried out with the thermal conductivities measured on compacted mine tailings and tire crumbs mixtures, which included four variables: water content (A); mixing ratio of tire crumbs (B); compactive effort (C); and tire crumbs size (D); and their two way interactions with the water content (AB, AC and AD). The results of the ANOVA analysis are summarized in Table 4.3. It is shown that at a 95% confidence level, all factors affect the thermal conductivity significantly, and the mixing ratio of tire crumbs has the most significant influence. The significance of the four factors on the thermal conductivity of the compacted mixtures is identified in the following order: the mixing ratio of tire crumbs, water content, whereas the tire crumbs size and compactive effort show the similar significance level. On the other hand, the two way interactions between the water content and other two factors, the mixing ratio of tire crumbs and compactive effort, are statistically significant; while the interaction of water content and tire crumbs size is not significant statistically to the variations of the thermal conductivity.

A stepwise multiple linear regression analysis was utilized to develop an empirical model to capture the impact of the influencing factors on the thermal conductivity of the compacted mine tailings and tire crumbs mixtures. Since the compactive effort is not a quantitative variable, a multisource regression model that includes class independent variables as well as quantitative independent variables was established. The developments of the multisource regression model in geoenvironmental applications were reported in the literature (Benson and Trast 1995; Nazzal et al. 2007). In stepwise regression procedures, the regression model was optimized by repeating the procedures that add or delete an independent variable after checking its correlation with the

dependent variables until the selection of an additional independent variable did not increase the coefficient of determination (R^2) by a 5% level of significance (Brook and Arnold 1985). The significance of the variables in a regression model can be evaluated by comparing the calculated t value, defined as the ratio of the regression coefficient β_i and its standard error SE , and the student's t distribution. In other word, if the absolute value of calculated t value is less than the student's t distribution at a designed significance level, the variable is not affected significantly to the regression model.

According to the stepwise regression analysis, it is found that the following equation best fits the data:

$$\lambda = 0.989 + 0.021w - 2.177 R_m + 0.053 CE \quad (4.4)$$

in which w is the water content, R_m is the mixing ratio of tire crumbs. CE is the integer class index representing compactive effort (compactive effort index): the $CE = 1$ is designated to the energy level of the modified Proctor compaction; the $CE = 0$ is designated to the energy level of the standard Proctor compaction; and the $CE = -1$ is designated to the energy level of the reduced Proctor compaction. The tire crumbs size did not give any additional information with statistical significance. One of possible reasons for this is that the data set is limited to only two. The values of regression coefficient of the variables suggest that increasing water content and compactive effort leads to the increase in the thermal conductivity whereas increasing mixing ratio of tire crumbs results in the decrease in the thermal conductivity. This is consistent with the trends observed in Figures 4.4-4.6.

Table 4.4 presents the results of regression analysis on Eq. (4.4) under a confidence level of 95%. The coefficient of determination and standard error of the regression model are 0.867 and

0.113, respectively, indicating Eq. (4.4) fits the measured data very well. Figure 4.9 shows that the predicted thermal conductivity λ_p , using the proposed model yields good agreement with the measured thermal conductivity λ_m . The overall F value is 688.6, much greater than the F value at the probability of 95% = 2.633. This indicates that the regression equation (Eq. (4.4)) with four variables is statistically significant. Moreover, all absolute t values in Table 4.4 are greater than the t value = 1.968 at the probability of 95%, implying that the water content, mixing ratio of tire crumbs, compactive effort index and intercept are contributed significantly to the regression model. Comparing to the t values obtained, the effect of the mixing ratio of tire crumbs to the observed trend is greater than those other influencing factors, which is consistent with the results from the four factor ANOVA test. Consequently, the regression equation relating to the water content w , mixing ratio of tire crumbs R_m and compactive effort index CE is highly significant at 95% confidence limits as indicated by statistical analyses. The results provide a insight to the thermal conductivity of the compacted mine tailings and tire crumbs mixtures as affected by the water content, mixing ratio of tire crumbs, compactive effort and tire crumbs size.

4.6 Conclusions

Mine tailings and tire crumbs are recycled solid wastes, and their mixtures can be beneficially used as reduced weight fill materials with improved thermal insulation for geoen지니어ing applications. Results of thermal conductivity tests performed on compacted mixtures of mine tailings and tire crumbs were presented, and analyzed to identify the effect of water content, mixing ratio of tire crumbs, compactive effort and tire crumbs size on the thermal conductivity. The anisotropy of thermal conductivity was observed on compacted mixtures. The following is the main conclusion of this study.

The thermal conductivity of the compacted mine tailings and tire crumbs mixtures depends on the water content, mixing ratio of tire crumbs, compactive effort and tire crumbs size. The thermal conductivity is sensitive to the water content when it is lower than a critical water content, while it is almost independent of the water content after the critical water content is exceeded. The thermal conductivity decreases with increasing the mixing ratio of tire crumbs. A higher compactive effort leads to a higher thermal conductivity, and the compacted mixtures with small tire crumbs have lower thermal conductivity than those with large tire crumbs. Linear relationship is established between the thermal conductivity and bulk density for all specimens tested.

There is a clear indication of thermal conductivity anisotropy of the compacted mixtures: the horizontal thermal conductivities are higher than the vertical thermal conductivities with a difference less than 15%. The anisotropy ratio of the thermal conductivity is estimated to be 1.05. The thermal conductivity anisotropy is dependent on the water content: as the water content increases, the thermal conductivity anisotropy reduces. In contrast, the mixing ratio of tire crumbs, compactive effort and tire crumbs size show little influence on the thermal conductivity anisotropy.

The ANOVA results indicate that the thermal conductivity of the compacted mixtures is significantly affected by the water content, mixing ratio of mine tailings and tire crumbs, compactive effort and size of tire crumbs at a confidence level of 95%. The stepwise multiple linear regression analysis shows that the thermal conductivity of the compacted mixtures can be predicted using a general model consisting of the mixture composition as quantitative variable and compaction condition as an index variable.

The findings and interpretation methods presented in this study will be helpful for comprehending the thermal conductivity behaviors of compacted rubberized geomaterials.

References

- Abu-Hamdeh, N.H., and Reeder, R.C. (2000). "Soil thermal conductivity: effects of density, moisture, salt concentration, and organic matter." *Soil Science Society of America Journal*, 64(4), 1285-1290.
- Amaratunga, L.M. (1995). "Cold-bond agglomeration of reactive pyrrhotite tailings for backfill using low cost binders: Gypsum β -Hemihydrate and cement." *Minerals Engineering*, 8(12), 1455-1465.
- ASTM. (2007). "Standard test methods for laboratory compaction characteristics of soil using standard effort [12,400 ft-lb/ft³ (600 kN-m/m³)]." *D698-07*, West Conshohocken, Pa.
- ASTM. (2008). "Standard practice for use of scrap tires in civil engineering applications." *D6270-08*, West Conshohocken, Pa.
- ASTM. (2009). "Standard test methods for laboratory compaction characteristics of soil using modified effort [56,000 ft-lb/ft³ (2,700 kN-m/m³)]." *D1557-09*, West Conshohocken, Pa.
- Bachmann, J., Horton, R., Ren, T., and Van Der Ploeg, R.R. (2001). "Comparison of the thermal properties of four wettable and four water-repellent soils." *Soil Science Society of America Journal*, 65(6), 1675-1679.
- Benson, C.H., and Trast, J.M. (1995). "Hydraulic conductivity of thirteen compacted clays." *Clays and Clay Minerals*, 43(6), 669-681.
- Brook, R.J., and Arnold, G.C. (1985). *Applied regression analysis and experimental design*, Marcel Dekker, New York.
- Bussiere, B. (2007). "Colloquium 2004: hydrogeotechnical properties of hard rock tailings from metal mines and emerging geoenvironmental disposal approaches." *Canadian Geotechnical Journal*, 44(9), 1019-1052.

- Cetin, H., Fener, M., and Gunaydin, O. (2006). "Geotechnical properties of tire-cohesive clayey soil mixtures as a fill material." *Engineering Geology*, 88(1-2), 110-120.
- Christ, M., and Park, J. (2010). "Laboratory determination of strength properties of frozen rubber-sand mixtures." *Cold Regions Science and Technology*, 60(2), 169-175.
- Daniel, D.E., and Benson, C.H. (1990). "Water content-density criteria for compacted soil liners." *Journal of Geotechnical and Geoenvironmental Engineering*, 116(12), 1811-1830.
- Delage, P., Audiguier, M., Cui, Y., and Howat, M.D. (1996). "Microstructure of a compacted silt." *Canadian Geotechnical Journal*, 33(1), 150-158.
- Edinçliler, A., Baykal, G., and Saygili, A. (2010). "Influence of different processing techniques on the mechanical properties of used tires in embankment construction." *Waste Management*, 30(6), 1073-1080.
- Horai, K.I. (1971). "Thermal conductivity of rock-forming minerals." *Journal of Geophysical Research*, 76(5), 1278-1308.
- Kluitenberg, G.J., Bristow, K.L., and Das, B.S. (1995). "Error analysis of heat pulse method for measuring soil heat capacity, diffusivity, and conductivity." *Soil Science Society of America Journal*, 59(3), 719-726.
- Lade, P.V., Liggió, C.D., and Yamamuro, J.A. (1998). "Effects of non-plastic fines on minimum and maximum void ratios of sand." *Geotechnical Testing Journal*, 21(4), 336-347.
- Mitchell, J.K., and Soga, K. (2005). *Fundamentals of soil behavior*, 3rd ed., John Wiley & Sons, New Jersey.
- Montgomery, D.C., Runger, G.C., and Hubele, N.F. (2004). *Engineering statistics*, 3rd ed., John Wiley & Sons, New York.
- Narsilio, G.A., Kress, J., and Yun, T.S. (2010). "Characterization of conduction phenomena in soils at the particle-scale: finite element analyses in conjunction with synthetic 3D imaging." *Computers and Geotechnics*, 37(7-8), 828-836.

- Nazzal, M., Abu-Farsakh, M., and Mohammad, L. (2007). "Laboratory characterization of reinforced crushed limestone under monotonic and cyclic loading." *Journal of Materials in Civil Engineering*, 19(9), 772-783.
- Ochsner, T.E., Horton, R., and Ren, T. (2001). "A new perspective on soil thermal properties." *Soil Science Society of America Journal*, 65(6), 1641-1647.
- Ouellet, S., Bussiere, B., Mbonimpa, M., Benzaazoua, M., and Aubertin, M. (2006). "Reactivity and mineralogical evolution of an underground mine sulphidic cemented paste backfill." *Minerals Engineering*, 19(5), 407-419.
- Salomone, L.A., and Kovacs, W.D. (1983). "The use of property tests to determine the thermal properties of soils." *Geotechnical Testing Journal*, 6(4), 173-180.
- Salomone, L.A., and Kovacs, W.D. (1984). "Thermal resistivity of soils." *Journal of Geotechnical Engineering*, 110(3), 375-389.
- Steiner, G., and Komle, N.I. (1991). "A model of the thermal conductivity of porous water ice at low gas pressure." *Planetary and Space Science*, 39(3), 507-513.
- Tarnawski, V.R., Leong, W.H., and Bristow, K.L. (2000). "Developing a temperature-dependent Kersten function for soil thermal conductivity." *International Journal of Energy Research*, 24(15), 1335-1350.
- Wang, H.L., Shang, J.Q., Kovac, V., and Ho, K.S. (2006). "Utilization of Atikokan coal fly ash in acid rock drainage control from Musselwhite Mine tailings." *Canadian Geotechnical Journal*, 43(3), 229-243.
- Woodsinde, W., and Messmer, J.M. (1961). "Thermal conductivity of porous media." *Journal of Applied Physics*, 32(9), 1688-1706.
- Yun, T.S., Dumas, B., and Santamarina, J.C. (2011). "Heat transport in granular materials during cyclic fluid flow." *Granular Matter*, 13(1), 29-37.

Table 4.1 Physical properties of mine tailings and tire crumbs

Properties	Mine tailings	Tire crumbs	
		Small size	Large size
Specific gravity, G_s	3.37	1.19	1.16
Effective size, D_{10} (mm)	0.0028	0.24	1.0
Median size, D_{50} (mm)	0.0256	0.46	2.1
Coefficient of uniformity, C_u	11.4	2.08	2.20
Coefficient of curvature, C_c	1.6	0.96	0.89

Table 4.2 Summary of horizontal, vertical and overall thermal conductivities of compacted mixtures tested

Specimen ID	λ_h^*			λ_v^*			λ^{**}		
	Median (W/mK)	Mean (W/mK)	SD (W/mK)	Median (W/mK)	Mean (W/mK)	SD (W/mK)	Media (W/mK)	Mean (W/mK)	SD (W/mK)
TC0.0-SP-S-W5	1.011	1.017	0.059	0.869	0.869	0.055	0.943	0.943	0.095
TC0.0-SP-S-W10	1.303	1.302	0.007	1.179	1.180	0.008	1.243	1.241	0.066
TC0.0-SP-S-W15	1.635	1.638	0.015	1.579	1.582	0.011	1.611	1.610	0.032
TC0.0-SP-S-W20	1.604	1.600	0.018	1.557	1.558	0.004	1.570	1.579	0.026
TC0.0-SP-S-W25	1.593	1.599	0.033	1.606	1.604	0.011	1.600	1.601	0.023
TC0.1-SP-S-W5	0.731	0.733	0.066	0.645	0.645	0.059	0.687	0.689	0.075
TC0.1-SP-S-W10	1.151	1.147	0.062	1.073	1.074	0.049	1.109	1.111	0.065
TC0.1-SP-S-W15	1.216	1.219	0.013	1.169	1.170	0.013	1.197	1.195	0.029
TC0.1-SP-S-W20	1.202	1.211	0.018	1.174	1.176	0.007	1.190	1.194	0.024
TC0.1-SP-S-W25	1.232	1.243	0.030	1.220	1.219	0.003	1.222	1.231	0.024
TC0.2-SP-S-W5	0.593	0.587	0.051	0.511	0.509	0.052	0.554	0.548	0.063
TC0.2-SP-S-W10	0.784	0.786	0.049	0.724	0.723	0.042	0.749	0.755	0.054
TC0.2-SP-S-W15	0.943	0.940	0.013	0.911	0.910	0.017	0.925	0.925	0.021
TC0.2-SP-S-W20	0.947	0.945	0.023	0.907	0.904	0.028	0.928	0.925	0.035
TC0.2-SP-S-W25	0.933	0.933	0.020	0.927	0.926	0.029	0.933	0.930	0.023
TC0.3-SP-S-W5	0.442	0.443	0.050	0.401	0.400	0.047	0.417	0.422	0.051
TC0.3-SP-S-W10	0.610	0.612	0.029	0.559	0.560	0.027	0.584	0.586	0.038
TC0.3-SP-S-W15	0.748	0.746	0.023	0.737	0.738	0.026	0.744	0.742	0.023
TC0.3-SP-S-W20	0.766	0.766	0.030	0.742	0.744	0.012	0.756	0.755	0.016
TC0.3-SP-S-W25	0.805	0.802	0.008	0.792	0.790	0.006	0.795	0.796	0.009

Note: TC = tire crumbs; SP = standard Proctor; MP = modified Proctor; RP = reduced Proctor; S = small tire crumbs; L = large tire crumbs; W = water content; SD = standard deviation; the numbers that follow the TC and W indicate the mixing ratio of tire crumbs (g/g) and water content (%) in the compacted specimen, respectively; an asterisk indicates the statistical estimates of four measurements of the specimen and a double asterisk indicates the statistical estimates of eight measurements of the specimen.

Table 4.2 Summary of horizontal, vertical and overall thermal conductivities of compacted mixtures tested (continued)

Specimen ID	λ_h^*			λ_v^*			λ^{**}		
	Median (W/mK)	Mean (W/mK)	SD (W/mK)	Median (W/mK)	Mean (W/mK)	SD (W/mK)	Median (W/mK)	Mean (W/mK)	SD (W/mK)
TC0.4-SP-S-W5	0.361	0.361	0.026	0.316	0.317	0.026	0.339	0.339	0.034
TC0.4-SP-S-W10	0.457	0.462	0.027	0.418	0.420	0.032	0.444	0.441	0.035
TC0.4-SP-S-W15	0.559	0.558	0.057	0.527	0.527	0.048	0.538	0.543	0.051
TC0.4-SP-S-W20	0.620	0.619	0.012	0.592	0.591	0.017	0.604	0.605	0.022
TC0.4-SP-S-W25	0.681	0.681	0.004	0.645	0.647	0.008	0.668	0.664	0.019
TC0.2-MP-S-W5	0.644	0.642	0.079	0.556	0.555	0.078	0.602	0.599	0.086
TC0.2-MP-S-W10	0.898	0.897	0.113	0.832	0.832	0.084	0.853	0.865	0.098
TC0.2-MP-S-W15	0.983	0.981	0.008	0.933	0.932	0.005	0.954	0.957	0.027
TC0.2-MP-S-W20	0.970	0.973	0.045	0.932	0.942	0.040	0.957	0.957	0.043
TC0.2-MP-S-W25	0.965	0.965	0.007	0.925	0.927	0.007	0.947	0.946	0.021
TC0.2-RP-S-W5	0.485	0.491	0.058	0.417	0.415	0.055	0.450	0.453	0.066
TC0.2-RP-S-W10	0.679	0.681	0.047	0.634	0.639	0.042	0.656	0.666	0.047
TC0.2-RP-S-W15	0.830	0.832	0.061	0.783	0.782	0.066	0.812	0.807	0.065
TC0.2-RP-S-W20	0.955	0.950	0.012	0.944	0.933	0.015	0.945	0.941	0.015
TC0.2-RP-S-W25	0.945	0.945	0.012	0.925	0.927	0.016	0.935	0.936	0.016
TC0.2-SP-L-W5	0.663	0.666	0.027	0.581	0.578	0.028	0.623	0.622	0.053
TC0.2-SP-L-W10	0.863	0.864	0.005	0.796	0.795	0.008	0.832	0.830	0.037
TC0.2-SP-L-W15	0.969	0.976	0.016	0.937	0.938	0.020	0.964	0.957	0.026
TC0.2-SP-L-W20	1.040	1.052	0.049	1.025	1.025	0.056	1.040	1.039	0.051
TC0.2-SP-L-W25	1.045	1.041	0.037	1.011	1.006	0.032	1.027	1.024	0.037

Note: TC = tire crumbs; SP = standard Proctor; MP = modified Proctor; RP = reduced Proctor; S = small tire crumbs; L = large tire crumbs; W = water content; SD = standard deviation; the numbers that follow the TC and W indicate the mixing ratio of tire crumbs (g/g) and water content (%) in the compacted specimen, respectively; an asterisk indicates the statistical estimates of four measurements of the specimen and a double asterisk indicates the statistical estimates of eight measurements of the specimen.

Table 4.3 Results of ANOVA for response variable

Source of variation	Degree of freedom	Sum of squares	Mean sum of squares	$F_{\text{calculated}}$	F_{critical}	p - value
Water content (A)	4	0.827	0.270	94.618	2.404	< 0.0001
Mixing ratio (B)	4	19.553	4.888	2236.871	2.404	< 0.0001
Compactive effort (C)	2	0.221	0.111	50.618	3.028	< 0.0001
Tire crumbs size (D)	1	0.121	0.121	55.219	3.875	< 0.0001
A×B	16	0.781	0.049	22.346	1.680	< 0.0001
A×C	8	0.139	0.017	7.948	1.972	< 0.0001
A×D	4	0.015	0.004	1.704	2.404	0.149

Table 4.4 Results of stepwise multiple linear regression analysis

Observations	320		
R - squared	0.867		
Standard error	0.113		
Overall F - statistic	688.6		
Variables	Coefficients	Standard error	t - statistic
Intercept	0.989	0.019	53.017
w (%)	0.021	0.001	23.843
R_m (-)	-2.177	0.057	-38.471
CE (-)	0.053	0.013	4.151

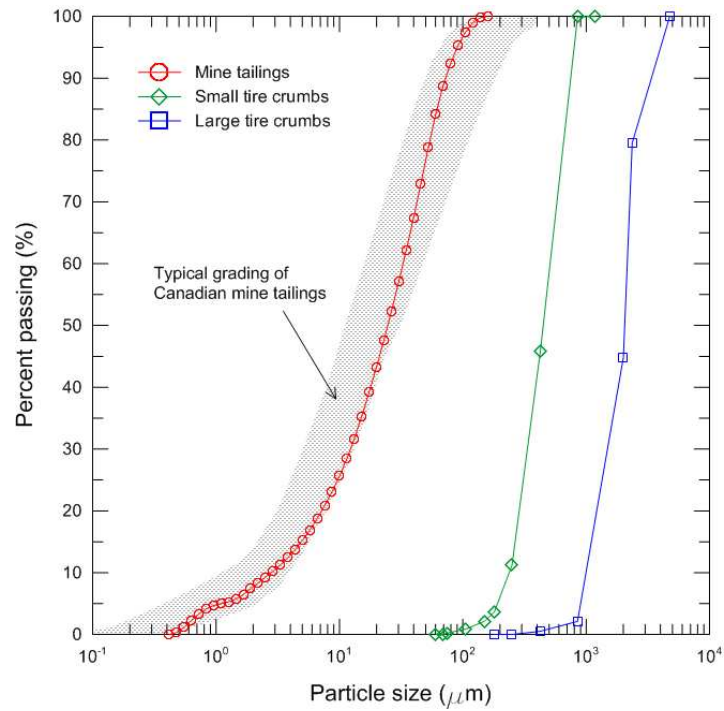


Figure 4.1 Particle size distributions of test materials

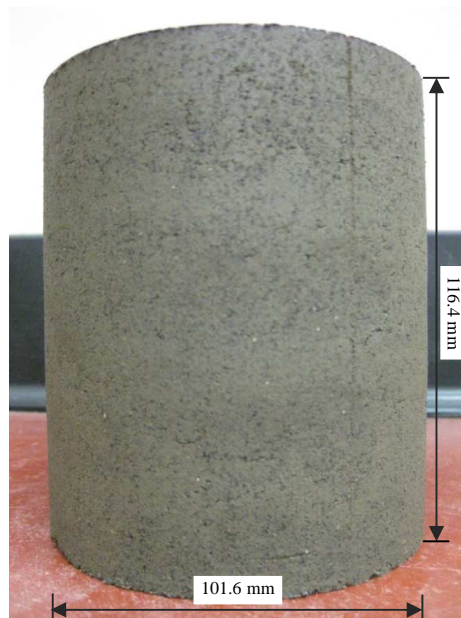


Figure 4.2 A compacted specimen of mine tailings and small tire crumbs mixtures with the mixing ratio of tire crumbs of 0.2 and the water content of 15% (i.e., TC0.2-SP-S-W15)

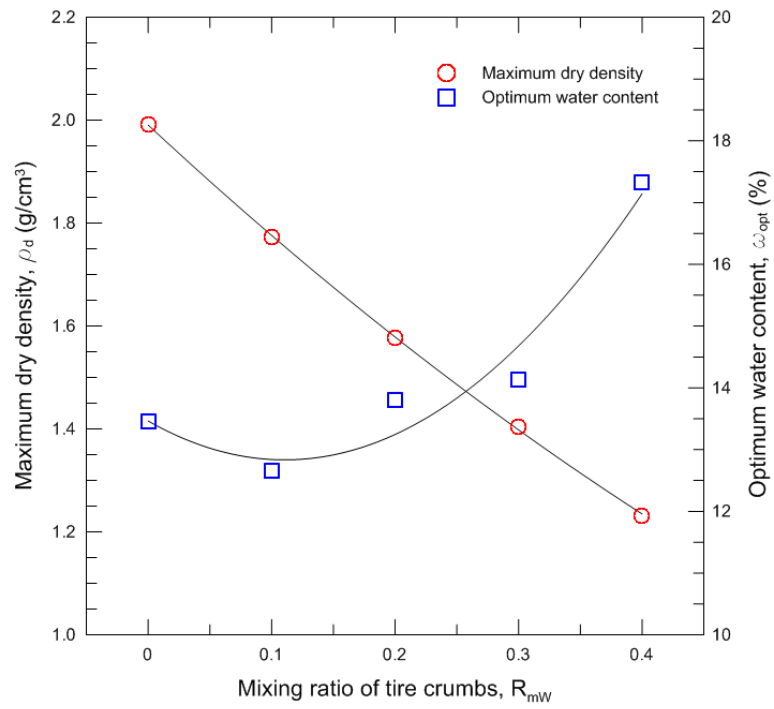
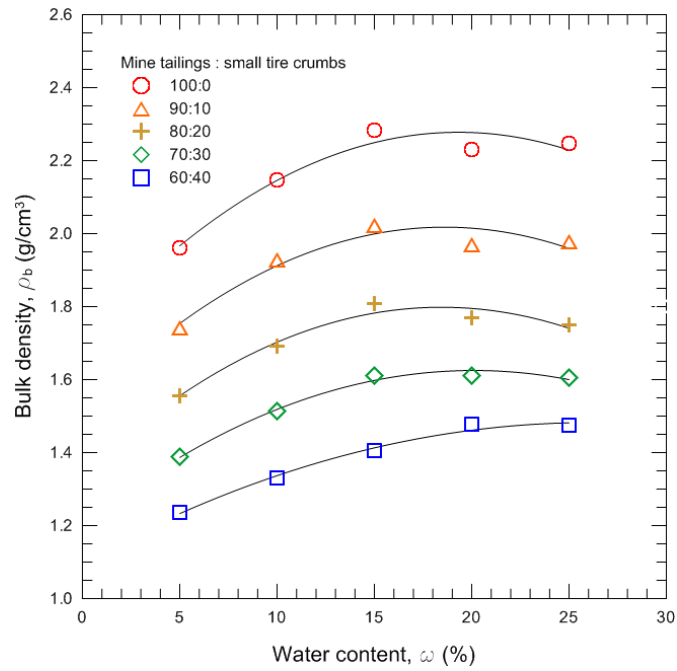
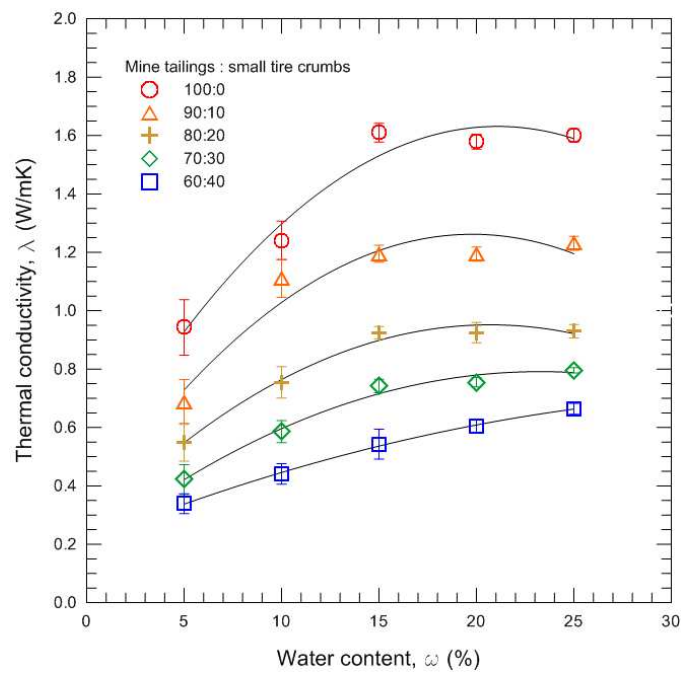


Figure 4.3 Variations of maximum dry density and optimum water content with mixing ratio of tire crumbs

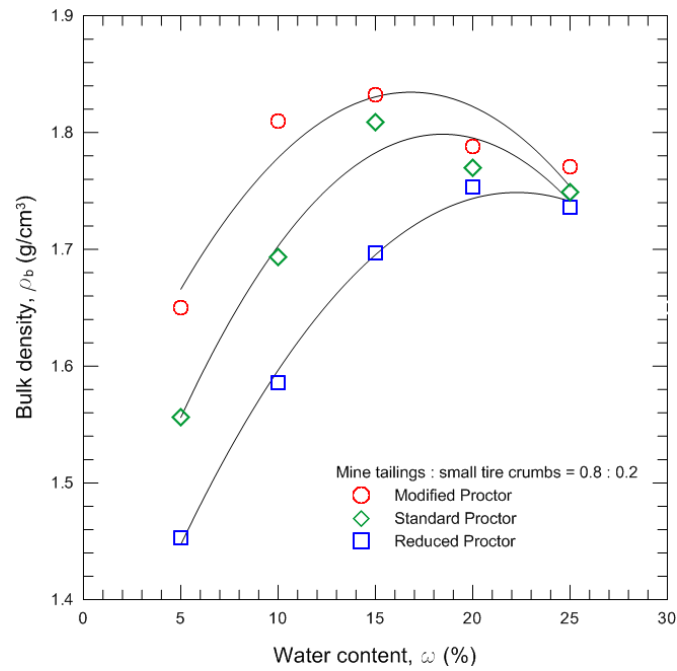


(a)

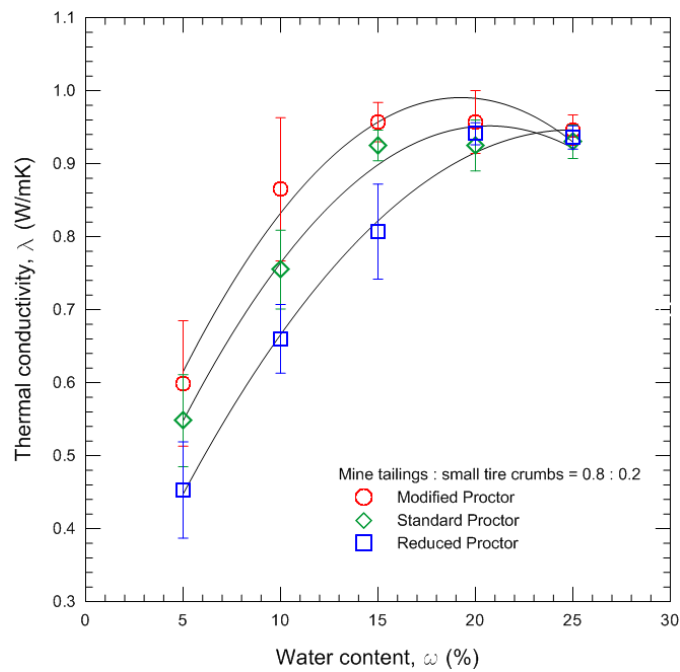


(b)

Figure 4.4 Variations of bulk density and thermal conductivity with water content for compacted mine tailings and small tire crumbs mixtures with different mixing ratios of tire crumbs

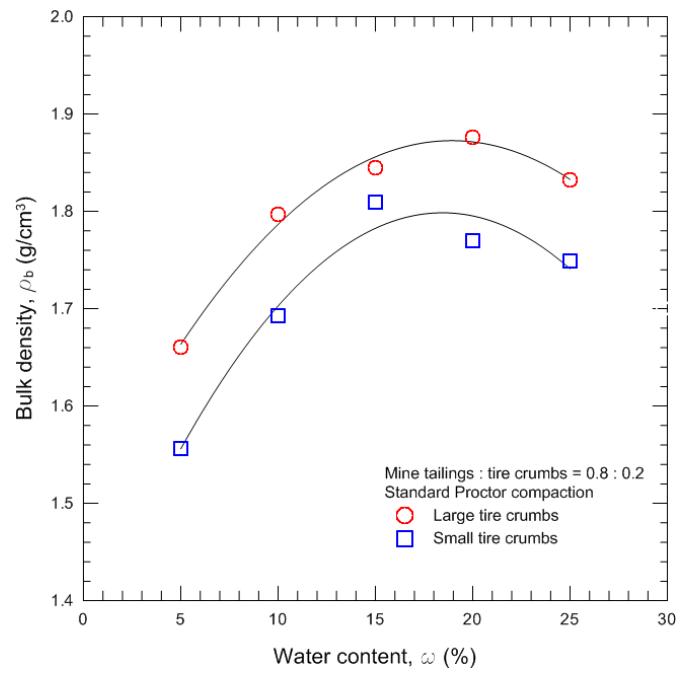


(a)

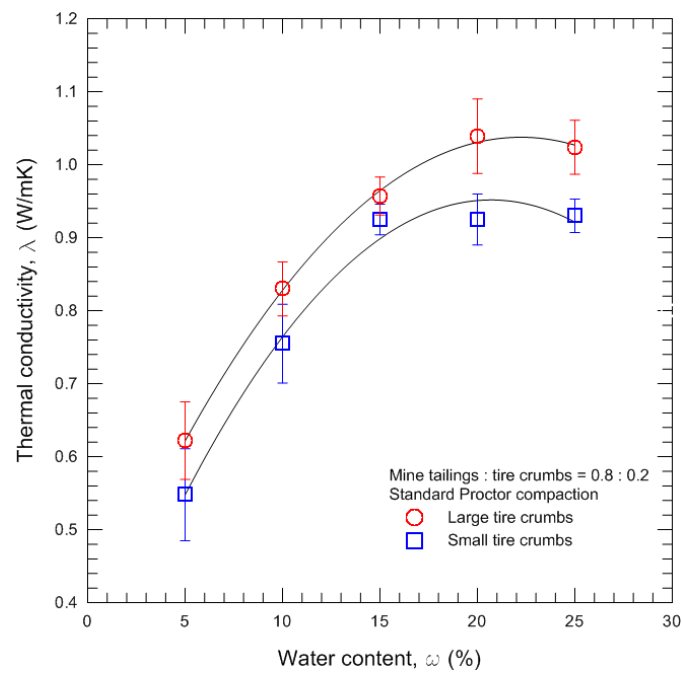


(b)

Figure 4.5 Variations of bulk density and thermal conductivity with water content for compacted mine tailings and small tire crumbs mixtures with different compactive efforts



(a)



(b)

Figure 4.6 Variations of (a) bulk density, (b) thermal conductivity, and (c) volumetric air content with water content for compacted mixtures with different tire crumbs sizes

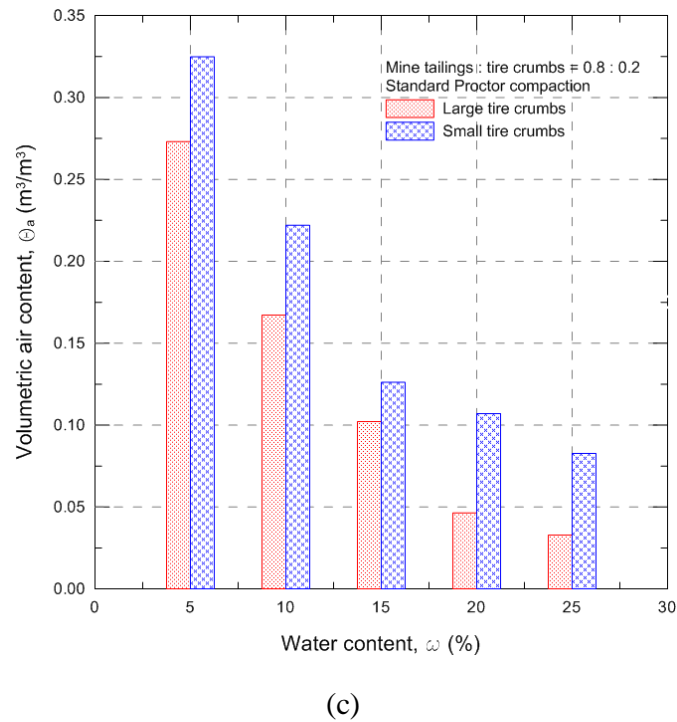


Figure 4.6 Variations of (a) bulk density, (b) thermal conductivity, and (c) volumetric air content with water content for compacted mixtures with different tire crumbs sizes (continued)

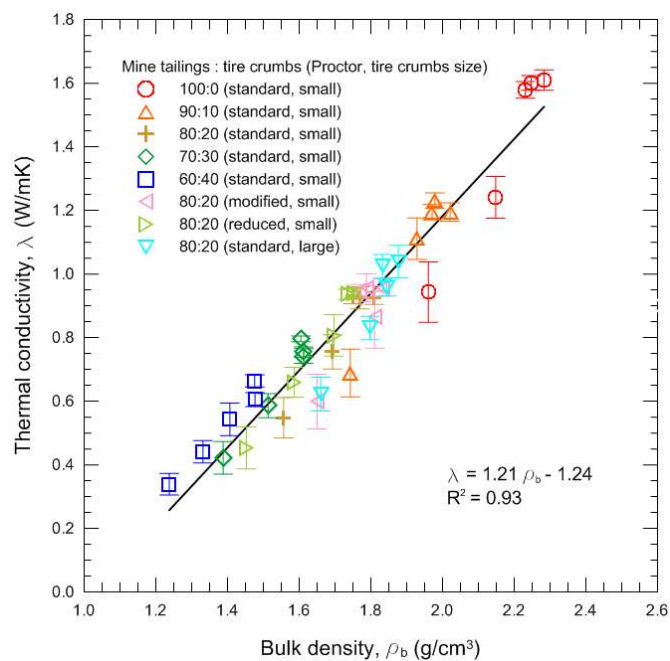
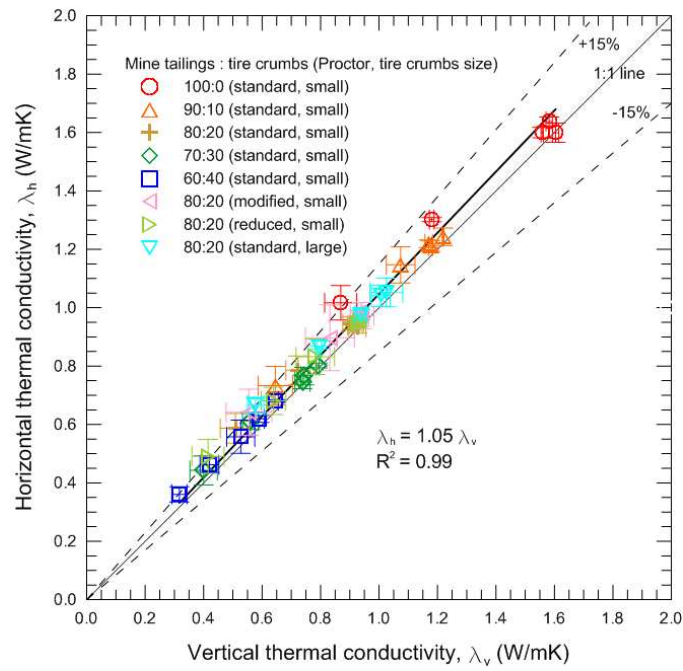
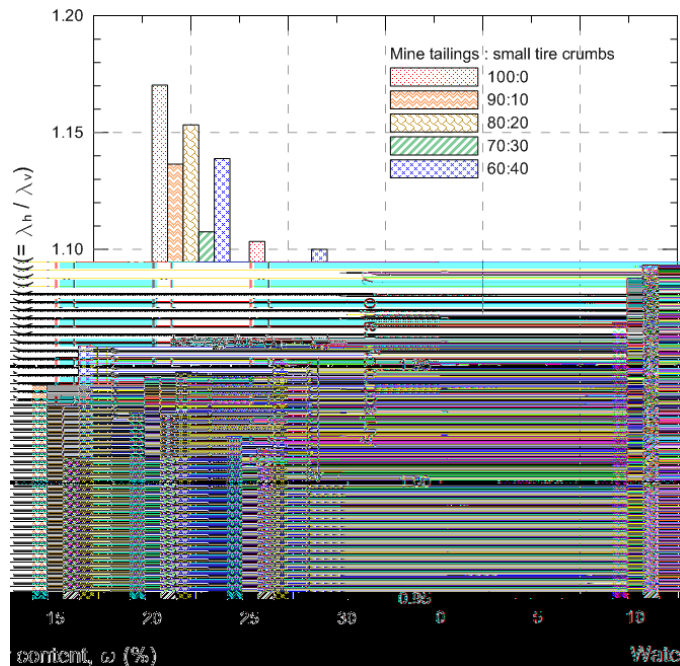


Figure 4.7 Relationship between thermal conductivity and bulk density for all compacted mixtures

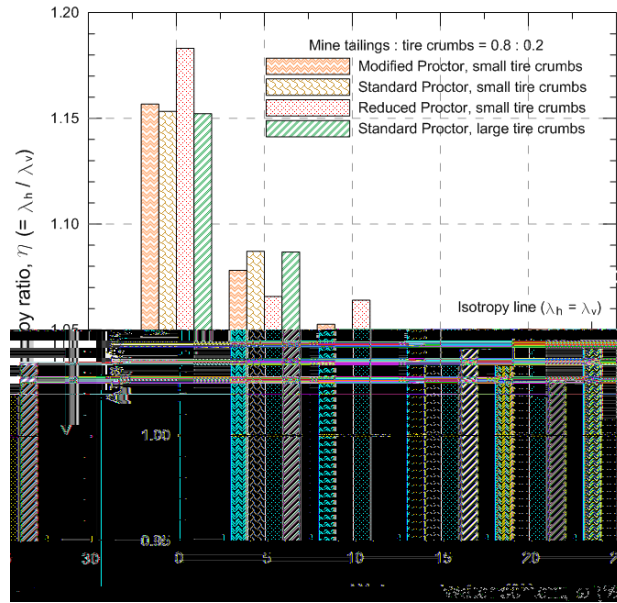


(a)



(b)

Figure 4.8 Anisotropy of thermal conductivity for compacted mine tailings and tire crumbs mixtures: (a) horizontal versus vertical thermal conductivity; (b) effects of water content and mixing ratio of tire crumbs on anisotropy ratio; (c) effects of water content, compactive effort and tire crumbs size on anisotropy ratio



(c)

Figure 4.8 Anisotropy of thermal conductivity for compacted mine tailings and tire crumbs mixtures: (a) horizontal versus vertical thermal conductivity; (b) effects of water content and mixing ratio of tire crumbs on anisotropy ratio; (c) effects of water content, compactive effort and tire crumbs size on anisotropy ratio (continued)

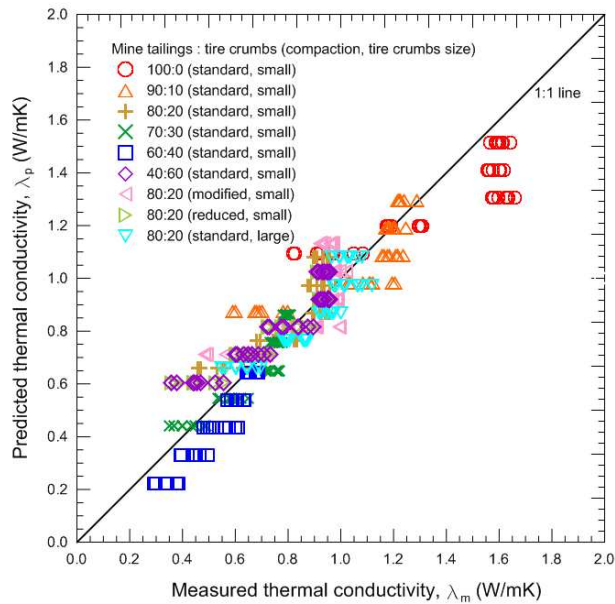


Figure 4.9 Predicted thermal conductivity of compacted mine tailings and tire crumbs mixtures using the statistical model versus actual data

CHAPTER 5

EVOLUTION OF THERMAL AND MECHANICAL PROPERTIES OF MINE TAILINGS AND FLY ASH MIXTURES DURING CURING PERIOD

5.1 Introduction

Fly ash is a by-product of the combustion process in coal-fired power generating plants, which mostly consists of smooth spherical particles of silicon, alumina, iron and calcium oxides, along with residual carbon. Coal fly ash is commonly used alone or as an admixture in construction owing to its pozzolanic, cementitious and alkaline nature. The classification and characterizing method of fly ash for use in civil engineering applications are reviewed in ASTM C 618 (ASTM 2008a) and ASTM D 5239 (ASTM 2004). When fly ash is added to a soil-water system, lime (CaO), the reactive component, reacts with water and soil solids, resulting in cation exchange, flocculation, carbonation and pozzolanic reactions. These reactions lead to significant changes in the geochemical and mineralogical properties and the microfabric of the geomaterial (Choquette et al. 1987; Al-Rawas 2002; Peethamparan et al. 2008; Horpibulsuk et al. 2009). The variations in the physicochemical properties of the fly ash also cause changes to the thermal and mechanical properties of the geomaterial. Since thermal conductivity is related to the structure of geomaterials, including the size, shape, gradation and aggregation of particles, and binding agents that can be of natural and/or artificial origins (Cote and Konrad 2009), it is often used to assess the thermal properties of geomaterials. Also, as hydration of lime usually accompanies exothermic reactions, the fly ash added to a particular geomaterial induces temperature variations during the process. On the other hand, the addition of fly ash into geomaterials can often improve their engineering properties, such as strength and stiffness. These potential enhancements result

A version of this chapter has been submitted for publication in *Canadian Geotechnical Journal*, NRC Research Press.

from the formation of cementitious compounds such as calcium silicate hydrate (CSH) and calcium aluminate hydrate (CAH). The effectiveness of fly ash as a binder to stabilize geomaterials has been studied by examining compaction and compressibility characteristics (Nalbantoglu and Tuncer 2001), swelling (Phanikumar and Sharma 2007), California bearing ratio (Edil et al. 2006), unconfined compressive strength (Tastan et al. 2011) as well as elastic and resilient moduli (Solanki et al. 2009). Even though numerous studies have been carried out to explore the role of fly ash as a geomaterial amendment, most works have highlighted effects on the mechanical performance in particular. In contrast, the effects of fly ash on thermal properties change have not been reported in the literature and the relationship of the thermal conductivity with the strength gain for fly ash treated geomaterials is not fully understood.

The global mining industry generates massive residue or tailings after extracting valuable metals and minerals from ore. The management and disposal of tailings pose major challenges to efforts to protect the environment. Typically, mine tailings are stored on site in the form of impoundments. In order to improve disposal efficiency, new and modified tailings management approaches have been studied and implemented: these include densification, desulphurization, and co-disposal of tailings and waste rock (Bussiere 2007). To control and mitigate the impact of acid mine drainage (AMD), several researchers (Wang et al. 2006; Yeheyis et al. 2009) have assessed the feasibility of utilizing fly ash in tailings management. It has been shown that the pozzolan stabilized tailings exhibit resistance to AMD generation and migration because of two factors, namely, the neutralization effect of the coal fly ash and formation of hydration products that act as oxygen and infiltration barriers. Mine tailings have been used in geoenvironmental applications, for instance, cemented tailings backfill (Helinski et al. 2011), engineering barrier of bentonite-tailings mixtures (Fall et al. 2009) and tailings-based pavement subbase (Qian et al.

2011). Mine tailings can be employed as fill materials if the potential of AMD generation is prohibited by adding binders such as cement, lime and fly ash where natural soils are not available in abundant quantity. In addition, knowledge of both the thermal and mechanical properties of fill materials with binders added is important for thermo-mechanical analyses of underground structures such as oil and gas pipelines, electric transmission lines, energy piles and nuclear waste repositories.

This study is concerned with the beneficial use of mine tailings for fills with fly ash as a binder. A series of laboratory tests were conducted on compacted mixtures of mine tailings and coal fly ash obtained from a mine site and a power generating station, respectively, both in Ontario, Canada. The test specimens were prepared by controlling the amount of fly ash added to mine tailings, molding water content and compaction energy. Changes in thermal conductivity, temperature, unconfined compressive strength and elastic modulus of the specimens were monitored during the curing period. The microfabrics of the specimens were examined in terms of pore size distribution and particle surface characteristics. The relationships between thermal conductivity and the bulk unit weight and unit pore volume were established. Additionally, the correlation between thermal conductivity and the compressive strength of the specimens was observed.

5.2 Materials

In this study, mine tailings, fly ash and water were the host materials used to make the compacted mixtures of mine tailings and fly ash. The physical properties and oxide composition of mine tailings and fly ash are summarized in Tables 5.1 and 5.2, respectively. The particle size distributions of both the mine tailings and fly ash are shown in Figure 5.1.

5.2.1 Mine Tailings

The mine tailings were taken in a dry state from the Musselwhite gold mine located in northern Ontario, Canada. The specific gravity of the tailings is 3.37, which is greater than that of most soils due to predominant amphibole minerals with high specific gravity. The tailings are primarily comprised of silt-sized particles (83.2%) with some sand-sized (9.4%) and clay-sized (7.4%) particles. According to the Unified Soil Classification System, the tailings are classified as silts of no plasticity (ML), similar to most of the tailings produced in Canadian hard rock mines (Bussiere 2007). Meanwhile, the major oxides in the tailings include silica (50.82%), alumina (8.87%) and ferric oxide (28.97%), which account for a total amount of 88.66% by weight (Wang et al. 2006). The calcium oxide is relatively low at 3.19%.

5.2.2 Fly Ash

The coal fly ash was collected in a dry state from the Atikokan Thermal Generating Station located in Ontario, Canada. The specific gravity of the fly ash is 2.54, and it does not exhibit any plasticity. The fly ash is made up 98.7% fines (< 75 μ m) with predominately silt-sized particles. The major oxides identified include silica (37.99%), alumina (19.92%) and ferric oxide (6.17%), with a total of 64.08% by weight (Wang et al. 2006). Thus, the Atikokan fly ash is classified as neither Class C nor Class F fly ash in accordance with ASTM C 618 (ASTM 2008a). The fly ash has a high content of calcium oxide (15.66%), which is the source of pozzolan. The ratios of CaO/SiO_2 and $\text{CaO}/(\text{SiO}_2 + \text{Al}_2\text{O}_3)$, which are indicators of cementing potential (Cetin et al. 2010; Tastan et al. 2011), are calculated to be 0.41 and 0.27, respectively.

5.2.3 Water

Deionized water with a temperature of 22.5 ± 0.2 °C was used in this study. The deionized water has a pH of 6 and electrical conductivity below 1 S/m.

5.3 Specimen Preparation and Testing Conditions

The fly ash ratio R_{FA} is based on the dry weight of solid minerals and defined as

$$R_{FA} = \frac{W_{FA}}{W_{MT}} \times 100 (\%) \quad (5.1)$$

where W_{FA} is the weight of fly ash and W_{MT} is the weight of mine tailings. The eight slurries of mine tailings and fly ash mixtures were prepared by adding various weights of fly ash into tailings of 25 g dispersed in 100 mL deionized water. The fly ash ratios of the mixtures ranged from 0 to 60%. The slurries were shaken at a constant temperature of 25 °C. The pH of the slurry was measured using a pH meter calibrated before measurement. The pH of each slurry was measured at 1, 24, 72 and 120 hours after mixing. It was observed that the slurry pH reached equilibrium within 1 hour after mixing the mine tailings and fly ash. Figure 5.2 shows the pH values measured in slurries with different fly ash ratios at 1 hour after mixing. The original tailings are slightly alkaline with pH 8.35. This is mainly due to the addition of lime during the milling process and the presence of carbonate. With increasing fly ash contents in the mixtures, the pH increases until it reaches a constant when the fly ash ratio is above 20%. Based on these results, fly ash ratios of 20, 40 and 60% were selected for the mixture specimens in this study because these fly ash ratios will sustain the physicochemical reactions required to bind the tailings.

The mixtures with the fly ash ratios of 20, 40 and 60% were thoroughly mixed in a dry state. A series of standard Proctor compaction tests [ASTM D 698 (ASTM 2007)] were carried out to determine the optimum water content (OWC) and maximum dry unit weight (MDW) of all mixtures that were produced by mixing 30 minutes after adding water into the dry mixtures. In this study, all mixtures were compacted at their specific OWC and MDW. Figure 5.3 compares the compaction results on the mixtures with fly ash ratios of 20, 40 and 60%.

In the case of mixtures with a fly ash ratio of 20%, three compaction states were considered in order to explore effects on the thermal, mechanical and microfabric characteristics of the specimens: (1) at the water content of 0.85 OWC (representing the dry side of optimum) under standard Proctor energy (590 kJ/m^3); (2) at the water content of 1.15 OWC (representing the wet side of optimum) under standard Proctor energy; and (3) at the OWC under high Proctor energy ($1,190 \text{ kJ/m}^3$). The high Proctor compaction was implemented using the same procedure specified for standard Proctor compaction but the compacted layers were increased from 3 to 5 and the number of blows per layer was increased from 25 to 30. It is noted that the high Proctor energy applied in this study is less than the modified Proctor energy ($2,690 \text{ kJ/m}^3$) declared in ASTM D 1557 (ASTM 2009a) because the thermal properties analyzer used could not be inserted to the specimen compacted under the modified Proctor energy without a pre-drilled hole. The compaction states were designed to simulate possible field conditions.

In this study, the specimens were named in three terms. The first term indicates the fly ash (FA) ratio; the second term indicates the compaction energy, i.e., standard Proctor (SP) energy or high Proctor (HP) energy; and the third term indicates the specimen under optimum water content (OWC), dry water content (DWC) or wet water content (WWC). For example, a specimen with the fly ash ratio of 20% compacted at the standard Proctor energy and optimum

water content is designated as FA20-SP-OWC. A total of six specimens were tested: FA20-SP-OWC, FA40-SP-OWC, FA60-SP-OWC, FA20-SP-DWC, FA20-SP-WWC and FA20-HP-OWC. Table 5.3 presents the water contents and dry unit weights for all specimens studied.

Five identical samples were made under each Specimen ID. One was used to measure the thermal conductivity and temperature during the curing period as well as to study pore size distribution and surface fabric, whereas the other four were used to evaluate changes in unconfined compressive strength and elastic modulus over time. To minimize internal variability of the samples, an automatic compaction apparatus was utilized.

5.4 Experiments

The experimental program included the measurement of the thermal conductivity, temperature, compressive strength, elastic modulus, mercury intrusion porosimetry and scanning electron microscopy of compacted mixtures of mine tailings and fly ash. The experimental devices, techniques and methodology adopted in this study are described in the following sections.

5.4.1 Thermal Properties Analyzer

The thermal conductivity and internal temperature during the curing of compacted mine tailings and fly ash mixtures were measured by using a KD2 Pro thermal properties analyzer. The analyzer is comprised of a micro-controller and a sensor. The controller displays automatic readings of the thermal properties and allows a user to program the analyzer to periodically measure and store these properties. The sensor has a single probe of 2.4 mm diameter and 100 mm length, mounted with a heater and a thermistor. The operating principle of the measurement system is based on the transient line heat source theory, which conforms to ASTM D 5334

(ASTM 2008b). A heat pulse is applied to the heater and the temperature change within the probe is simultaneously recorded by the thermistor: the higher thermal conductivity of the medium exhibits a higher rate of heat dissipation that leads to a lower rate of temperature increase detected with the thermistor. Thermal conductivity is determined by the temperature response with time. The KD2 Pro analyzer reproduces the thermal conductivity of reference materials with $\pm 5\%$ accuracy within the temperature range of - 50 to 150 °C.

After preparing the compacted specimen, comprised of mine tailings and fly ash mixtures, the single probe sensor was vertically inserted into the specimen in the mold. In order to minimize frictional resistance between the probe and specimen, the probe was coated with a thin layer of thermal grease. Afterward, the specimen was extruded from the mold using a hydraulic jack and immediately placed in an environmental chamber at 60% relative humidity and 24.6 °C temperature for curing. The first measurements of the thermal conductivity and temperature of the specimen were carried out within 5 minutes after compaction and were continuously monitored every 30 minutes up for a period of 120 hours.

5.4.2 Unconfined Compression Test

To characterize the strength and stiffness of compacted mixtures of mine tailings and fly ash, unconfined compression tests were conducted according to ASTM D 5102 (ASTM 2009b). Cylindrical specimens (101.6 mm diameter and 116.4 mm height) compacted in the standard Proctor mold were tested at a loading speed of 0.5 mm/min. For each specimen, four compression tests were performed on four sub-samples with identical properties, i.e., immediately after compaction, and then 24, 72 and 120 hours after compaction. The unconfined compressive strength was determined as the peak normal stress of a stress-strain curve and the

corresponding elastic modulus was calculated as the slope between the origin and maximum stress, as shown in Figure 5.4. It is noted that the compressive strength is influenced by the height to diameter ratio (h/d) of a specimen. Ozyildirim and Carino (2006) pointed out that the compressive strength of concrete specimens with $h/d = 1.15$ will be approximately 10% greater than that of a cylindrical specimen with the standard $h/d = 2$. In this study, the h/d ratios of all specimens for unconfined compression tests were kept constant at $h/d = 1.15$.

5.4.3 Mercury Intrusion Porosimetry

Mercury intrusion porosimetry (MIP) was used to quantify the pore size distribution (PSD) of the mine tailings and fly ash mixtures. The principle of the technique is that mercury, a non-wetting fluid, will not intrude the voids of a porous medium unless a sufficient pressure is applied. According to Laplace's capillarity law (known as Washburn's equation), a theoretical relation between the intrusion pressure and the pore diameter, assuming the pore is cylindrical, can be expressed as (Washburn 1921)

$$d_p = \frac{4T_s \cos \theta}{P} \quad (5.2)$$

where d_p is the pore diameter (m), P is the applied intrusion pressure (MPa), T_s is the surface tension (N/m) and θ is the contact angle (degrees). As indicated in Eq. (5.2), the pore diameter is governed by the surface tension of the mercury and the contact angle between the mercury and the pore wall. The interfacial mercury-vacuum tension at 25 °C is 0.480 N/m and the contact angle of the mercury-air interface to the solid is assumed to be equal to 140° as cited by Cuisinier et al. (2011) on lime-treated soils. The MIP device used was the Micromeritics AutoPore IV 9500 V 1.07 with a maximum intrusion pressure of 207 MPa. The MIP device measures the pore

volume of mercury intruded to the medium corresponding to stepped intrusion pressures until it reaches the capacity of the system. Given the values of T_s and θ , the pore diameters intruded by mercury under each intrusion pressure is calculated by Eq. (5.2) and the cumulative mercury volume injected versus the pore diameter of the medium can be obtained. It is noteworthy that the MIP does not provide the measurement of the true diameter of irregular pores but of the equivalent cylindrical diameter of entrance pores. The pore size distribution by the MIP is dependent on sample pretreatment, sample size and applied mercury pressure (Aligizaki 2006). Delage (2010) suggested that the freeze-drying technique appears to be the most suitable method to avoid fabric alteration owing to shrinkage through traditional techniques such as air drying and oven drying. Penumadu and Dean (2000) recommended that the sample volume of 1,000 to 2,000 mm³ should be used for dehydration. They also revealed that for soft soil samples, the applied pressure has impact on the sample fabric, and the internal and external pressure difference in the sample at the early stage may cause changes in the inherent fabric. According to Simms and Yanful (2004), however, this effect is less important for compacted soils. Based on these considerations, the following methodology was used to remove pore water with minimum matrix deformation of compacted mine tailings and fly ash mixtures: after the completion of thermal properties measurement, a sample with the volume of about 1,000 mm³ was carefully taken from the middle of the specimen and placed immediately in liquid nitrogen. Thereafter, the frozen sample was vacuum-sublimated for 24 hours in a desiccator.

The results of a MIP test are commonly presented in terms of the cumulative pore volume per unit weight V_c versus the logarithm of the pore diameter d_p and the derivative of the cumulative pore volume V_d ($=dV_c/d(\log d_p)$) versus the logarithm of the pore diameter d_p , which are known as the cumulative intrusion curve and differential distribution curve,

respectively. The larger V_d in the differential distribution curve represents the greater presence of the corresponding pore diameter in the medium.

5.4.4 Scanning Electron Microscopy

Scanning electron microscopy (SEM) was used for direct observation of the spatial configuration of particles in the mine tailings and fly ash mixtures, including sizes, shapes and associated pores at micro scales. The technique provides qualitative information that can be interpreted along with results of the MIP test. The sample was prepared for SEM imaging following the same procedures as in the MIP test. The sample surface was not polished in order to preserve the macro and micro textures. The image was taken by an LEO 440 scanning electron microscope, which allows a wide range of magnification up to 1,000 times.

5.5 Results and Discussion

5.5.1 Compaction Characteristics

Figure 5.3 shows the relationship between the dry unit weight, γ_d , and molding water content, w , for compacted mine tailings and fly ash mixtures with different fly ash ratios. The maximum dry unit weights vary from 18.9 to 19.5 kN/m³, while the optimum water contents range from 11.0 to 12.4%. With the increase in the fly ash ratio the compaction curve moves downward and toward the left, indicating that MDW and OWC decrease as the fly ash ratio increases. Similar behaviors were reported for fly ash treated soils in the literature (Osinubi 1998; Degirmenci et al. 2007). The decrease in the MDW with increasing fly ash addition is attributable to the lower specific gravity of the fly ash, i.e., 2.54, as compared to 3.37 for the mine tailings. Since the mixtures become lighter, they can be advantageous for use in fill

applications. It should be noted that the pore spaces of the specimens decrease as the fly ash ratio increases, which slightly compensates for the reduction of the MDW. This is explained by the packing mechanism, namely that in a mixture of particles of different sizes, the finer particles fill voids between coarser particles (Lade et al. 1998; Yilmaz 2009). On the other hand, the decrease in the OWC with the increase of the fly ash ratio is likely due to the chemical and physical reactions involving cation exchange and surface sorption as well as flocculation and agglomeration (forming flocks of particles) brought by fly ash. When the fly ash is added to mine tailings, the mixture becomes drier and more friable under the same water content owing to hydration effects: less water will be available for the reorientation of particles in the mixture. This can be advantageous in compaction works. Furthermore, the formation of large aggregates changes the gradation of the mine tailings and fly ash mixtures, resulting in denser packing.

5.5.2 Thermal Conductivity

The thermal conductivity, λ , versus the logarithm of time, t , for compacted mixtures of mine tailings and fly ash are shown in Figure 5.5. Generally, the thermal conductivities of the specimens decrease as curing time increases. Moreover, the initial thermal conductivity (i.e., the first measurement after compaction) and the development characteristics of thermal conductivity with time are sensitive to the fly ash ratio and compaction conditions.

Figure 5.5(a) illustrates the thermal conductivity of the specimens with different fly ash ratios. The initial thermal conductivities are 1.262, 1.133 and 1.074 W/mK for the fly ash ratios of 20, 40 and 60%, respectively, indicating the specimens with higher fly ash content have lower initial thermal conductivities. This is mainly attributed to the fact that the thermal conductivity of fly ash is normally lower than that of minerals in natural geomaterials (Kolay and Singh 2002).

Also, the initial thermal conductivity of pure fly ash compacted at optimum water content is 0.625 W/mK, which is much lower than those of the compacted specimens with the fly ash ratios of 20, 40 and 60%. Meanwhile, as the curing time increases, the thermal conductivity difference in the specimens decreases. However, the thermal conductivities of all specimens converge at the end of the curing period. The change in the thermal conductivity within the curing time at different fly ash ratios can be explained as follows: immediately after compaction, the thermal conductivity of the specimens is affected by the thermal conductivities of their constituents; as the curing time progresses, water is consumed by evaporation and hydration. As a result, cementation develops because of cementing and pozzolanic activities in the mixtures, which generates bonding between particles; finally, at the end of the curing period, the thermal conductivities of the specimens are governed primarily by the newly formed structure.

Figure 5.5(b) highlights the effect of molding water content on the thermal conductivities of the specimens with a fly ash ratio of 20%. The highest initial thermal conductivity is achieved at the optimum compaction, followed by the wet side of optimum and the dry side of optimum. At the OWC, the solid particles are in the closest arrangement, with smallest pore spaces occupied by water and air. The magnitudes of the initial thermal conductivity of the specimens compacted at the OWC, WWC and DWC can be explained by the fact that the thermal conductivity of solid minerals (1 - 10 W/mK) is much higher than that of water (0.57 W/mK) or air (0.026 W/mK). However, the significant thermal conductivity difference at different water contents disappears in the middle of the curing period (after about 5 hours) because the specimens with the same amount of fly ash result in similar levels of hydration although they have different molding water contents, as the curing time increases.

Figure 5.5(c) compares the thermal conductivities of two specimens with the same molding water content but different compaction energies. The higher compaction energy induces higher initial thermal conductivity, resulting from the higher density of the specimen, which means better contact between neighboring particles for heat conduction. However, the variations of thermal conductivity against curing time are relatively independent of the compaction energy.

5.5.3 Temperature

The internal temperature, T , of all compacted specimens of mine tailings and fly ash mixtures during curing period, t , was monitored and the results are shown in Figure 5.6. The trend of the temperature fluctuation of the specimens over time is similar in all specimens: the initial temperatures of the mine tailings and fly ash mixtures are within the range of 22 to 23 °C, which decreases in the first 5 hours of curing; then the trend is reversed, i.e., the specimen temperature increases with time until it reaches equilibrium with the environmental chamber temperature of 24.6 °C after about 90 hours. The decrease in temperature at the early curing stage for all specimens is unexpected, based on the understanding that the exothermic hydration reaction of lime (CaO) provokes the release of heat energy. One of the possible reasons for this is that the hydration of specimens releases less heat compared to the endothermic thermal energy consumed by water evaporation. This is consistent with the observation that temperature increase is related to the fly ash ratio: the higher the fly ash ratio, the higher temperature of the specimens up to a curing time of 50 hours (Figure 5.6(a)). It should be also noted that the temperature change is less influenced by the molding water content and compaction energy as seen in Figure 5.6(b).

5.5.4 Unconfined Compressive Strength

Figure 5.7 shows the unconfined compressive strength, q_u , of the specimens under various fly ash ratios, molding water contents and compaction energies. Figure 5.7(a) plots the effect of fly ash ratio on the compressive strength of mine tailings and fly ash mixtures compacted under their optimum water contents. It is observed that the compressive strength of the specimens increases as the fly ash ratio increases. For instance, after 120 hours curing, the compressive strengths of the specimens with fly ash ratios of 20, 40 and 60% are 121, 178, and 293% higher, respectively, compared with the compressive strength (0.2 MPa) of untreated mine tailings. The incidence of higher compressive strength with increasing fly ash ratio is a result of denser packing as well as cementation owing to pozzolanic reactions. On the other hand, it is found that the rate of compressive strength gain depends on the fly ash ratio: the compressive strengths of specimens with the fly ash ratios of 20 and 40% increase rapidly in 24 hours and then approach equilibrium with further increase in curing time, whereas the compressive strengths for specimens with 60% fly ash ratio increase progressively over a period of 120 hours, as seen in Figure 5.7(a). This indicates that higher fly ash content requires a longer period of curing time for the development of full strength. This result is consistent with the results of fly ash treated soils reported in the literature (Indraratna et al. 1999; Koliass et al. 2005; Ghosh and Subbarao 2007). However, the development of long term strength of mine tailings and fly ash mixtures is needed to be further investigated.

Figure 5.7(b) presents the unconfined compressive strength of the specimens with a constant fly ash ratio of 20% as influenced by the molding water content and compaction energy. The results show a similar trend of compressive strength gain against curing time. Meanwhile, the compressive strengths of the specimens compacted at the DWC are higher than that of the

specimens at the OWC and WWC. It is also noted that despite the higher dry unit weight of the specimen compacted at the OWC as compared to that compacted at the DWC, the compressive strength of the former is lower than that of the latter. This is because the strength of compacted geomaterials is affected not only by the dry unit weight and water content, but also by matric suction. Many researchers (Daniel and Benson 1990; Daniel and Wu 1993; Yang et al. 2005; Guney et al. 2006; Sawangsuriya et al. 2008) have observed that higher suction leads to higher soil strength and stiffness. In addition, the strength difference that is attributable to varying water contents results in the difference in microfabrics formed during compaction. For example, Thom et al. (2007) studied the impacts of water content variation on the fabric of a compacted clayey soil. They reported a progressive growth of smaller pores linked to larger pores attenuation with the increase in the compaction water content. Therefore, the differences in the strength characteristics of the specimens are the combination of varying water content and structural differences. On the other hand, for the specimens obtained with the same molding water but different compaction energies, higher compressive strength is observed at higher compaction energy (Figure 5.6(b)), as expected. The compressive strengths of specimens compacted under high Proctor energy are 27 to 38% higher than those compacted using standard Proctor energy in all four curing periods.

5.5.5 Elastic Modulus

Elastic modulus is an indication of the ductility or brittleness of a material, which is related to settlement of fly ash treated mine tailings based on elasticity theory. Figure 5.8 shows the development of the secant elastic modulus, E , of specimens during curing as related to the fly ash ratio, molding water content and compaction energy. It is seen that the development of elastic modulus is similar to that of the unconfined compressive strength presented in Figure 5.7.

In the case of the specimen compacted at the WWC, however, the increase of the elastic modulus with time is slower than the specimens molded at the OWC and DWC. This is most likely due to the fact that the WWC compacted specimens contain more water during the curing period, which lubricates interparticle contacts and facilitates the rolling and sliding of particles. As a result, the specimen can sustain larger deformation before failure.

5.5.6 Pore Size Distribution

Figure 5.9 shows the effect of fly ash ratio on the pore size distribution of compacted mixtures of mine tailings and fly ash. In Figure 5.9(a), the cumulative intrusion curves are well-graded with smooth boundaries, indicating that all pore sizes lie within the detectable range. More importantly, the cumulative pore volume decreases with increasing fly ash ratio. This is attributed to the higher density as a result of better packing, as noted previously. The differential pore volume distribution curves of the specimens with the fly ash ratio are illustrated in Figure 5.9(b). In the case of the fly ash ratio of 20%, the PSD exhibits a bimodal feature, namely a peak at the pore diameter of 4.083 μm and another at 1.563 μm . The apparent diameter boundary between the two predominant pore diameters is 2.948 μm . Consequently, this specimen can be characterized as having a double porosity fabric that contains significant families of both micropores and macropores. Such a microporosity fabric can be also found in other graded soils, such as compacted mixtures of sand and clay (Juang and Holtz 1985) and compacted clayey till (Simms and Yanful 2001). From the MIP results, it is believed that the characteristics of a double porosity fabric are associated with the size, shape and gradation of particles. The specimen with the fly ash ratio of 40% also displays bimodal pore distribution, but the two distinct pore diameters slightly decreases with the increase in the corresponding peak intensity when compared with the specimen with the 20% fly ash ratio. Finally, the differential distribution

curve of the specimen with the fly ash ratio of 60% in Figure 5.9(b) shows a smooth unimodal distribution with a dominant pore diameter of 0.984 μm . The difference between the differential distribution curves of the specimens with the fly ash ratio is explained by the packing theory of a binary mixture: when a small amount of finer particles is added to coarser particles, the mixture will have dual porosity fabric; and with increasing proportion of finer particle in the specimen, the “tightest” packing is attained, in which the fine particles more fully occupy the pores between coarser particles, resulting in a single porosity matrix. Further discussion can be made by defining a fly ash proportion, i.e.,

$$P_{FA} = \frac{W_{FA}}{W_{FA} + W_{MT}} \quad (5.3)$$

where parameters have been stated in Eq. (5.1). The results of this study show that the densest packing of compacted mine tailings and fly ash mixtures is obtained at the fly ash proportion in the mixture, P_{FA} , of 37.5%, which is corresponding to the fly ash ratio, $R_{FA} = 60\%$. The results are consistent with previous studies on porosity behaviors of binary mixtures (Piloto and Martin 2001; Thevanayagam et al. 2002; Yilmaz 2009), which found that the minimum voids of a finer and coarser particles mixtures are achieved at a proportion of finer particles ranging between 30 and 40%.

Figure 5.10 highlights the influence of molding water content on the PSD of the specimens with the fly ash ratio of 20%. The lowest cumulative pore volume at a given pore diameter of 3.6 μm is obtained at the OWC, followed by the DWC and WWC, as seen in Figure 5.10(a). This is in consistent with the relative order of magnitude of the corresponding dry unit weights presented in Figure 5.3. Meanwhile, the differential distribution curves of all three specimens are bimodal with noticeable differences in the macropore mode, as shown in Figure 5.10(b). The

families of macropores shift toward the left as the water content increases from the DWC to OWC, indicating a reduction in the mean size of the macropores as the water content increases. However, there is a minor difference between the specimens compacted at the OWC and WWC. As seen in Figure 5.10(b), the peak intensity of the specimen compacted at the DWC is approximately two times higher than those compacted at the OWC and WWC. In other words, the micropores remain essentially unchanged and the macropores vary correspondingly with the molding water contents. This result supports the idea that the difference in the unconfined compressive strength of the specimens with different molding water contents of mine tailings and fly ash mixtures is partially related to the difference in the microfabrics formed during the compaction process. In fact, according to Delage et al. (1996), the soil compacted on the dry side of optimum leads to aggregate-dominated fabric while the soil compacted on the optimum and the wet side of optimum creates the matrix-dominated fabric without apparent aggregates.

Figure 5.10 also shows comparison of the pore size characteristics of two specimens with the same fly ash ratio (20%) under different compaction energies. At a given water content, the higher compaction energy generates a specimen of lower cumulative pore volume with closely packing (Figure 5.10(a)). As seen in Figure 5.10(b), the increase in the compaction energy has an effect on both macropores and micropores, although the influence on the former is more pronounced. It is also observed that the specimen compacted under high Proctor energy has a weak bimodal distribution.

5.5.7 SEM Image

Figure 5.11 shows the SEM images of compacted specimens of mine tailings and fly ash mixtures with different fly ash ratios (20, 40 and 60%) at 150 times magnification. Glassy

spherical fly ash particles are coated and embedded in a tailings matrix of irregular bulky tailings minerals, which can be characterized as mine tailings-dominated fabric. It is visible in these images that two particles with different shapes are closely packed and bonded with particle-to-particle contact. More detailed observation reveals that matrices of particles in the specimens with the fly ash ratios of 20 and 40% have a more irregular prominence in the form of particle assemblages and more diversified pore sizes and larger pores in their fabrics. On the other hand, the specimen with the fly ash ratio of 60% appears to be homogeneous with a uniform distribution of pores. This observation is generally consistent with the results of pore size distributions discussed above, although a distinct bimodal porosity feature is not observed. Interestingly, most pores diameters appear to be smaller than 100 μm , which seems in agreement with the MIP results showing in Figures 5.9 and 5.10. This can corroborate the fact that in the case of compacted soils, the pore size distribution detected by MIP is a good estimate of the real pore size distribution, as reported by Simms and Yanful (2004).

5.5.8 Thermal Conductivity as Related to Packing and Mechanical Properties

The relationship between the initial thermal conductivity, λ_i , and bulk unit weight, γ_b , of compacted mixtures of mine tailings and fly ash is shown in Figure 5.12. The initial bulk unit weight is defined as the weight of solids and water per unit volume of specimens immediately after compaction. The initial thermal conductivity increases with increasing initial bulk unit weight with a linear correlation ($R^2 = 0.86$). Similar linear relation between the thermal conductivity and bulk density is found for compacted natural soils (Ekwue et al. 2006; Hotz and Ge 2010). Meanwhile, a linear correspondence exists between the final thermal conductivity, λ_f (i.e., the thermal conductivity measured at 120 hours of curing period) and cumulative pore

volume, V_c , by the MIP test, as seen in Figure 5.13. The final thermal conductivity is inversely proportional to the cumulative pore volume per unit weight ($R^2 = 0.87$). From such correlations, one may deduce that the thermal conductivity of mine tailings and fly ash mixtures is strongly dependent on the packing properties represented by the initial bulk unit weight and the cumulative pore volume after curing. Hence, these parameters play predominant roles in the heat transfer of wet and dry geomaterials and are key parameters for understanding the microfabrics of geomaterials.

Since the changes of thermal conductivity and strength result from the physicochemical processes of compacted specimens of mine tailings and fly ash mixtures, the relationship between these two properties is considered. Figure 5.14 illustrates the unconfined compressive strength, q_u , versus the thermal conductivity, λ , for all specimens, which is obtained by combining the relations depicted in Figures 5.5 and 5.7. An almost linear trend between compressive strength and thermal conductivity can be observed: as the curing time increases, compressive strength increases and thermal conductivity decreases; however, the rate of compressive strength gain per the reduction of thermal conductivity decreases with time.

5.6 Summary and Conclusions

The thermal conductivity, compressive strength, elastic modulus and temperature changes of compacted specimens of mine tailings and fly ash mixtures during the curing period were investigated as functions of the fly ash ratio, molding water content and compaction energy of the specimens. The pore size distribution and microfabrics of the fly ash treated mine tailings were also examined. The thermal conductivity of the compacted mine tailings and fly ash

mixtures was analyzed to relate with their packing and mechanical properties. The significant findings are summarized as follows:

1. The addition of fly ash to mine tailings leads to a decrease in the initial thermal conductivity of the specimens. The highest value of the initial thermal conductivity is obtained at the specimen compacted under the optimum water content. The higher compaction energy causes increases in the initial thermal conductivity of the specimens. As the curing time increases, the difference in the initial thermal conductivities decreases.
2. For all specimens cured in a temperature-controlled environment, a similar trend of internal temperature variations over time is observed: the temperature decreases at the early stage of the curing period and then increases until it reaches the environmental temperature. The higher fly ash content in specimens induces higher initial temperature of the specimens.
3. The unconfined compressive strength of the specimens increases with increasing curing time, though most of the strength gain is attained within the first 24 hours of curing. The increase in the fly ash ratio leads to the increase in the compressive strength of the specimens, indicating that the fly ash is effective in improving the strength of mine tailings by causing cementation. An increase in the molding water content results in a decrease in the compressive strength of the specimens under the same compaction energy, while a higher compressive strength is achieved at higher compaction energy. In general, the change characteristic of the elastic modulus of the specimens is similar to that of the corresponding unconfined compressive strength.

4. A double porosity fabric represented by macropores and micropores is identified in the specimens of mine tailings and fly ash mixtures. As the fly ash ratio increases, both the unit pore volume and mean pore size decreases owing to denser packing. The specimen with the fly ash ratio of 60% displays a monomodal pore size distribution, representing the highest packing density. The mean pore size of the specimen compacted at the dry side of optimum water content is larger than those compacted at the optimum and the wet of optimum, which is mostly attributed to the redistribution of macropores. Increasing compaction energy leads to a substantial reduction in both the macropores and micropores but the bimodal fabric remains unchanged. The surface fabrics of the specimens were investigated using SEM observation, which correlated well with the corresponding pore size distribution indicated by the MIP test.
5. Linear relationships are established between the initial thermal conductivity and bulk unit weight as well as between the final thermal conductivity and cumulative pore volume per unit weight for all specimens tested. The relationships between the thermal conductivity and compressive strength in mine tailings and fly ash mixtures suggest that the thermal conductivity measurement can potentially be useful for quality control/quality assurance in field applications.

The findings presented in this study will be beneficial for understanding the short-term development of thermal and mechanical behaviors of mine tailings treated with fly ash.

References

Aligizaki, K.K. (2006). *Pore structure of cement-based materials: testing, interpretation and requirement*, Taylor and Francis, London and New York.

- Al-Rawas, A.A. (2002). "Microfabric and mineralogical studies on the stabilization of an expansive soil using cement by-pass dust and some types of slags." *Canadian Geotechnical Journal*, 39(5), 1150-1167.
- ASTM. (2004). "Standard practice for characterizing fly ash for use in soil stabilization." *D5239-04*, West Conshohocken, Pa.
- ASTM. (2007). "Standard test methods for laboratory compaction characteristics of soil using standard effort [12,400 ft-lb/ft³ (600 kN-m/m³)]." *D698-07*, West Conshohocken, Pa.
- ASTM. (2008a). "Standard specification for coal fly ash and raw for calcined natural pozzolan for use in concrete." *C618-08a*, West Conshohocken, Pa.
- ASTM. (2008b). "Standard test method for determination of thermal conductivity of soil and soft rock by thermal needle probe procedure." *D5334-08*, West Conshohocken, Pa.
- ASTM. (2009a). "Standard test methods for laboratory compaction characteristics of soil using modified effort [56,000 ft-lb/ft³ (2,700 kN-m/m³)]." *D1557-09*, West Conshohocken, Pa.
- ASTM. (2009b). "Standard test methods for unconfined compressive strength of compacted soil-lime mixtures." *D5102-09*, West Conshohocken, Pa.
- Bussiere, B. (2007). "Colloquium 2004: hydrogeotechnical properties of hard rock tailings from metal mines and emerging geoenvironmental disposal approaches." *Canadian Geotechnical Journal*, 44(9), 1019-1052.
- Cetin, B., Aydilek, A.H., and Guney, Y. (2010). "Stabilization of recycled base materials with high carbon fly ash." *Resources, Conservation and Recycling*, 54(11), 878-892.
- Choquette, M., Berube, M., and Locat, J. (1987). "Mineralogical and microtextural changes associated with lime stabilization of marine clays from Eastern Canada." *Applied Clay Science*, 2(3), 215-232.
- Cote, J., and Konrad, J. (2009). "Assessment of structure effects on the thermal conductivity of two-phase porous geomaterials." *International Journal of Heat and Mass Transfer*, 52(3-4), 796-804.

- Cuisinier, O., Auriol, J., Le Borgne, T., and Deneele, D. (2011). "Microstructure and hydraulic conductivity of a compacted lime-treated soil." *Engineering Geology*, 123(3), 187-193.
- Degirmenci, N., Okucu, A., and Turabi, A. (2007). "Application of phosphogypsum in soil stabilization." *Building and Environment*, 42(9), 3393-3398.
- Daniel, D.E., and Benson, C.H. (1990). "Water content-density criteria for compacted soil liners." *Journal of Geotechnical Engineering*, 116(12), 1811-1830.
- Daniel, D.E., and Wu, Y. (1993). "Compacted clay liners and covers for arid sites." *Journal of Geotechnical Engineering*, 119(2), 223-237.
- Delage, P. (2010). "A microstructure approach to the sensitivity and compressibility of some Eastern Canada sensitive clays." *Geotechnique*, 60(5), 353-368.
- Delage, P., Audiguier, M., Cui, Y., and Howat, M.D. (1996). "Microstructure of a compacted silt." *Canadian Geotechnical Journal*, 33(1), 150-158.
- Edil, T.B., Acosta, H.A., and Benson, C.H. (2006). "Stabilizing soft fine-grained soils with fly ash." *Journal of Materials in Civil Engineering*, 18(2), 283-294.
- Ekwue, E.I., Stone, R.J., and Bhagwat, D. (2006). "Thermal conductivity of some compacted Trinidadian soils as affected by peat content." *Biosystems Engineering*, 94(3), 461-469.
- Fall, M., Celestin, J.C., and Han, F.S. (2009). "Suitability of bentonite-paste tailings mixtures as engineering barrier material for mine waste containment facilities." *Minerals Engineering*, 22(9-10), 840-848.
- Ghosh, A., and Subbarao, C. (2007). "Strength characteristics of class F fly ash modified with lime and gypsum." *Journal of Geotechnical and Geoenvironmental Engineering*, 133(7), 757-766.
- Guney, Y., Aydilek, A.H., and Demirkan, M.M. (2006). "Geoenvironmental behavior of foundry sand amended mixture for highway subbases." *Waste Management*, 26(9), 932-945.

- Helinski, M., Fahey, M., and Fourie, A. (2011). "Behavior of cemented paste backfill in two mine stopes: measurements and modeling." *Journal of Geotechnical and Geoenvironmental Engineering*, 137(2), 171-182.
- Horpibulsuk, S., Rachan, R., and Raksachon, Y. (2009). "Role of fly ash on strength and microstructure development in blended cement stabilized silty clay." *Soils and Foundations*, 49(1), 85-89.
- Hotz, R.D., and Ge, L. (2010). "Investigation of the thermal conductivity of compacted silts and its correlation to the elastic modulus." *Journal of Materials in Civil Engineering*, 22(4), 408-412.
- Indraratna, B., Nutalaya, P., and Kuganenthira, N. (1991). "Stabilization of a dispersive soil by blending with fly ash." *Quarterly Journal of Engineering Geology*, 24(3), 275-290.
- Juang, C.H., and Holtz, R.D. (1986). "Fabric, pore size distribution, and permeability of sandy soils." *Journal of Geotechnical Engineering*, 112(9), 855-868.
- Kolay, P.K., and Singh, D.N. (2002). "Application of coal ash in fluidized thermal beds." *Journal of Materials in Civil Engineering*, 14(5), 441-444.
- Kolias, S., Kasselouri-Rigopoulou, V., and Karahalios, A. (2005). "Stabilization of clayey soils with high calcium fly ash and cement." *Cement and Concrete Composites*, 27(2), 301-313.
- Lade, P.V., Liggio, C.D., and Yamamuro, J.A. (1998). "Effects of non-plastic fines on minimum and maximum void ratios of sand." *Geotechnical Testing Journal*, 21(4), 1173-1188.
- Nalbantoglu, Z., and Tuncer, E.R. (2001). "Compressibility and hydraulic conductivity of a chemically treated expansive clay." *Canadian Geotechnical Journal*, 38(1), 154-160.
- Osinubi, K.J. (1998). "Influence of compactive efforts and compaction delays on lime-treated soil." *Journal of Transportation Engineering*, 124(2), 149-155.
- Ozyildirim, C., and Carino, N.J. (2006). "Concrete strength testing." *Significance of Tests and Properties of Concrete and Concrete-making Materials* edited by Lamond, J.E., and Pielert, J.H., ASTM STP 169D, 125-140.

- Peethamparan, S., Olek, J., and Lovell, J. (2008). "Influence of chemical and physical characteristics of cement kiln dusts (CKDs) on their hydration behavior and potential suitability for soil stabilization." *Cement and Concrete Research*, 38(6), 803-815.
- Penumadu, D., and Dean, J. (2000). "Compressibility effect in evaluating the pore-size distribution of kaolin clay using mercury intrusion porosity." *Canadian Geotechnical Journal*, 37(2), 393-405.
- Phanikumar, B.R., and Sharma, R.S. (2007). "Volume change behavior of fly-ash-stabilized clays." *Journal of Materials in Civil Engineering*, 19(1), 67-74.
- Pilito, C.P., and Martin, II J.R. (2001). "Effects of nonplastic fines on the liquefaction resistance of sands." *Journal of Geotechnical and Geoenvironmental Engineering*, 127(5), 408-415.
- Qian, G., Haung, T., and Bai, S. (2011). "Use of cement-stabilized granite mill tailings as pavement subbase." *Journal of Materials in Civil Engineering*, 23(11), 1575-1578.
- Sawangsurriya, A., Edil, T.B., and Bosscher, P.J. (2008). "Modulus-suction-moisture relationship for compacted soil." *Canadian Geotechnical Journal*, 45(7), 973-983.
- Simms, P.H., and Yanful, E.K. (2001). "Measurement and estimation of pore shrinkage and pore distribution in a clayey till during soil-water characteristics curve tests." *Canadian Geotechnical Journal*, 38(4), 741-754.
- Simms, P.H., and Yanful, E.K. (2004). "A discussion of the application of mercury intrusion porosimetry for the investigation of soils, including an evaluation of its use to estimate volume change in compacted clayey soils." *Geotechnique*, 54(6), 421-426.
- Solanki, P., Khoury, N., and Zaman, M.M. (2009). "Engineering properties and moistures susceptibility of silty clay stabilized with lime, class C fly ash, and cement kiln dust." *Journal of Materials in Civil Engineering*, 21(12), 749-757.
- Tarantino, A., and De Col, E. (2008). "Compaction behaviour of clay." *Geotechnique*, 58(3), 199-213.

- Tastan, E.O., Edil, T.B., Benson, C.H., and Aydilek, A.H. (2011). "Stabilization of organic soils with fly ash." *Journal of Geotechnical and Geoenvironmental Engineering*, 137(9), 819-833.
- Thevanayagam, S., Shenthan, T., Mohan, S., and Liang, J. (2002). "Undrained fragility of clean sands, silty sands and sandy silts." *Journal of Geotechnical and Geoenvironmental Engineering*, 128(10), 849-859.
- Wang, H.L., Shang, J.Q., Kovac, V., and Ho, K.S. (2006). "Utilization of Atikokan coal fly ash in acid rock drainage control from Musselwhite mine tailings." *Canadian Geotechnical Journal*, 43(3), 229-243.
- Washburn, E.W. (1921). "Note on a method of determining the distribution of pore sizes in a porous material." *Proceedings of the National Academy of Science*, 7(4), 115-116.
- Yang, S.R, Haung, W.H., and Tai, Y.T. (2005). "Variation of resilient modulus with soil suction for compacted subgrade soils." *Transportation Research Record*, 1913, 99-106.
- Yeheyis, M.B., Shang, J.Q., and Yanful, E.K. (2009). "Long-term evaluation of coal fly ash and mine tailings co-placement: a site-specific study." *Journal of Environmental Engineering*, 91(1), 237-244.
- Yilmaz, Y. (2009). "A study on the limit void ratio characteristics of medium to fine mixed graded sands." *Engineering Geology*, 104(3-4), 290-294.

Table 5.1 Physical properties of test materials

Properties	Mine tailings	Fly ash
Specific gravity, G_s	3.37	2.54
Optimum water content, w_{opt} (%) [†]	12.6	11.9
Maximum dry unit weight, $\gamma_{d\max}$ (kN/m ³) [†]	20.4	16.6
Effective size, D_{10} (μm)	2.8	0.8
Median size, D_{50} (μm)	25.6	15.2
Coefficient of uniformity, C_u	11.43	25.61
Coefficient of curvature, C_c	1.61	2.61

[†] ASTM D 698 (ASTM 2007)

Table 5.2 Oxide composition of test materials (adapted from Wang et al. 2006)

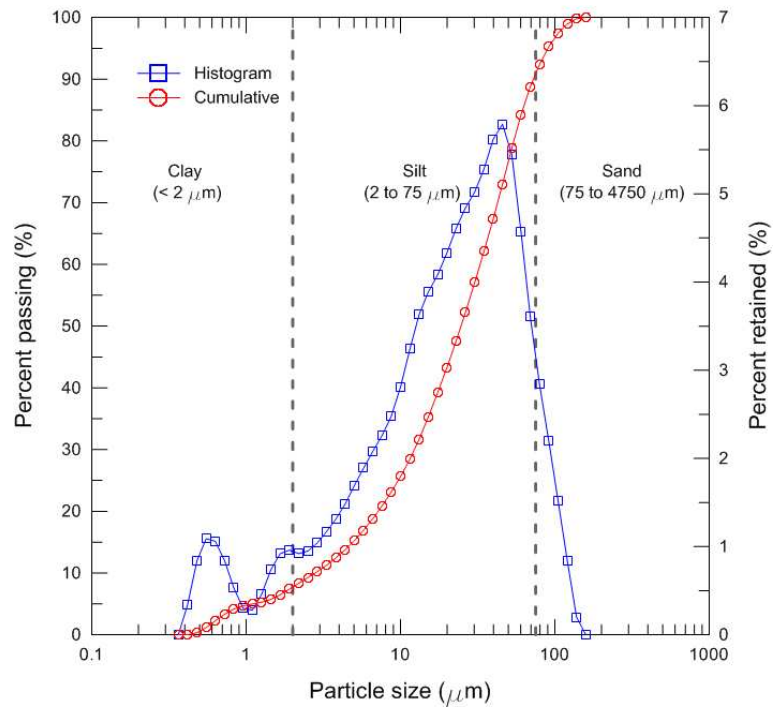
Component (%)	Mine tailings	Fly ash
SiO ₂	50.82	37.99
Al ₂ O ₃	8.87	19.92
Fe ₂ O ₃	28.97	6.17
MnO	0.36	0.03
MgO	3.39	3.52
CaO	3.19	15.66
K ₂ O	0.84	0.62
Na ₂ O	0.02	9.30
P ₂ O ₅	0.15	0.69
Cr ₂ O ₃	0.02	0.00
TiO ₂	0.45	0.84
Loss on ignition	0.05	0.68
Total	97.13	95.12

Table 5.3 Summary of specimens tested

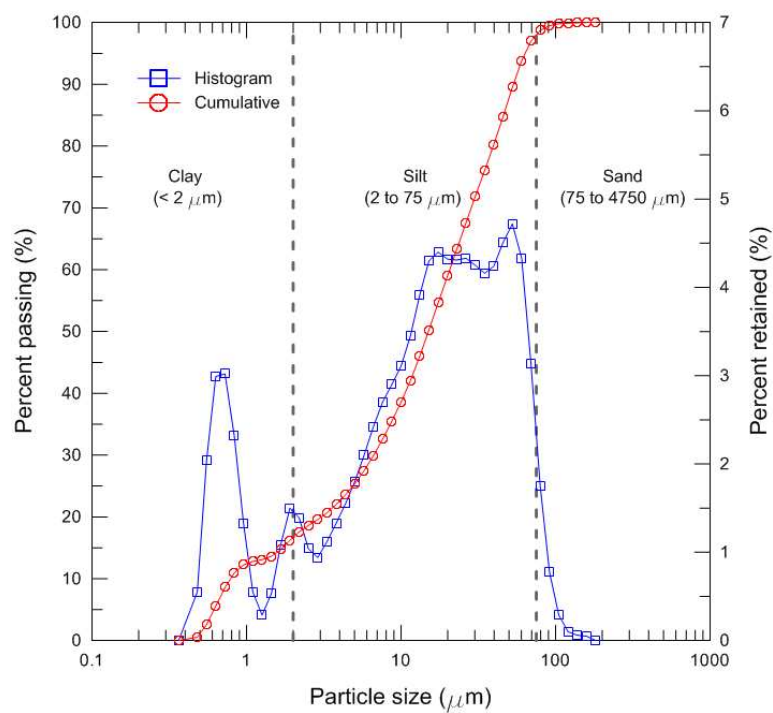
Specimen ID [†]	Water content, w (%)	Dry unit weight, γ_d (kN/m ³)
FA20 - SP - OWC	12.4	19.5
FA40 - SP - OWC	11.6	19.2
FA60 - SP - OWC	11.0	18.9
FA20 - SP - DWC	10.5	19.2
FA20 - SP - WWC	14.3	19.0
FA20 - HP - OWC	12.4	20.0

Note: FA = fly ash; OWC = optimum water content; DWC = dry water content; WWC = wet water content; SP = standard Proctor energy (590 kJ/m³); HP = high Proctor energy (1,190 kJ/m³); the numbers that follow the FA indicate the percentage by weight of fly ash added to the mine tailings, i.e., fly ash ratio.

[†] Each specimen consists of five samples with identical properties of mine tailings and fly ash mixtures.



(a)



(b)

Figure 5.1 Particle size distributions of (a) Musselwhite mine tailings and (b) Atikokan fly ash

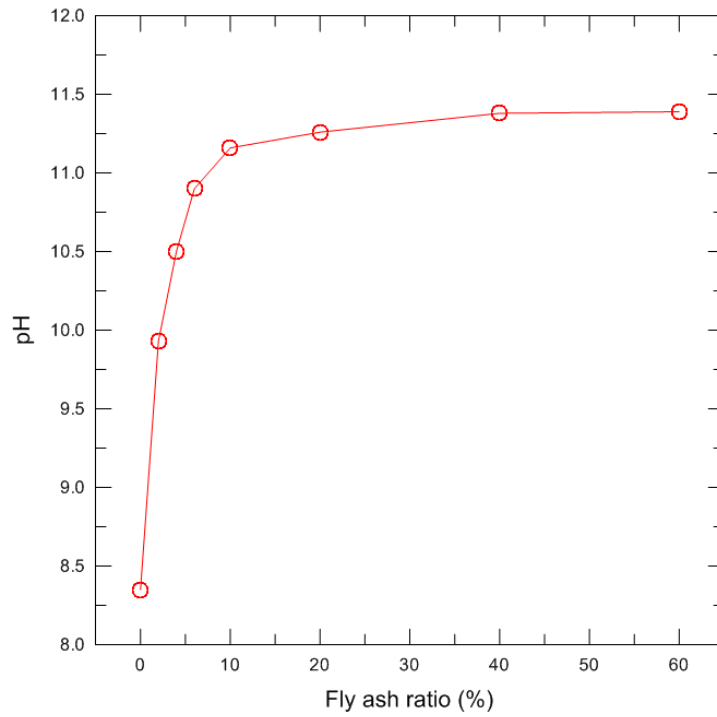


Figure 5.2 pH variation of mine tailings and fly ash slurries

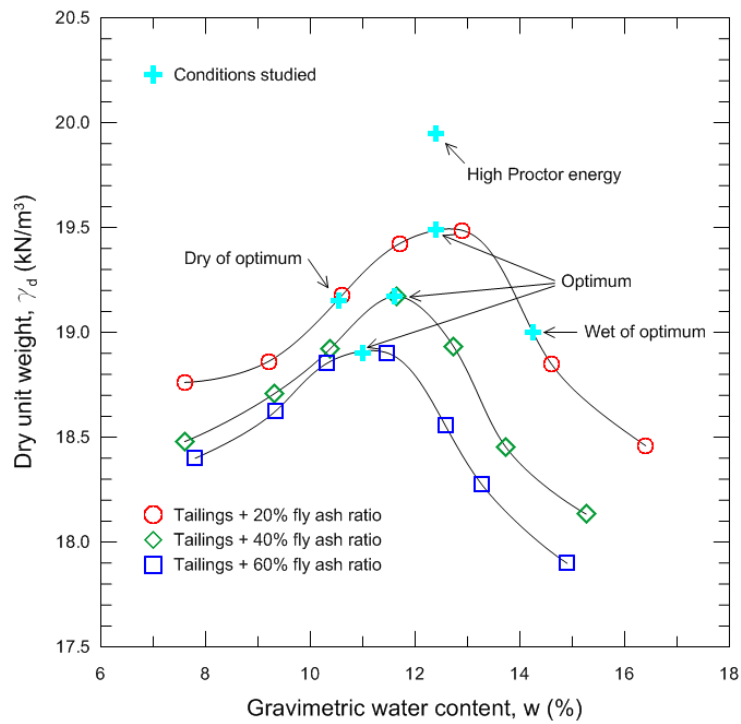


Figure 5.3 Compaction curves and conditions studied

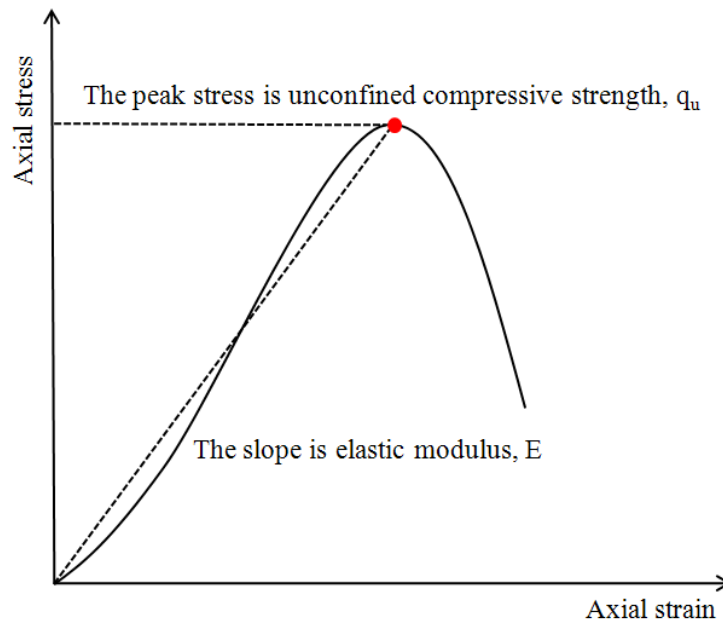
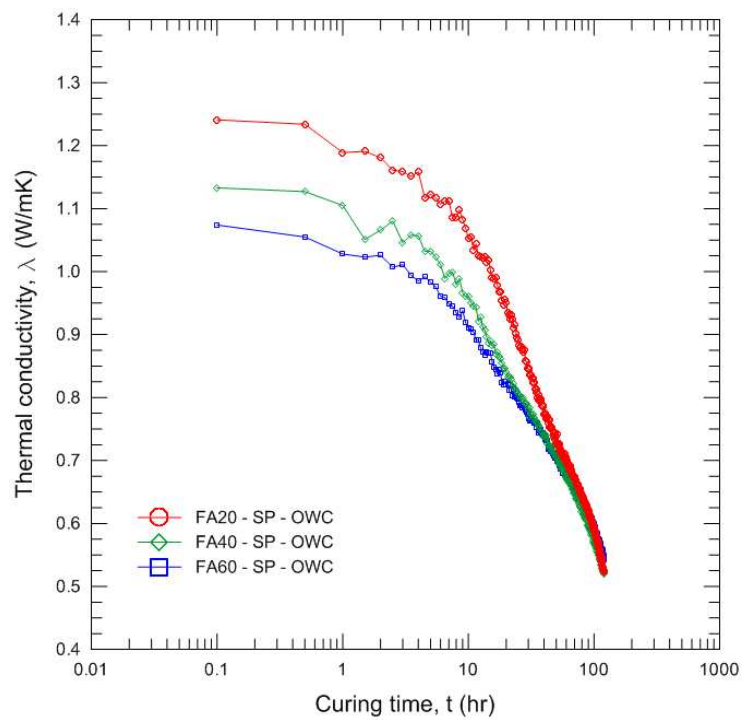
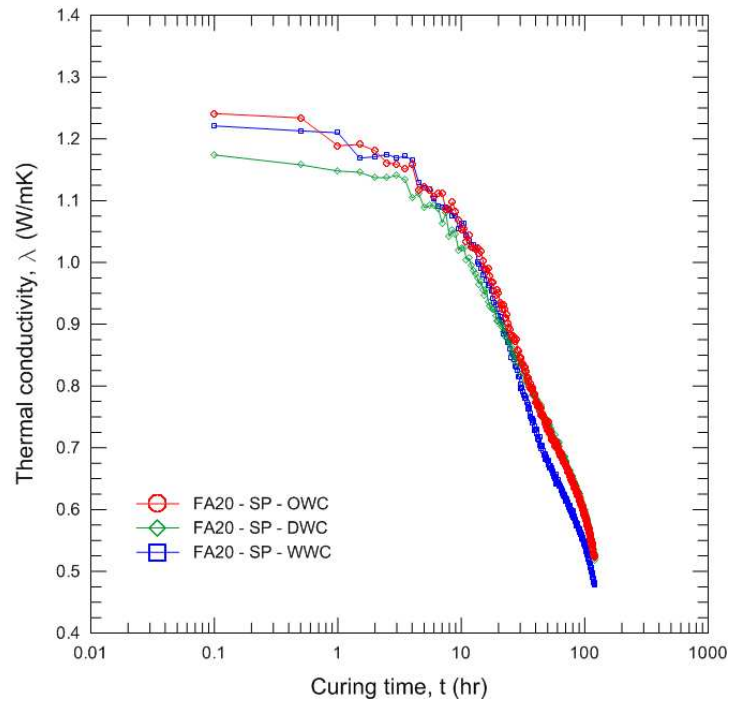


Figure 5.4 Typical stress and strain curve of compacted mine tailings and fly ash mixtures

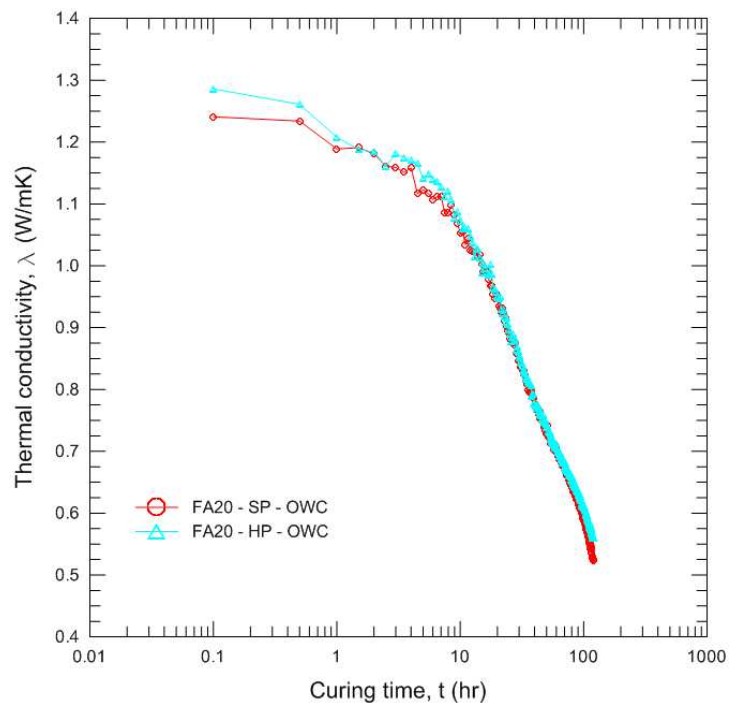


(a)

Figure 5.5 Variations of thermal conductivity with curing time: effects of (a) fly ash ratio, (b) molding water content, and (c) compaction energy

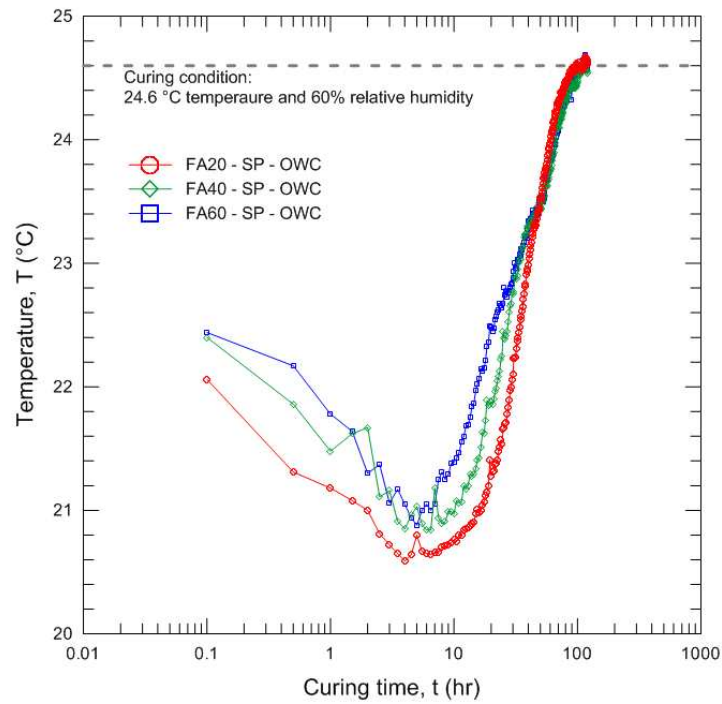


(b)

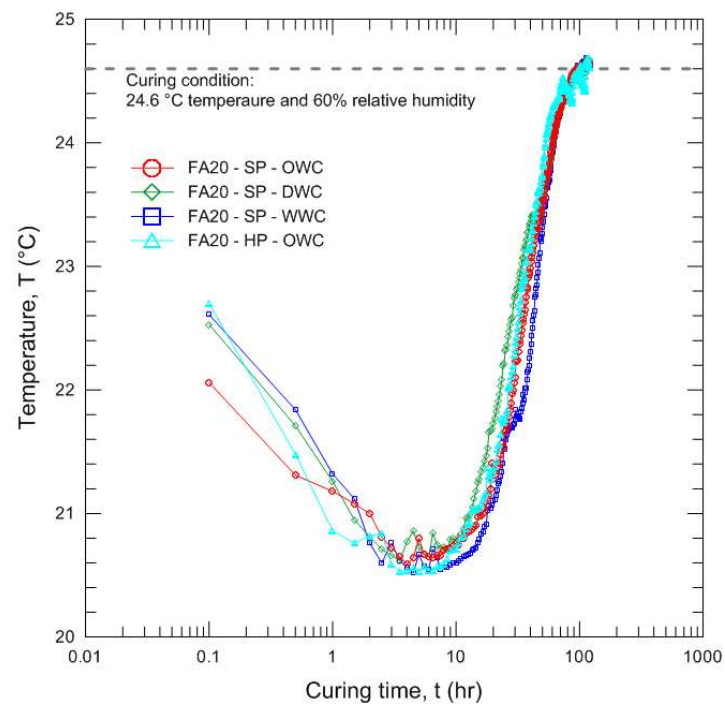


(c)

Figure 5.5 Variations of thermal conductivity with curing time: effects of (a) fly ash ratio, (b) molding water content, and (c) compaction energy (continued)

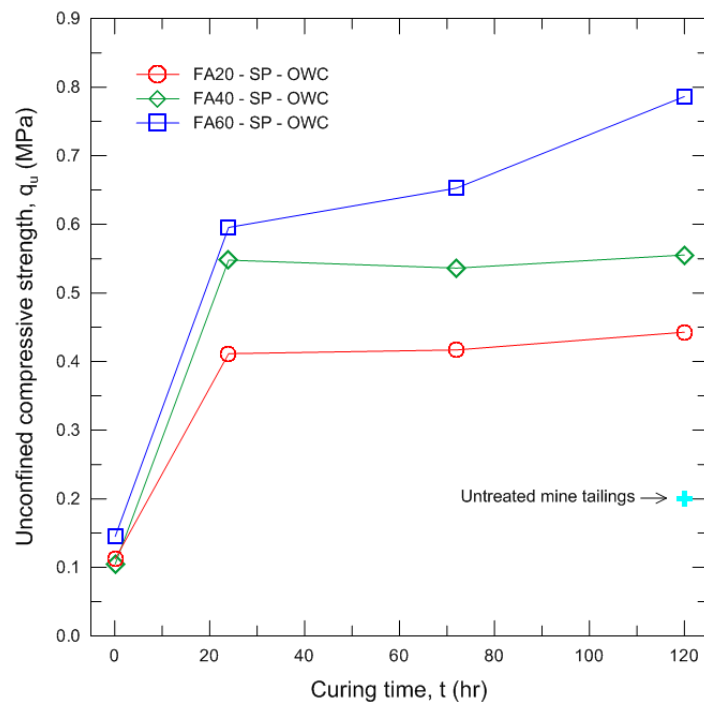


(a)

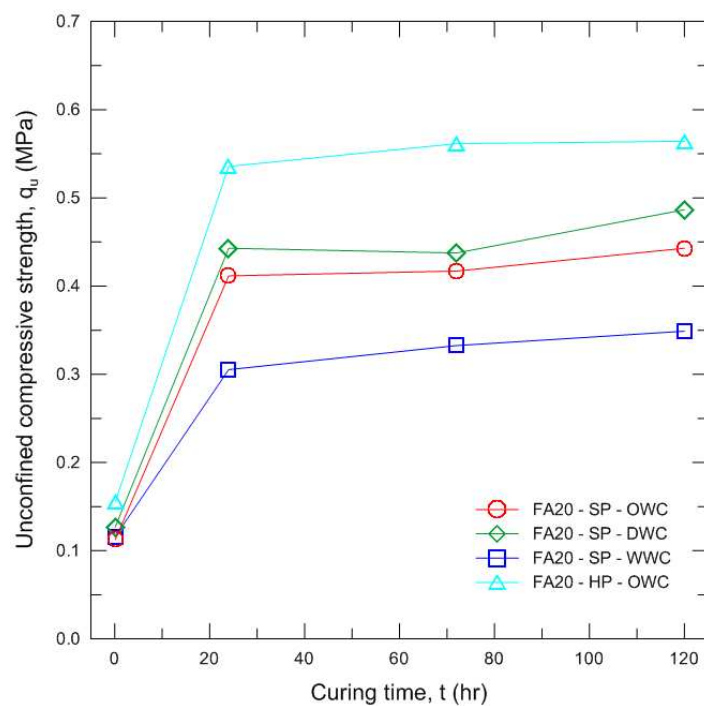


(b)

Figure 5.6 Variations of temperature with curing time: effects of (a) fly ash ratio and (b) molding water content and compaction energy

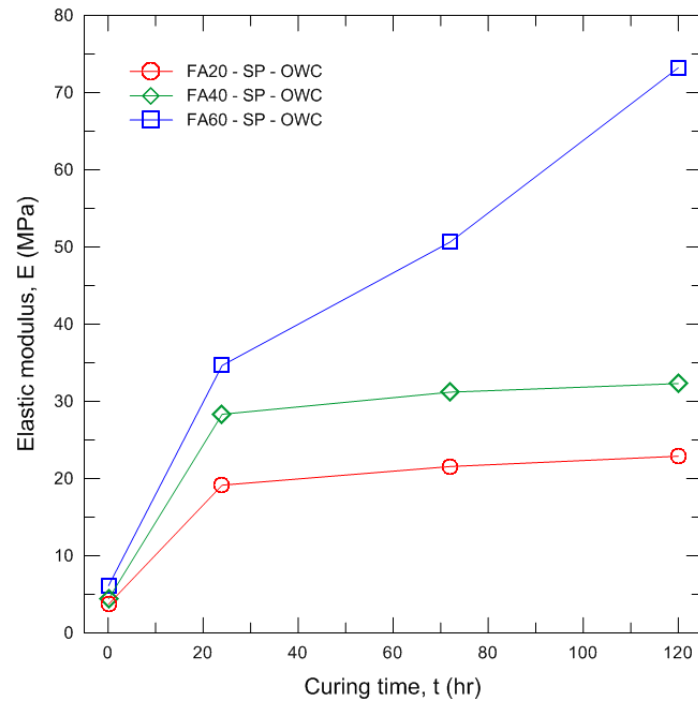


(a)

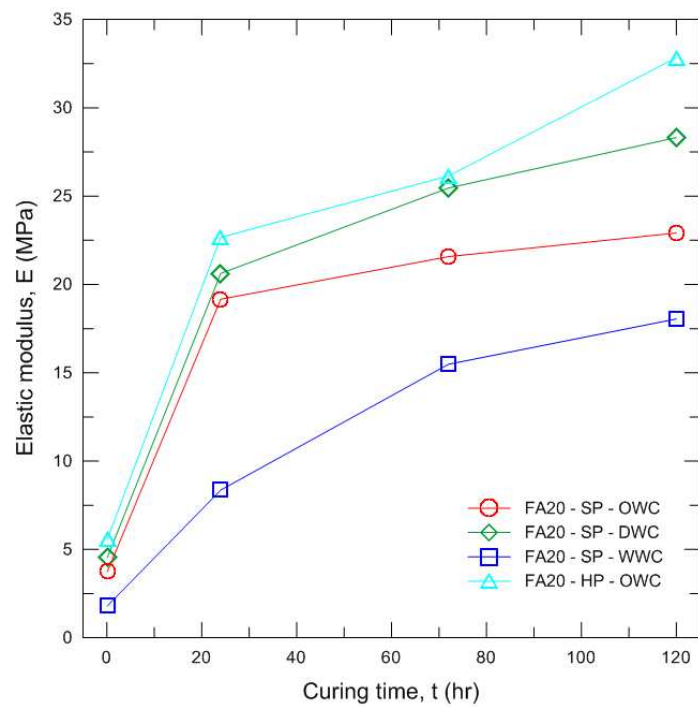


(b)

Figure 5.7 Variations of unconfined compressive strength with curing time: effects of (a) fly ash ratio and (b) molding water content and compaction energy

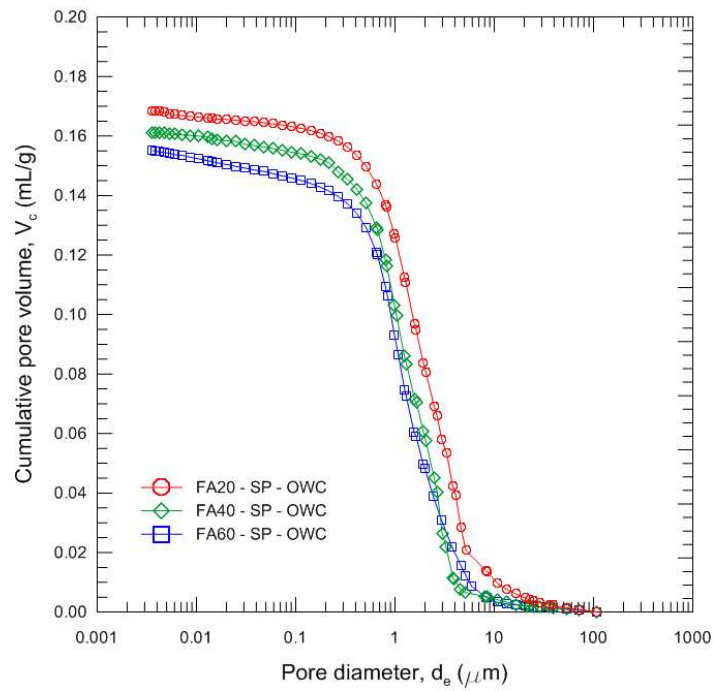


(a)

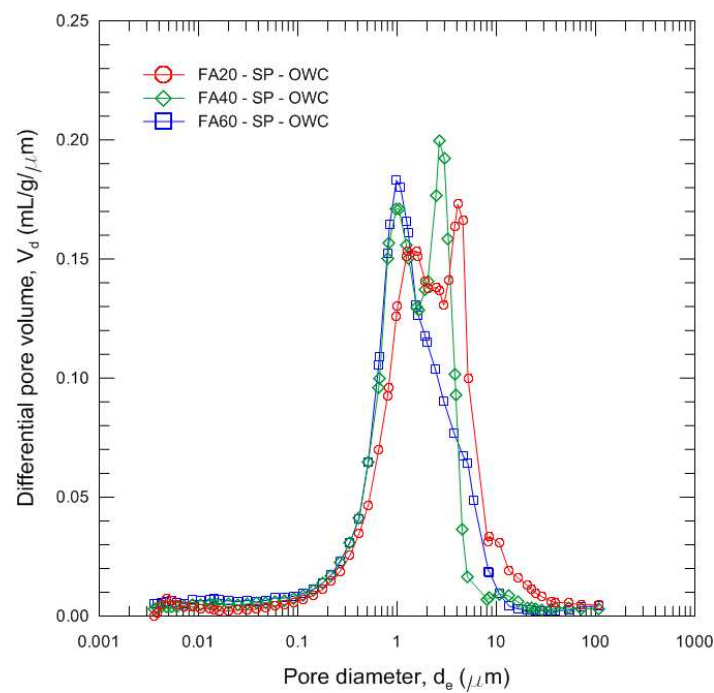


(b)

Figure 5.8 Variations of elastic modulus with curing time: effects of (a) fly ash ratio and (b) molding water content and compaction energy

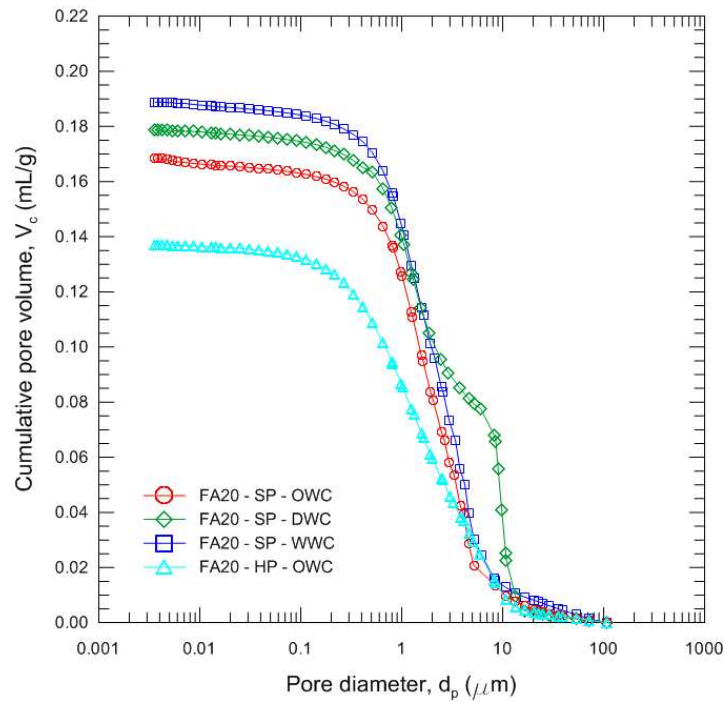


(a)

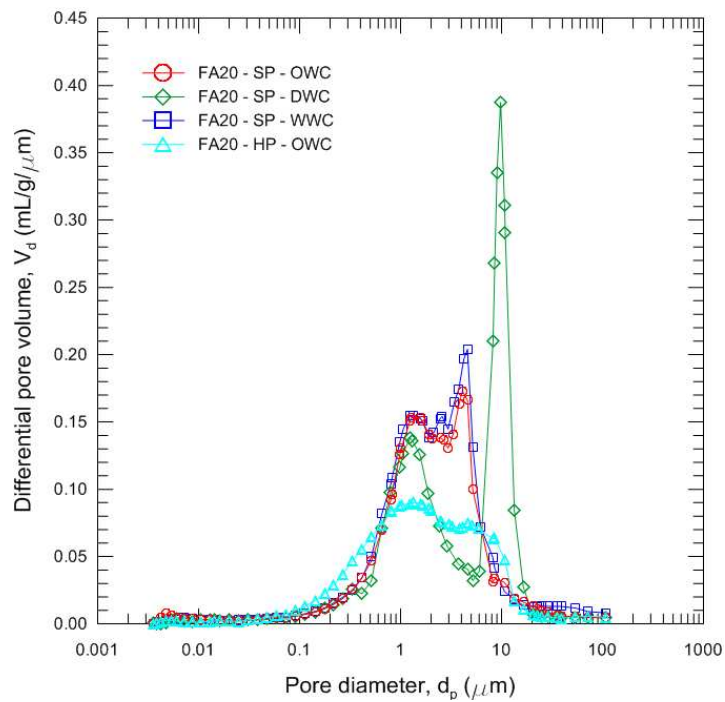


(b)

Figure 5.9 Mercury intrusion porosimetry results of the 120 hours-cured specimens with different fly ash ratios (20, 40 and 60%): (a) cumulative pore volume; (b) differential pore volume

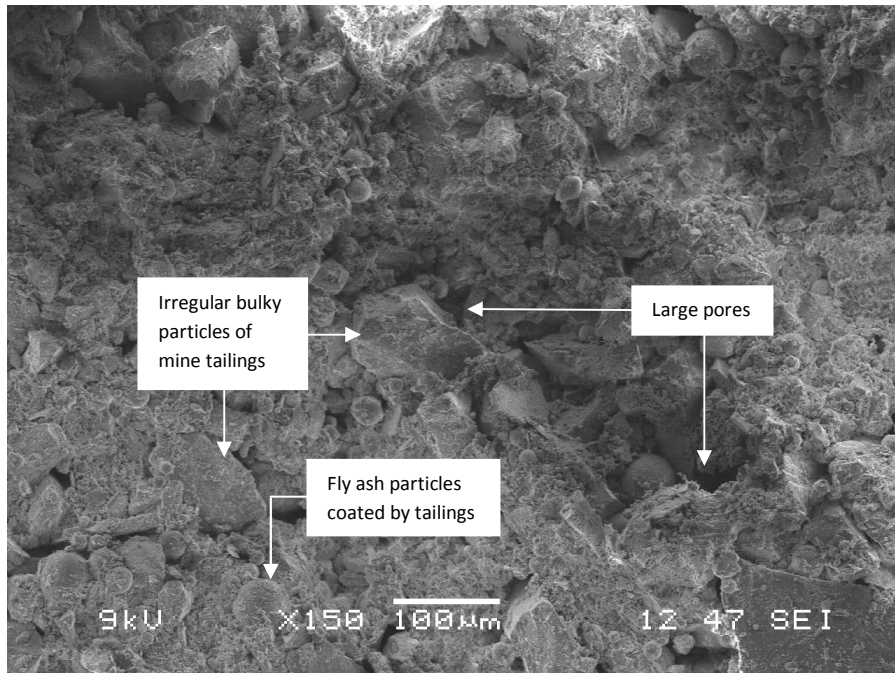


(a)

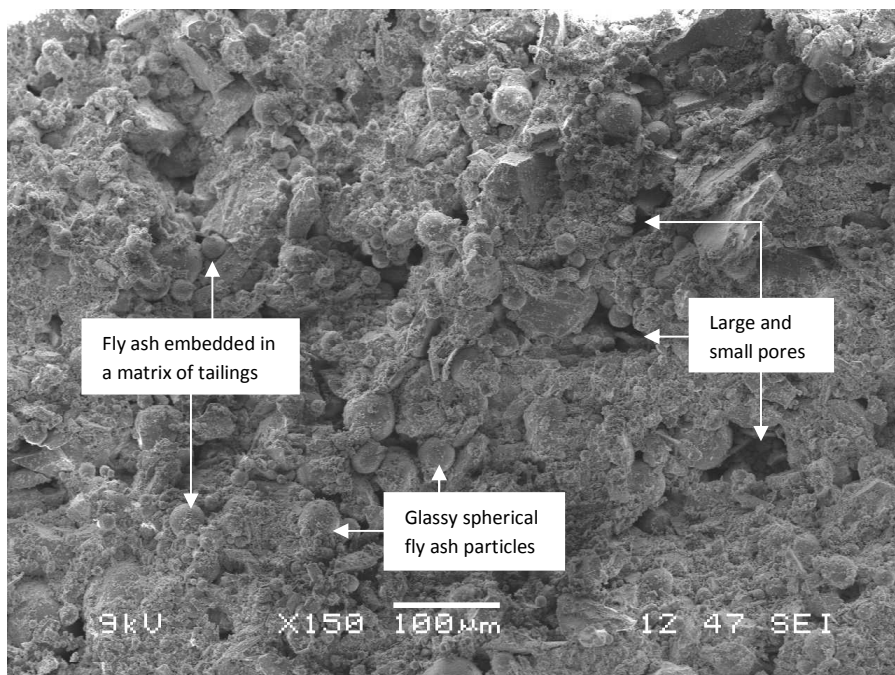


(b)

Figure 5.10 Mercury intrusion porosimetry results of the 120 hours-cured specimens compacted at different compaction conditions: (a) cumulative pore volume; (b) differential pore volume

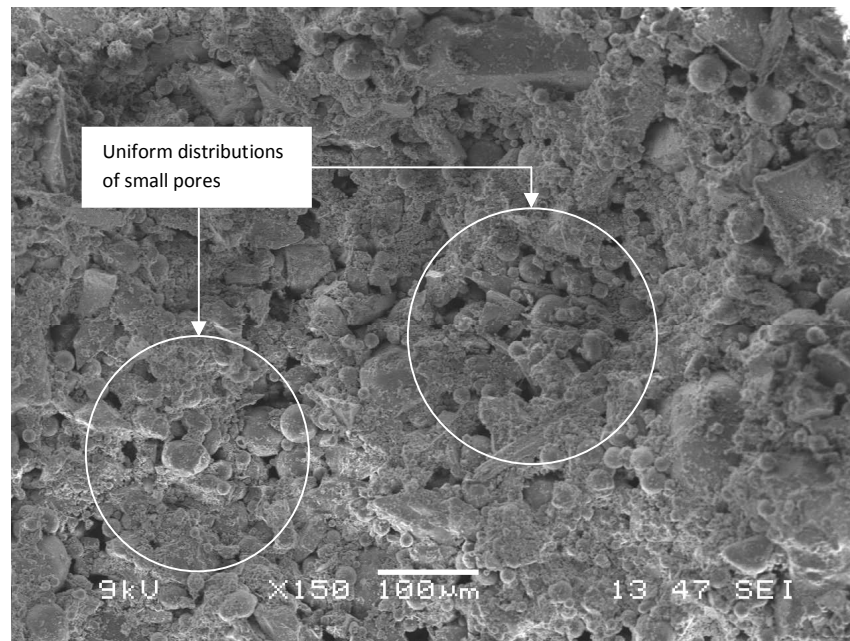


(a)



(b)

Figure 5.11 SEM images of the 120 hours-cured samples with different fly ash ratios: (a) FA = 20%; (b) FA = 40%; (c) FA = 60%



(c)

Figure 5.11 SEM images of the 120 hours-cured samples with different fly ash ratios: (a) FA = 20%; (b) FA = 40%; (c) FA = 60% (continued)

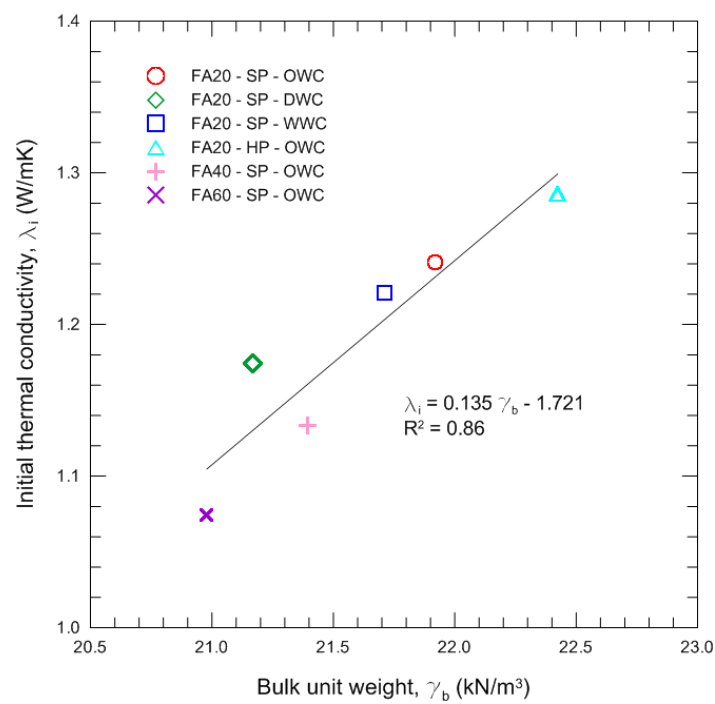


Figure 5.12 Relationship between initial thermal conductivity and bulk unit weight

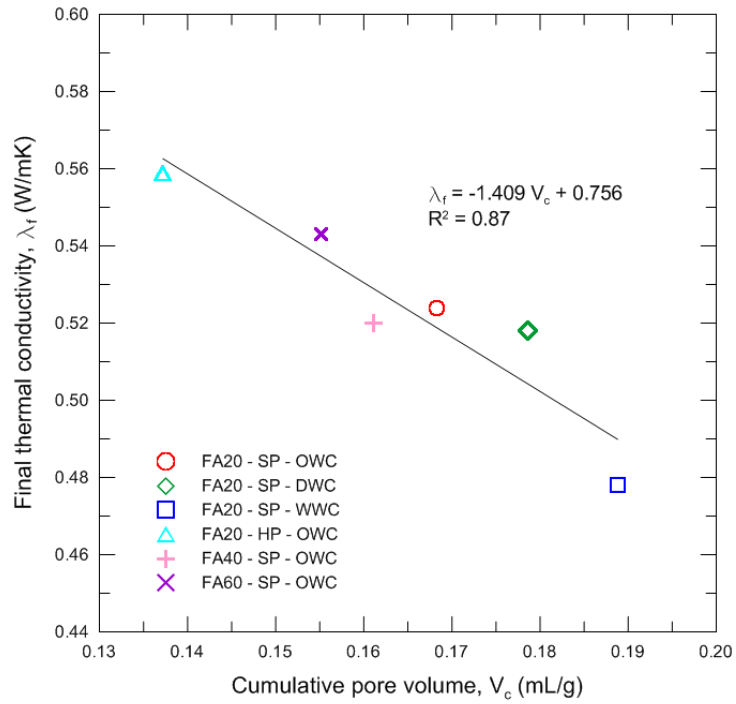


Figure 5.13 Relationship between final thermal conductivity and cumulative pore volume

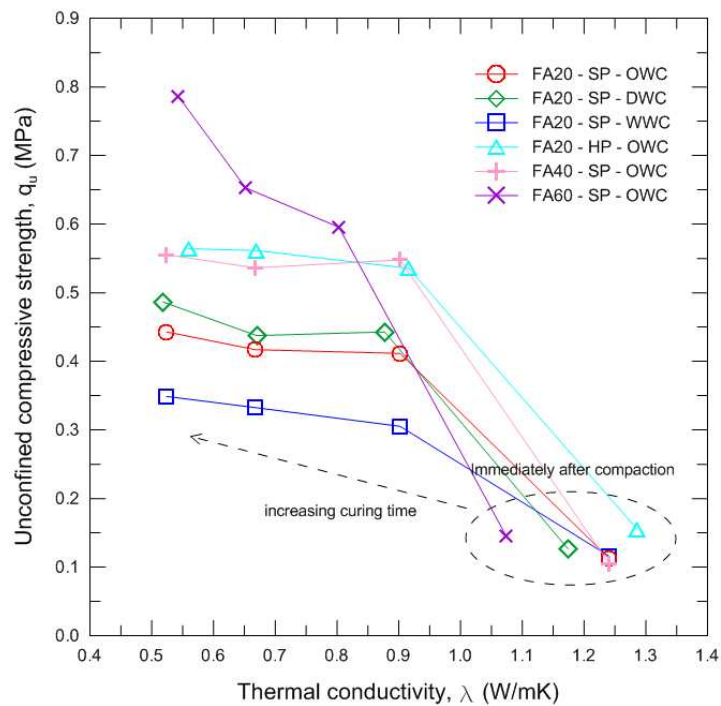


Figure 5.14 Relationship between unconfined compressive strength and thermal conductivity

CHAPTER 6

CONCLUSIONS

6.1 Summary and Conclusions

The thesis presents a comprehensive study on the thermal and electrical characteristics of selected geomaterials used in geotechnical engineering applications. The thermal and electrical properties (i.e., thermal conductivity, electrical conductivity and volumetric heat capacity) of the geomaterials investigated strongly depend on their compositions and fabrics. The specific findings regarding these aspects drawn from this study are as follows:

The electrical conductivity of compacted kaolin clay is influenced by the porosity, dry unit weight, pore water (gravimetric water content, degree of saturation and volumetric water content), as well as pore water salinity. It is found that for a constant pore water salinity, the electrical conductivity is most significantly related to the volumetric water content. The Rhoades model as a function of the volumetric water content and pore water salinity gives best estimate of the electrical behavior of the compacted kaolin clay comparing to other existing models.

In the case of the dry mixtures of mine tailings and tire crumbs, the factors affecting the packing properties (porosity and bulk unit weight) of the mixtures including the particle size, shape and gradation as well as the container wall effect and packing method control the thermal conductivity and volumetric heat capacity. The porosity of mixtures plays a preponderant role in heat transfer on the dry mixtures: the thermal conductivity and volumetric heat capacity increased linearly with decreasing porosity. At the volumetric mixing ratios of 0.55 to 0.75 for tire crumbs, the mixture fabric transits from a rigid (i.e., a mine tailings dominated fabric) to a soft (i.e., a tire crumbs dominated fabric) granular skeleton, which is directly related to the

thermal conductivity behavior of the mixtures. A prediction model for the thermal conductivity and an analysis diagram for estimating the volumetric heat capacity are developed as a function of the volumetric mixing ratio of tire crumbs and porosity.

The thermal conductivity of compacted mixtures of mine tailings and tire crumbs is dependent on the molding water content, mixing ratio of tire crumbs, compactive effort and tire crumbs size. It is shown that a clear correspondence exists between the thermal conductivity and bulk density of the compacted mixtures, irrespective of the influencing factors. The anisotropic thermal conductivity of the compacted mixtures is examined and the results reveal that the effect is more pronounced when the mixtures have lower water contents. The experimental data are processed via analysis of variance (ANOVA) and the results indicate that the factors included in the simulation are statistically significant. A multiple linear regression model is established to relate the thermal conductivity and the mixture composition and compaction conditions.

The change in the thermal conductivity of compacted mine tailings and fly ash mixtures over curing time as affected by the fly ash ratio, molding water content and compaction energy is evaluated. The thermal conductivities of the compacted mixtures decrease with increasing curing time. Importantly, the higher initial thermal conductivity is attained at lower fly ash ratios and higher compaction energy as well as under the optimum water content. Such results are highly associated to the fabric of the mixtures that reflects the proportions of their components, packing of solid particles and micropore structure. The decrease of the thermal conductivity is strongly related to the increase in compressive strength of the fly ash treated tailings.

6.2 Suggestions for Future Research

Although critical factors in the thermal and electrical behaviors of some geomaterials are investigated in this study, many issues should be studied in future research, for example,

1. Effects of temperature on the thermal and electrical characteristics of geomaterials;
2. Effects of pore fluid chemistry and organic matter on the thermal and electrical characteristics of geomaterials;
3. Relationship between thermal and electrical properties of geomaterials; and
4. Development of thermal and electrical properties of chemically treated geomaterials with high water content over time.

It is believed that the studies on these issues will be beneficial for understanding the thermal and electrical behaviors of geomaterials.

APPENDIX A: Definition and Meaning of Statistical Measures

The statistical measures, i.e., mode D_m , mean \bar{D} , standard deviation σ , skewness Sk and kurtosis K , can be used to demonstrate a particle size distribution characteristics, which is described succinctly by Blott and Pye (2001): those quantifying the size with the highest frequency; the average size; the spread (sorting) of the size around the average; the symmetry or preferential spread (skewness) to one side of the average; and the degree of concentration of the particles relative to the average (kurtosis). These measures are commonly calculated geometrically (based on log-normal distribution) using moment method, which are defined as follows:

$$\bar{D} = \exp \sum f \ln D \quad (\text{A.1})$$

$$\sigma = \exp \sqrt{\sum f (\ln D - \ln \bar{D})^2} \quad (\text{A.2})$$

$$Sk = \frac{\sum f (\ln D - \ln \bar{D})^3}{\ln \sigma^3} \quad (\text{A.3})$$

$$K = \frac{\sum f (\ln D - \ln \bar{D})^4}{\ln \sigma^4} \quad (\text{A.4})$$

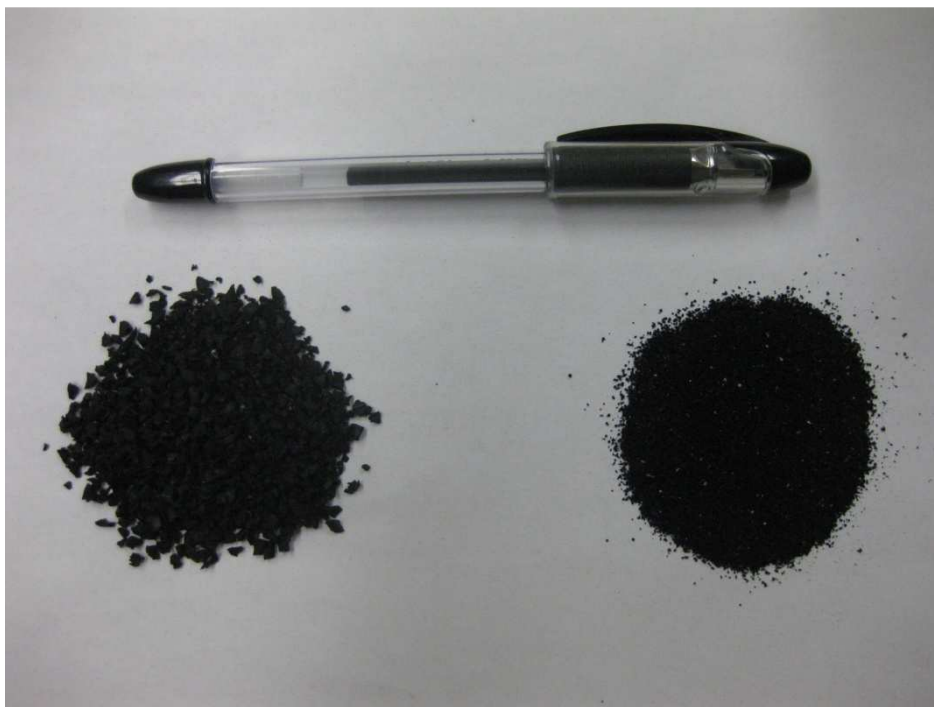
where f is the fraction of particles between two sieve sizes, and D is the average particle size between two sieve sizes.

APPENDIX B: Photographs of Materials and Experiments

This appendix provides supplementary information to the materials and experiments presented in Chapters 3 to 5. It contains the photographs taken during the performance of the experiments. The photographs are included in the thesis as a record.

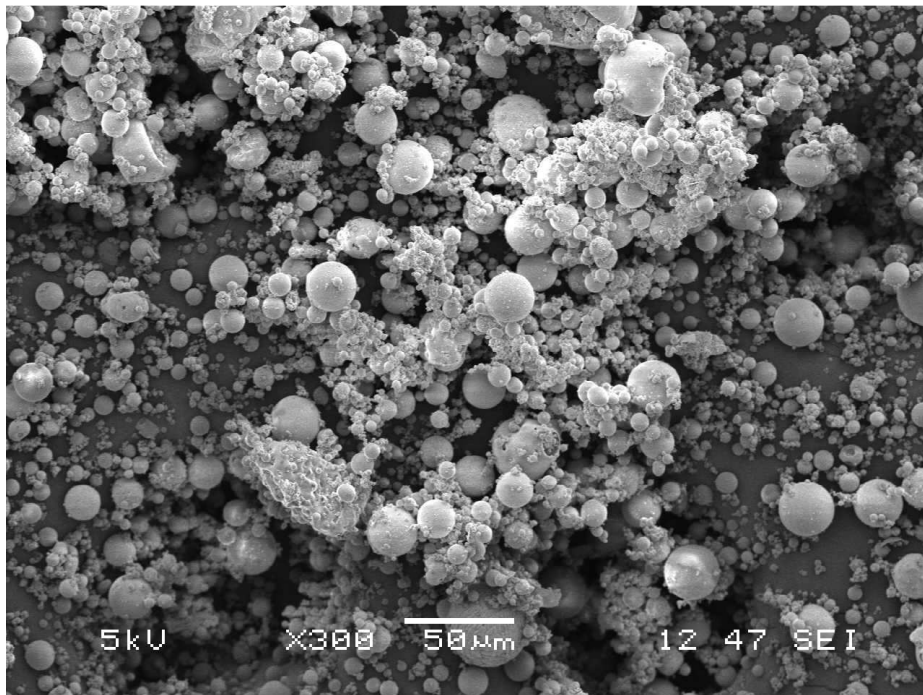


(a)

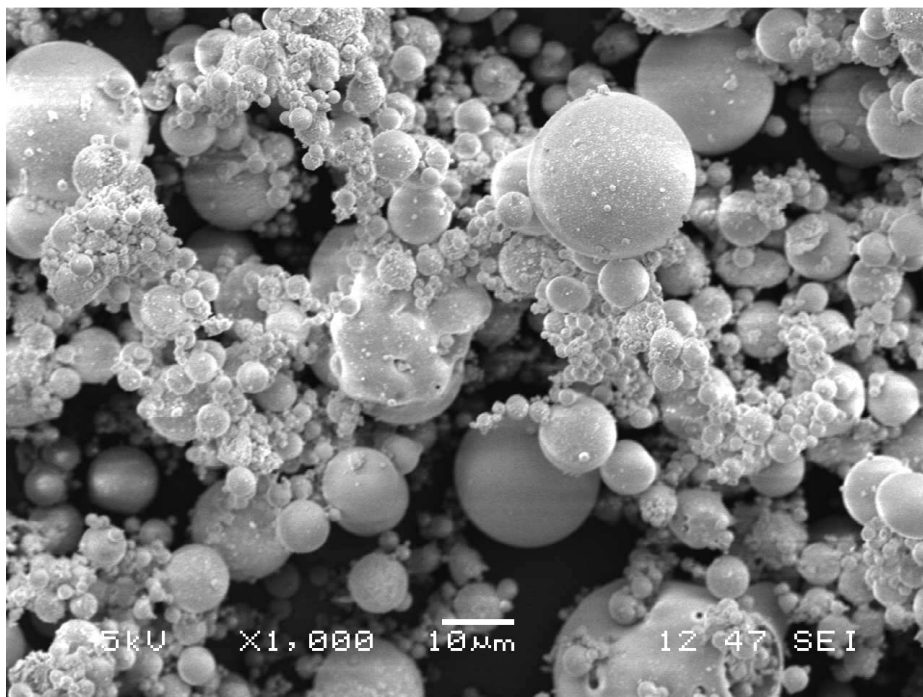


(b)

Figure B.1 By-product materials: (a) Musselwhite gold mine tailings and (b) scrap tire particles

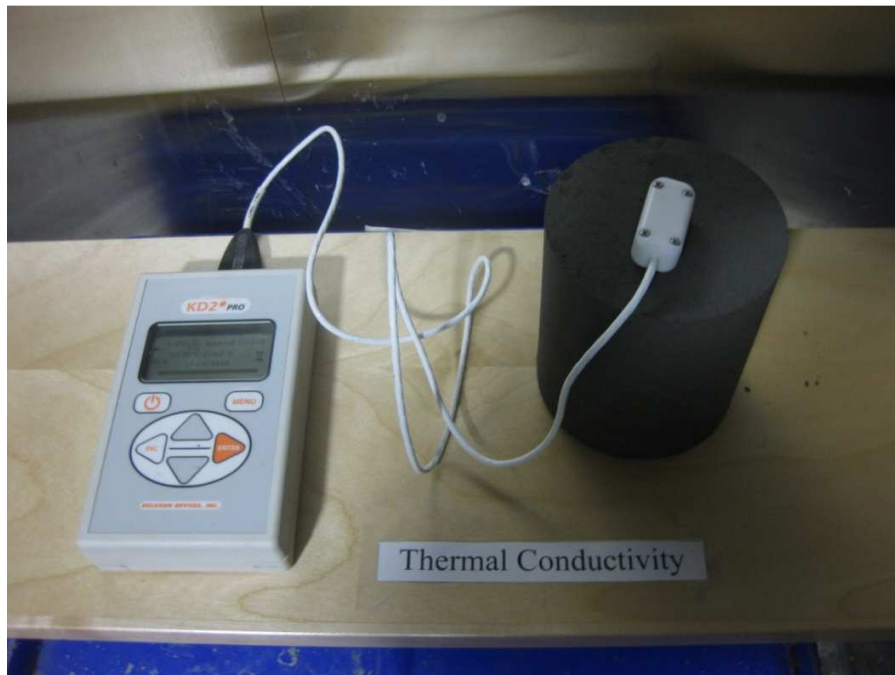


(a)

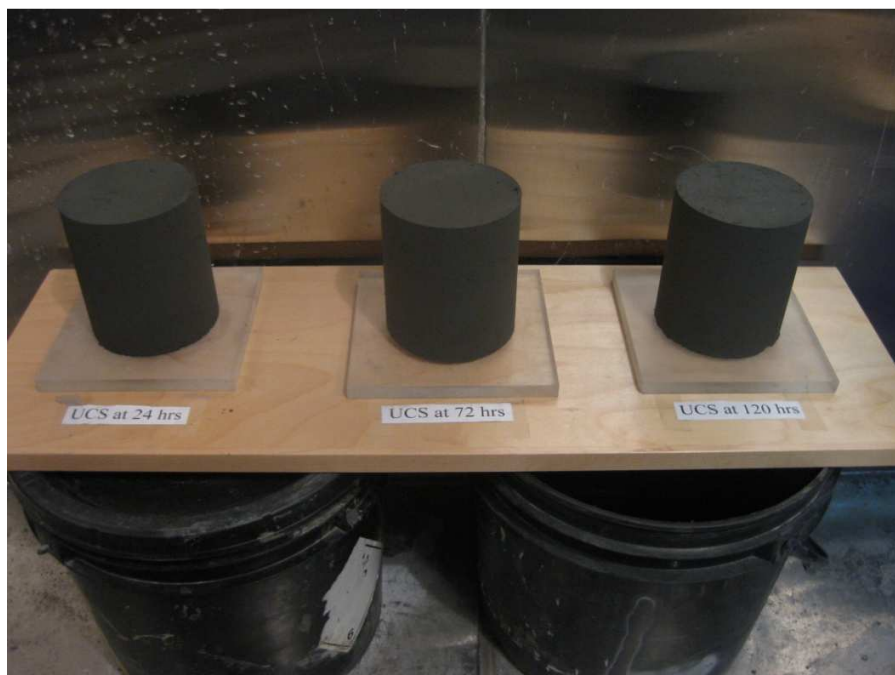


(b)

Figure B.2 SEM images of Atikokan coal fly ash: at (a) 300 times magnification and (b) 1,000 times magnification



(a)



(b)

Figure B.3 Thermal conductivity monitoring and curing of specimens of coal fly ash treated mine tailings in an environmental chamber



(a)



(b)

Figure B.4 Unconfined compression test - failure shapes of coal fly ash treated mine tailings (FA20-SP-OWC, immediately after compaction)



(a)



(b)

Figure B.5 Unconfined compression test - failure shapes of coal fly ash treated mine tailings (FA20-SP-OWC, 120 hours after compaction)

CURRICULUM VITAE

POST-SECONDARY EDUCATION	<p>Civil and Urban Engineering Yonsei University, Seoul, Korea 8/2005 B.Sc.</p> <p>Civil Engineering Yonsei University, Seoul, Korea 8/2007 M.Sc.</p> <p>Civil and Environmental Engineering University of Western Ontario, London, Canada 8/2012 Ph.D.</p>
RELATED WORK EXPERIENCE	<p>Research Assistant University of Western Ontario, London, Canada 9/2008 - 8/2012</p> <p>Teaching Assistant University of Western Ontario, London, Canada 1/2009 - 8/2012</p> <p>Research Assistant Yonsei University, Seoul, Korea 7/2005 - 8/2007</p> <p>Teaching Assistant Yonsei University, Seoul, Korea 9/2006 - 12/2006</p> <p>Construction Project Engineer Bosung Construction Co. (now, Han Yang Co.), Gwangju, Korea 9/2001 - 9/2004</p>

Summer Intern

Hanshin Engineering and Construction Co., Seoul, Korea

7/2000 - 8/2000

HONOURS AND
AWARDS

Western Engineering Scholarship

University of Western Ontario, London, Canada

9/2008 - 8/2012

BK21 (Brain Korea 21) Scholarship

Ministry of Education, Science and Technology, Seoul, Korea

3/2006 - 8/2007

Scholarship for Honor Student

Yonsei University, Seoul, Korea

3/2006

PUBLICATIONS

Lee, J.K. and Shang, J.Q. (2011). "Influencing factors on electrical conductivity of compacted kaolin clay." *Geomechanics and Engineering, An International Journal*, 3(2), 131-151.

Lee, J.K., Jeong, S.S., Kim, B.C., and Song, S.W. (2008). "Pseudostatic analysis of single column/shafts considering nonlinear soil behavior." *Journal of Korean Society of Civil Engineers*, 28(1C), 31-40 (in Korean).

Jeong, S.S., Kwak, D.O., Ahn, S.Y and Lee, J.K. (2006). "A study on the lateral behavior of pile-bent structures with P- effect." *Journal of the Korean Geotechnical Society*, 22(8), 77-88 (in Korean).